ATTENUATION OF A SHOCK WAVE BY A SINGLE TRANSVERSE SLIT

BY

P.P. OSTROWSKI

A THESIS SUBMITTED TO THE FACULTY OF GRADUATE STUDIES AND RESEARCH IN PARTIAL FULFILMENT OF THE REQUIREMENTS FOR THE DEGREE OF DOCTOR OF PHILOSOPHY

JANUARY, 1975

DEPARTMENT OF MECHANICAL ENGINEERING
McGILL UNIVERSITY
MONTREAL, CANADA

STATEMENT OF ORIGINALITY

To the author's knowledge, the specific problem treated in this thesis has not been attempted by any other researchers. Therefore all of the experimental results presented here are considered to be unique contributions to original knowledge.

Although many aspects of the ray-shock theory presented in this thesis have been well established previously, the solution of the ray-shock relations for the attenuated shock Mach number is believed to be an original contribution as well.

RESUME

On étudie l'atténuation d'une onde de choc plane causée par une fente simple transversale amenagée dans la paroi d'un tube rectangulaire, pour des chocs ayant un nombre de Mach allant jusqu'à 2.44 et pour des largeurs de fentes comprises entre 0.068 et 1.250 pouces. A l'aide de la photographie schlieren à étincelle, on étudie et on mesure l'atténuation près de la fente. La vitesse de l'onde est mesurée à une distance d'environ dix diamètres hydrauliques en aval de la fente à l'aide de jauges à pression. A l'aide de la théorie de Whitham sur le rayon-choc, on prédit l'atténuation initiale et on construit un diagramme qui décrit le mouvement des ondes transversales sur le front de choc.

On observe que l'atténuation provient de la diffraction du choc par la fente, même si cet effet est neutralisé en partie par une réflection de Mach se produisant sur le bord du coté aval de la fente. On montre que le mouvement de l'onde transversale résultante est pseudo-stationnaire. En accord avec la théorie, l'atténuation observée est faible et l'effet de la largeur de la fente est de second ordre. La plus grande réduction mesurée pour le nombre de Mach du choc est de 7%. On note un accord raisonnable avec la théorie pour toute la gamme des tests effectués. Enfin la stabilité du choc atténué est mise en évidence à partir du diagramme des ondes.

ABSTRACT

Attenuation of a planar travelling shock wave due to the interaction with a single transverse slit in the wall of a square tube is investigated for shock Mach numbers up to 2.44 and for slit widths between 0.068 and 1.250 inches. Spark schlieren photography is employed to examine and measure the attenuation near the slit. Wave speed measurements roughly ten hydraulic diameters downstream from the slit are performed using pressure transducers. Whitham's ray-shock theory is employed to predict the initial attenuation and to construct a wave diagram that describes the transverse wave motion on the shock front.

The attenuation is observed to result from the diffraction of the shock through the slit although this effect tends to be offset by a Mach reflection process at the downstream edge of the slit. The subsequent transverse wave motion is demonstrated to be essentially pseudo-stationary. In accordance with the theory the attenuation is observed to be weak and the effect of slit width secondary. The largest measured reduction in shock Mach number is 7%. Reasonable agreement with theory is observed over the range of the tests. Stability of the attenuated shock is demonstrated from the wave diagram.

ACKNOWLEDGEMENTS

The author wishes to express his appreciation to his research director, Dr. J.H.T. Wu, for his guidance and many helpful suggestions during the course of the present investigation. His constant encouragement and generous support is gratefully acknowledged.

Thanks are also extended to Dr. R.D. Archer of the University of New South Wales, Australia for his guidance during the early stages of the work while Dr. Wu was on sabbatical leave. The author is particularly indebted to Professor J.H.S. Lee for his advice and some very illuminating discussions regarding the theoretical aspects of the study. In addition, gratitude is expressed for the able assistance of Mr. Patrick Lee, Mr. Rafik Neemeh and Mr. Nabil Elabdin during the course of the experimental phase of the investigation.

Finally, the author wishes to express his sincere appreciation of the skillful efforts of Linda Porco and Ronnie Scallan who, in spite of some difficult operating conditions, cheerfully typed this thesis.

This work was supported by the National Research Council of Canada under Grant No. A-1225.

NOMENCLATURE

LATIN SYMBOLS

A	duct cross sectional area
C	shock-shock velocity
c	sound speed,speed defined by eq.22
e	specific internal energy
F	area-Mach number function
f	defined by eq. 14
f_1, f_2, f_3	defined by eq. 1
g	defined by eq. 14
h	duct width
K	Chester function, eq. 5
k	defined on page 32
L	shock stand-off distance
ℓ	slit width
M	Mach number
m	characteristic angle, eq. 25
n	2/K
P	positive characteristic variable
p	fluid pressure
Q	negative characteristic variable
R	gas constant
S	specific entropy
T	temperature
t	time
u	x component of fluid velocity

LATIN SYMBOLS (contd.)

v	fluid velocity
x	axial coordinate
Y	transverse coordinate
z	defined on page 65

GREEK SYMBOLS

α	ray-shock coordinate
β	ray-shock coordinate
γ	ratio of specific heats
δ	flow deflection angle
η	characteristic coordinate defined on Pages 27, 38
θ	flow direction
θ_d	detachment angle
μ	defined on page 28, also Mach angle
ν	Prandtl-Meyer angle
ξ	characteristic coordinate defined on pages 27, 38
ρ	fluid density
τ	time required for a sound wave to traverse the jet
ϕ	function defined on page 32, function defined on page 66
ψ	Mach stem contiguity direction
χ	shock-shock locus angle

SUBSCRIPTS

e	refers to expansion wave
j	refers to fluid jet
M	mean value
s	refers to shock wave

SUBSCRIPTS

t	tail of expansion wave
w	refers to the duct wall
x	ahead of shock
y	behind shock
o	ambient (undisturbed) conditions
1	behind undisturned shock
2	behind disturbed shock
*	refers to shock when just at downstream edge of slit, also critical (sonic) conditions

TABLE OF CONTENTS

CHAPTER I

INTRODUCTION

1.1 Relevance and Brief Description of the Problem

Recently, there has been a resurgence of interest in the interaction of blast waves with obstacles on account of the growing concern regarding unconfined vapor cloud explosions. Since the quantity of combustible gases that is being transported within many industrialized countries is steadily increasing, there is a real danger of catastrophe if large spills occur. Documented accounts[1] of industrial accidents have shown that in the last few years there has been a marked increase in both the number of such incidents and the damage inflicted by them.

Due to the ever increasing cost of energy, natural gas that was previously burned off in many large oil fields is soon to be stored and transported in large supertankers. These, with envisioned capacities of up to three million cubic feet of liquefied natural gas (LNG), are expected to present a significant danger to transport and storage facilities.[2] This concern has prompted a recent Dutch investigation[3] into the hazards associated with a planned LNG tanker terminal. The gas dynamic aspects of the problem constitute a major portion of the study.

Generally, the spillage and subsequent ignition of a large quantity of a combustible gas presents several distinct problems to the engineer. Among these is the ability of the surrounding structures to survive a catastrophic explosion. Obviously, the study and design of blast resistant structures can lead to a reduction in the damage done. Also associated with this aspect of the problem is the question of how far must a conventional structure be located from an explosive source in order to survive? This question arises in the placement of gas processing facilities relative to loading facilities, storage sites as well as population centers.

Another important consideration is the possible transition from deflagration to detonation in fuel-air explosions, the latter causing considerably more damage. It is well known that a deflagration wave often drives a precursor shock ahead of itself and that reflection of this shock from an obstacle may lead to temperatures and pressures sufficiently high to initiate detonation. This is especially true in the neighborhood of the triple point of Mach reflection. In addition, the shock waves produced by flying debris from an initial explosion may eventually initiate detonation. Thus it appears desirable to find some means of weakening these shocks before this can occur.

Similar dangers exist in coal mining operations as well, although in this case explosions are more confined and tend to propagate through branches of underground tunnels.

The same is true of gas line explosions in industrial plants. In these cases as well, there appears to be a real need to investigate practical methods of dissipating and attenuating shock waves which may be accidentally generated.

In general, shock wave attenuation is a complex process and since the equations which describe shock wave dynamics are nonlinear, there are no simple solutions to this type of problem. Aside from the natural tendency of blast waves to attenuate due to area divergence effects, shock wave attenuation usually results from the generation of an expansion wave somewhere in the flow field which overtakes the shock and weakens it. For an unconfined shock, this process can be rather gradual, especially if the expansion is quite localized initially. However, for shock waves in ducts, multiple reflection of an expansion wave from the duct walls provides a mechanism by which the attenuation process can be accelerated. In this case, the expansion wave can traverse the shock several times before it is dissipated.

The present study examines the attenuation of an initially planar shock wave as it passes over a single slit in the wall of a rectangular duct of constant cross section. Such attenuation clearly results from diffraction of the shock wave through the slit. The expulsion through the slit of gas originally compressed by the shock generates an expansion wave which overtakes the shock and tends to weaken it. This effect is compensated to some degree by the subsequent reflection of the diffracted shock from the downstream edge of the slit. The net result is, however, a reduction in shock strength. Since the energy flux through the slit depends mainly upon the strength of the incident shock, the attenuation rate depends upon this parameter also.

The simple shock tube facility employed here is not intended to simulate a blast wave. The latter always decays because the initiation energy is distributed over an ever increasing volume of fluid as it propagates away from its point of origin while for the former the shock is "pumped" at a constant shock Mach number. In the present case, this difference is desirable as the attenuating effect of the slit alone can then be evaluated.

1.2 The Nature of the Problem

Some of the characteristics of the shock-slit interaction process have been described previously[4] for the case where the particle velocity behind the incident shock is subsonic. The situation is depicted in the drawings of Figure 1.1 which shows the development of the wave interactions when the wall of the duct may be considered to be very thin. In (a) the initially planar shock is diffracted as it passes into the slit; the shock curves around the opening to maintain contact with the wall. At the same time a nearly cylindrical expansion wave is generated at the upstream edge of the slit. As time progresses this wave spreads out into the channel and is responsible for the attenuation of the shock. Since the particle velocity is taken to be subsonic, the head of the expansion wave also moves upstream. Furthermore, since there is no characteristic length involved, this initial stage of the interaction is self-similar, the configuration differs from instant to instant only by a scale factor.

However, the insertion of the downstream edge of the slit into the problem introduces a characteristic length (the slit width) and the self-similar nature of the flow is destroyed. In physical terms, this is accomplished by the reflection of the diffracting shock from the downstream edge which produces a secondary shock which also spreads out into the flow. This compression wave which is also nearly cylindrical then terminates the initial expansion and tends to reduce the attenuation of the main shock. It is interesting to note that when the secondary shock progresses upstream, it eventually collides with the opposite edge of the slit to produce a third shock which then moves downstream to collide with the other edge. This reflection process continues until the colliding waves become so weak that the motion is entirely acoustic.

The experimental evidence indicates that the reflection of the diffracting shock is a Mach reflection i.e., a three shock configuration with a Mach stem which is normal to the duct wall at its foot. While there is no reason to suppose that conditions can not be found for which the reflection process is regular, only the Mach configuration will be considered here. It is the Mach stem which is in fact the attenuated wave and since this wave must lag behind the incident (undisturbed) portion of the main shock, significant shock curvature is exhibited in the vicinity of the triple point.

After some time the wave configuration becomes more or less fixed with the internal flow characterized by the four traveling waves described above. Outside, the external traveling waves move far away from the slit and for all practical purposes, no longer influence the flow there. A steady fluid jet is established at the slit which is inclined at some angle θ_j to the duct axis. This situation for purely subsonic flow behind the attenuated shock is depicted in

Figure 1.1 (c).

In general, the jet structure depends upon the pressure ratio across the slit as well as the particle velocity behind the shock. Three flow regions may be distinguished for the jet. These are (i) purely subsonic flow, (ii) mixed sub and supersonic flow i.e., choking and (iii) purely supersonic flow for which there is a Prandtl-Meyer expansion at the upstream edge of the slit. Troshin[5] has analyzed steady, two-dimensional irrotational compressible flow through an aperture in the wall of a duct using compressible hodograph theory and his results may be applied to case (i) above. This analysis gives an approximate theory for the jet angle θ_j as well as the contraction ratio. In principle, it is possible to use this method to compute the jet structure also.

Regime (iii) exists when the particle velocity behind the incident shock is supersonic. For this case the internal waves are not able to propagate upstream and they remain essentially attached to their point of origin. Thus a Prandtl-Meyer expansion exists at the upstream edge of the slit and a slightly detached shock exists at the downstream edge as shown in Figure 1.1 (d). The jet structure is quite complex due to the reflection of the detached shock from the jet boundary. However, it will be shown later than an approximate theory due to Moeckel[6] can be used to compute the shape of this detached shock and the method of characteristics can then be employed to compute the jet structure. Unfortunately, little or no information exists concerning regime (ii) and little more can be said about it. For shocks in air, choking (Regime (ii)) is theoretically possible for shock Mach numbers greater than 1.21 and supersonic particle velocities (Regime (iii)) exist for shock Mach numbers beyond 2.07.

Clearly, the development of the jet structure is tied to the wave interactions that take place in the immediate vicinity of the slit and as mentioned above, these become acoustic in nature as time progresses. A theory by Rudinger[7] for the reflection of a shock wave from the open end of a duct provides some information about such processes. Acoustic theory is employed to describe the reflection of shocks from a duct end fitted with an orifice plate as well. According to the theory the pressure adjustment is asymptotic although it is virtually complete in a time $t \approx 4\tau$ where τ is the time required for an acoustic wave to traverse the exist section of the duct or orifice.

From the foregoing description of the shock-slit interaction it can be seen that the strength of the attenuated shock is constant along the wall downstream of the slit provided that the duct is infinitely wide. Of course in the practical case it is not and both the expansion wave and secondary (reflected) shock will undergo multiple reflections from the walls of the tube as the main shock propagates down the tube. Thus the attenuation as measured at the wall containing the slit, will proceed in distinct jumps corresponding to the arrival of the reflected waves at the wall. Furthermore the frequency of the reflections, and hence the attenuation rate, will depend upon the width of the duct. However, in a practical case, multiple slits would provide more efficient attenuation and this effect would become secondary.

1.3 Shock Diffraction and Reflection Processes

Over the last thirty years or so, a considerable effort has been directed towards the understanding of blast waves and their effects. Studies have been mainly concerned with the production and propagation, theoretical description and experimental measurement of blast waves as well as the blast loading of various structures. A comprehensive summary of these efforts and an extensive bibliography are presented in Reference 8. Attention has also been focused on the inverse problem, that is, the modification of blast and shock waves by various structures and obstacles. The latter topic falls into a rather broad aspect of gas dynamics which might be termed "shock wave interactions" and has been the subject of considerable research over the years. It was mentioned in Section 1.2 that the shock-slit interaction involves both diffraction and reflection of the incident wave, therefore some of the more pertinent contributions in this field will now be discussed briefly. The early work of Lighthill[9,10] provided a viable theory for the motion of a shock at an expansion or compression corner as well as the head on reflection of a plane shock from an irregular surface. However, since the theory is based on a linearization of the equations of motion its validity appears to be restricted to small deflections of the shock wave.

The complexities and limitations of Lighthill's theory led to a search for alternate methods of solution to shock diffraction problems. Numerical schemes were developed, most notably by Ludloff and Friedman[11,12] who not only solved the equations of motion in their usual hyperbolic form but also in the elliptical form associated with the "pseudo-stationary" or similarity coordinates x/t, y/t. They note that the former method is to be preferred due to its relative simplicity and effectiveness. The same approach has been employed by Rusanov[13] in the Soviet Union to solve several shock diffraction and reflection problems. Numerical solution of shock propagation through channels with sudden and gradual enlargements as well as branches has been accomplished by Gururaja and Dekker.[14] An excellent overall review of the numerical methods in gas dynamics has been given by Belotserkovskii and Chushkin,[15] although this work focuses mainly on the efforts of Soviet researchers. A summary of the mathematical techniques, both analytic and numeric, that have been applied to many shock diffraction and reflection problems has been presented by Pack.[16]

Perhaps the most versatile method of solution for shock wave motion problems is the ray-shock theory due to Whitham.[17] Based on some concepts from geometrical acoustics, the method employs successive shock positions and their orthogonal trajectories (the rays) as coordinates. This leads to one differential equation relating shock Mach number M and ray-tube area A. A second relation between A and M is approximated from the well known CCW (Chester-Chisnell-Whitham) Theory[18] for the motion of a shock wave down a tube of varying cross section. The resulting equations turn out to be hyperbolic and a solution is conveniently expressed by the method of characteristics which describes the motion of kinematic waves on the shock front. These are interpreted as the intersection of acoustic waves with the shock and the case where these waves break is termed a "shock-shock" which corresponds to the well known phenomenon of Mach reflection. Thus the theory is able to describe the trajectory of the triple point of Mach reflection but unfortunately it is unable to provide any information concerning the flow field behind the main shock front.

The ray-shock method is so general and flexible that it has been applied successfully to a wide variety of shock dynamics problems. In his original paper, Whitham[17] examined the diffraction of plane shocks by an expansion or compression corner, shock motion along an arbitrarily shaped wall and the stability of plane and cylindrical shocks. The method was extended to three dimensions[19] for which shock stability and the diffraction of a plane shock by a cone or an arbitrary slender body is examined. It is also shown that a direct analogy with linearized supersonic flow problems exists.

Experimental verification of the ray-shock theory has been undertaken by many investigators covering a wide variety of problems. Diffraction of a planar shock at an expansion corner has been studied by Skews for both sharp[20] and rounded[21] corners via schlieren photography in a shock tube. As anticipated by Whitham, reasonable agreement between the experimental and theoretical shock profiles is observed only for shock Mach numbers M greater than about 3.0. For lower values of M Whitham observed that the theory concentrates the disturbance over too small a segment of the shock. In actuality, the disturbance is spread over the entire region encompassed by the sonic circle emanating from the corner, as is verified by Skew's experiments.

For a given initial shock Mach number, the ray-shock theory predicts a critical diffraction corner angle which corresponds to a wall shock Mach number which is just unity. Beyond this angle, no solution is possible corresponding to the degeneration of the shock into a Mach wave. Again, at lower shock Mach numbers a considerable discrepency is noted by Skews. For example at $M = 1.5$ the critical diffraction angle is roughly 90^0 while the experiments show a finite shock strength even for $M = 1.2$ and a diffraction angle of nearly 180^0. For corner angles less than 90^0 the theory is observed to predict the wall shock Mach number fairly well throughout the entire range of the tests ($M = 1.0$ to 5.0 approximately).

A fundamental assumption in Whithams formulation of the ray-shock theory is that there is no interaction of any kind between neighboring ray tubes. Oshima et. al.[22] have incorporated shear stresses due to turbulent mixing across ray tubes into the theory and claim a significant improvement. However, since they employed a constant value of the

Chester Mach number function K(M) in the integration of the characteristic relations, these results should be treated with some reserve until more experimental evidence is accumulated. An improvement of this theory for weak shocks has also been given.[23]

Miles[24] has studied theoretically, the problem of the head on collision of a blast wave with the bow wave attached to a thin wedge moving at supersonic speed. In this case the diffracted shock is oblique to the (relative) upstream flow and a tangential velocity component is conserved across it. This is incorporated into the ray-shock theory according to a modification originally proposed by Chisnell.[25]

The ray-shock theory has been employed successfully by Bryson and Gross[26] to predict shock-shock trajectories for diffraction of a plane shock by cones, cylinders and spheres at shock Mach numbers of the order of 3.0. The independence of the diffraction pattern from shock Mach number as predicted by Whitham in this range was observed by these authors for the case of a cylinder. Other applications of the theory include the prediction of the trajectories of transverse distrubances to a converging cylindrical deton-ation wave[27] and the amplification of a shock wave as it progresses into a conically convergent channel.[28] With the aid of the ray-shock theory Skews[29] has demonstrated the analogy in shock shape for diffraction at an expansion corner and regular reflection at a compression corner.

An interesting use of Whithams technique is employed in the concept of shock wave shaping[30] for which collapse of a shock in a convergent channel is accomplished without finite reflections from the walls. This leads to significant amplification of the shock and the production of high enthalpy gas near the point of collapse. It has been shown[31,32] that from ray-shock theory the correct wall shape for a two-dimensional channel is a logrithmic spiral contraction and this has been studied extensively by Milton[33] who also confirmed these results with experiments and investigated axisymmetric shock collapse as well. Additional experimental results have also been given.[34,35]

An important consideration in shock propagation problems is an analysis of shock reflection processes. Normal reflection and the regular (two shock) configuration of oblique reflection of shock waves are well described by invisid analyses which may be found in any gasdynamics textbook.[36,37] However, for the oblique case if the angle of incidence is too large or the shock too weak the more complicated Mach (three shock) configuration occurs. In this case if the shocks are assumed to be straight in the immediate vicinity of their point of confluence (the triple point), two-dimensional invisid theory also gives a straightforward solution. This is most easily accomplished from hodograph theory i.e., the intersection of two shock wave polars,[16,38,39] and although this method is widely used, agreement with experiment is adequate for strong shocks and decidedly inaccurate for weak shocks. The deficiency of the three shock theory has lead to the proposal[40] that the flow near the triple point can not be described by the usual jump (Rankine-Hugoniot) conditions. Most investigators agree that the usual scale of laboratory experiments does not afford sufficient resolution to accurately examine the flow phenomena near the triple point.

The transition from regular to Mach reflection is not yet completely understood and it is not known whether this occurs when the deflection across the reflected shock is maximum or when the flow behind it is just sonic. Kawamura and Saito[39] concluded from their shock tube experiments that the flow is singular at the triple point when the flow behind the reflected shock is subsonic. Guderley (see 16) inserted a Prandtl-Meyer expansion at the triple point to give a different, but plausible type of intersection of the shock polars for those cases where intersection was previously thought not to exist. The reflection of curved shocks in a steady flow of Mach number 2.8 has been studied by Molder[41] who showed that a smooth transition from regular to Mach reflection occurs as shock strength is decreased.

For the case where a traveling planar shock is incident upon a stationary wedge or ramp and the Mach reflection configuration occurs, it is well known that it grows uniformly with time and is termed "pseudo-stationary" in the similarity coordinates x/t, y/t. The locus of the triple point then follows a linear path from the apex of the wedge and this angle (which is just the "shock-shock" trajectory described by Whitham) can be computed from the ray-shock theory. It was demonstrated by Whitham[17] that for strong shocks the theory is not especially accurate for such calculations (maximum error of about 25%) except for large ramp angles. For incident shock Mach numbers of 1.51 and 2.42 Milton[33] used known experimental results to show that the ray-shock theory adequately predicts the triple point locus angle except for ramp angles less than about 10-15 degrees. For ramp angles approaching zero, acoustic theory is observed to give better results. For the same shock Mach numbers, the ray-shock theory is seen to give a good estimate of the stem shock Mach number, except at large ramp angles. Thus in general, the theory is good for predicting wall shock Mach number but poor for estimating the triple point locus.

1.4 Shock Wave Attenuation

To date, most of the work on attenuation of traveling shock or blast waves has been focused on nearly plane waves moving through ducts. For the case of shocks propagating through diverging channels the decay in shock Mach number can be estimated from the CCW theory for which Whitham's formulation[17] is the simplest. Available experimental evidence[42] indicates reasonable agreement with theory for weaker shocks and duct divergence angles up to 45^0 although the measured decay rate is not quite as rapid as predicted.

Attenuation of shocks traveling in ducts can be accomplished by mass, momentum or energy transfer either ahead or behind a wave which would otherwise propagate at a uniform velocity. A general analysis of shock bounded flows with mass, momentum and energy transfer has been presented by Mirels [43]. However, since a linearized theory is employed it is restricted to weak shocks or cases where the variation in fluid properties is small. A further study[44] demonstrates that self similar shock attenuation is possible provided the mass, momentum and energy flux terms have a very specific form. Unfortunately, for most practical problems it appears unlikely that these conditions can be met.

Since disturbances are often communicated to traveling shocks by acoustic waves, the method of characteristics is a likely method of analysis for shock propagation problems. This approach has been employed by Rosciszewski.[45] His method is essentially a linearization of the one dimensional characteristic equations which presumably limits application to cases where disturbances in the flow field are relatively small. However, it is demonstrated that the method is simply a generalization of the CCW theory thus its applicability is wider than might be supposed.

One of the problems specifically treated by Rosciszewski is the attenuation of a plane shock travelling in a perforated tube. Expansion waves are generated by the expulsion of fluid through the perforations which then overtake and gradually weaken the travelling shock. The problem has been studied for square tubes[46] using the CCW theory and round tubes[47] via the method of characteristics. Experimental measurements from both studies show good agreement with theory and also demonstrate that Rosciszewski's calculations predict a much too rapid shock decay rate and this is attributed to errors in evaluation of the mass, momentum and energy flux through the perforations rather than a flaw in the general analysis.

An alternate scheme for shock attenuation is to reflect the energy of the wave upstream by placing obstacles in the path of a travelling shock. This can be accomplished with cylinders, grids[48] and similar objects. For one study, orifice plates were also suspended normal to the axis of a duct and measurements of the reflected and transmitted shock strengths were recorded.[49] The transmission of a weak shock wave through orifice plates with and without baffles as well as abrupt area contractions and expansions was investigated by Davies and Dwyer.[50] A simple one dimensional theory was found to give good results. A similar approach has been employed by Deckker and Male[51,52] to describe the passage of a shock wave through the juncture of two equal area ducts. The theory is found to predict the attenuation of the transmitted shock fairly well but not for the strength of the shock propagated into the side branch. The discrepency is attributed to wave reflection from the walls of the juncture.

1.5 Scope of the Present Investigation

According to the previous discussions, the flow phenomena associated with the shock-slit interaction are fairly complex hence the greater part of the present study is experimental. However, some attention is paid to a theoretical description of the problem and it will be shown below that the ray-shock theory provides an adequate description of the attenuation process.

A simple air/air shock tube with a two inch (nominal) square cross section is employed for the tests. Using an evacuated driven section, the practical range of operation of this tube is for shock Mach numbers up to about 2.5. This range is considered adequate to describe the present problem as it extends into the regime where supersonic particle velocities exist behind the incident shock. Thus the testing capability of the shock tube covers all three regimes described in section 1.2. A square cross section is chosen so that the simpler two dimensional interaction may be studied.

Two types of tests are performed. The first is a photographic study, the aim of which is largely definitive. Spark schlieren photography is employed to examine the physical features of both the internal and external flow fields over the entire range of shock Mach numbers. In this way, the intuitive description of the shock-slit interaction presented previously can be confirmed. At the same time, measurements taken from the photographs can be used to verify some of the theoretical descriptions that have been offered. Using a time delayed spark system parameters appropriate to the external flow field such as jet angle, development time and contraction ratio can be easily measured. For the internal flow field, velocities of both the undisturbed and attenuated waves, secondary shock and expansion wave radii and triple point trajectories can be obtained from the photographs. However, since only one photograph can be obtained for each firing of the shock tube repeatability of the test conditions is of paramount importance in order to obtain an accurate time history of the events.

The second phase of the tests is a straight forward measurement of the incident and attenuated wave velocities upstream and downstream of the slit. This is accomplished with six barium titanate piezo-electric pressure transducers used as shock detectors. These are employed in the usual way mounted in the shock tube wall in two groups of three (one trigger, two pickups) and connected to the vertical input terminals of a dual beam oscilloscope. A complete description of the experimental apparatus is given in Chapter IV.

For theoretical considerations, the ray-shock theory is chosen as this is the simplest approach. Although this theory assumes the working fluid to be inviscid and perfect, it has been used successfully to describe many other problems and is expected to be adequate for the present purposes.

Thus viscous effects are ignored completely despite the fact that boundary layer attenuation of shock waves is a well documented phenomenon. (It will be shown later that calibration of the shock tube indicates that viscous attenuation is not significant under the present test conditions). A critique and generalization of the ray-shock theory will be presented in Chapters II and III. Analytic solutions of the ray-shock theory for shock diffraction and Mach reflection processes appropriate to the present problem are then given. However, the resulting transcendental equations for the attenuated shock Mach number must be solved by iteration. Unfortunately the ray-shock theory does not provide any information concerning the flow field behind the attenuated shock therefore, aside from some of the experimental results, this matter will not be considered in the present study.

The ray-shock theory can be used to construct a wave diagram depicting the Mach reflection and expansion wave interaction processes as the attenuated shock progresses down the duct after passing over the slit. However, since the ray-shock theory does not give a very good estimate of the triple point trajectory within the Mach number range of the present study a somewhat crude empirical relation is substituted. For one of the test conditions, approximately two and one-half cycles of the motion (one cycle is taken to be when the triple point has traversed the duct twice) are plotted out on a wave diagram and comparison with experiment for one cycle shows fairly good agreement. The role of the wave diagram in a stability analysis of the attenuated wave is demonstrated.

CHAPTER II

A REVIEW OF THE CCW THEORY

2.1 The Area-Mach-Number Relation

The ray-shock theory developed by Whitham makes use of what is often termed the "CCW Relation", which describes the motion of an initially planar shock wave as it travels along a duct of non-uniform cross section. In particular, this description takes the form of a unique relation between the local duct cross sectional area and the (averaged) shock Mach number over that local cross sectional area. In order to understand the limitations and approximations inherent in the ray-shock theory, it is worthwhile to first examine the CCW theory in some detail.

Chester[53] was the first to derive the differential form of the CCW relation by using a quasi-one dimensional linearized analysis appropriate to small area variations, which was shown to be valid locally. Shortly afterward, Chisnell[54] obtained the same result with a strictly one dimensional "steady state" analysis, again on the basis of small area variations but valid only far away from the non-uniform region. It was thus concluded that the shock strength averaged over the cross sectional area does not vary as the shock progresses along a uniform tube downstream of an arbitrary (but still small) area change. However, since disturbances generated at the area change may still continually overtake the shock from behind, it was reasoned that these disturbances , which modify the shock locally, must effectively cancel each other when averaged across the shock surface. Finally, Whitham[18] derived the same relation using the differential characteristic form of the unsteady ~~one-dimensional equations of motion.~~ These efforts have been summarized by Chester[55] in a later paper. Whitham's derivation is the simplest, so it will be given first. Then the more illuminating contributions of Chester and Chisnell will be discussed.

Consider the equations of motion for an arbitrary one-dimensional flow of a perfect gas

$$\frac{\partial \rho}{\partial t} + u\frac{\partial \rho}{\partial x} + \rho\frac{\partial u}{\partial x} + \rho u\frac{\partial \ln A}{\partial x} = \frac{\rho}{c} f_1(x,t) \qquad (1)$$

$$\rho\frac{\partial u}{\partial t} + \rho u\frac{\partial u}{\partial x} + \frac{\partial p}{\partial x} = \rho f_2(x,t)$$

$$\frac{\partial p}{\partial t} + u\frac{\partial p}{\partial x} - c^2\left(\frac{\partial \rho}{\partial t} + u\frac{\partial \rho}{\partial x}\right) = \frac{\gamma-1}{R}\, p\left(\frac{\partial s}{\partial t} + u\frac{\partial s}{\partial x}\right)$$
$$= \rho c f_3(x,t)$$

where the functions f_1, f_2 and f_3 express the fact that there may be mass, momentum or energy exchange between the surroundings and a control volume encompassing the fluid. In this form, the terms on the right side of equations (1) represent the volumetric mass, momentum and energy flux across the control surface. These may be due to (1) mass flow across the sides of the control volume, (2) viscous shear and body forces (electromagnetic, gravity) and (3) external heat transfer, external work and work against body forces, respectively. For example, in a recent study[56] of shock propagation along a porous duct for which momentum and energy defects are not considered ($f_2=f_3=0$), $\rho f_1\ (x,t) = -2c\eta\xi\phi$ where the last three factors are the perforation ratio, discharge coefficient and ideal mass flow through the perforations, respectively. Oshima[22] et al examined the diffraction of planar shocks around a corner using the ray-shock theory and taking into account turbulent shear forces alone and not the work done by them ($f_1 = f_3 = 0$). In this case $\rho f_2(x,t) = \tau_y$ where τ_y is the turbulent shear stress.

Whitham considered the simple situation where there is area variation alone, $f_1 = f_2 = f_3 = 0$. In this case the differential characteristic form of equations (1) is

$$dp + \rho c\, du + \frac{\rho c^2 u}{u+c}\frac{dA}{A} = 0 \qquad \text{along } C+$$

$$dp - \rho c\, du + \frac{\rho c^2 u}{u-c}\frac{dA}{A} = 0 \qquad \text{along } C- \tag{2}$$

$$dp - c^2 d\rho = 0 \qquad \text{along } S$$

where the differential operators correspond to the directional derivatives

$$\frac{d}{d\xi} = \frac{1}{u+c}\frac{\partial}{\partial t} + \frac{\partial}{\partial x}, \quad \frac{d}{d\eta} = \frac{1}{u-c}\frac{\partial}{\partial t} + \frac{\partial}{\partial x}, \quad \frac{D}{Dt} = \frac{1}{u}\frac{\partial}{\partial t} + \frac{\partial}{\partial x}$$

in the respective characteristic directions

$$C+: \frac{dx}{dt} = u+c, \quad C-: \frac{dx}{dt} = u-c, \quad S: \frac{dx}{dt} = u$$

Now, Whitham's reasoning is as follows: if equations (2) describe the flow field behind a propagating shock, the positive (C+) characteristics will follow a trajectory that is close to that of the shock itself (Figure 2.1). Then, the first of equations (2), which is valid along a C+ characteristic, can be applied to the shock itself as a first approximation. This is done with the aid of the Rankine-Hugoniot equations, which express the change in the dependant flow variables across the shock

$$\begin{aligned}
\frac{p}{\rho_0 c_0^2} &= \frac{2}{\gamma+1} M^2 - \frac{\gamma-1}{\gamma(\gamma+1)} \\
\frac{u}{c_0} &= \frac{2}{\gamma+1}\left(M - \frac{1}{M}\right) \\
\frac{\rho}{\rho_0} &= \frac{(\gamma+1) M^2}{2+(\gamma-1) M^2} \\
\frac{c}{c_0} &= \mu \frac{[2\gamma M^2-(\gamma-1)]}{(\gamma+1) M}
\end{aligned} \tag{3}$$

where

$$\mu^2 = \frac{2+(\gamma-1)M^2}{2\gamma M^2-(\gamma-1)}$$

and M is the shock Mach number. It is assumed that the flow ahead of the travelling shock (subscript 0) is uniform and quiescent.

Therefore, differentiating equations (3) with respect to M and substituting this into the first of equations (2) (this process is Whitham's well-known "characteristic rule") yields

$$-\frac{dA}{A} = \frac{2M\,dM}{(M^2-1)\,K(M)} \tag{4}$$

where

$$K(M) = 2\left[\left(1+\frac{2}{\gamma+1}\,\frac{1-\mu^2}{\mu}\right)\left(1+2\mu+\frac{1}{M^2}\right)\right]^{-1} \tag{5}$$

is a slowly varying function of shock Mach number ($K(M) \rightarrow 0.5$, 0.395 as $M \rightarrow 1, \infty$ respectively) often called the "Chester Function" as Chester was the first to derive it, although in a somewhat different form. The variation of $K(M)$ is shown in Figure 2.2. Equation (4) expresses the fact that for a given change in area A, the change in shock Mach number M depends only on M and A. This A-M relation is the well-known CCW relation. It is important to note that the relation holds for finite area changes since no linearization has been employed in its derivation, although large area variations will likely lead to a violation of the quasi-one dimensional flow model. Furthermore, equation (4) should be quite accurate for weak shocks since, in this case, the shock trajectory is very close to that of the positive characteristics; as $M \rightarrow 1$ they are the same.

At this juncture, the nature of the approximations that have been made in order to obtain the CCW relation, are not apparent. In order to clarify matters somewhat, the Chester and Chisnell analysis must be examined in more detail. Chester arrived at an equivalent form of equation (4) by employing the full three dimensional equations of motion and considering only small area variations i.e. the linearized case where the flow is perturbed about the initial flow behind the undisturbed travelling shock. It is shown that pressure disturbances brought about by area changes are propagated back into the flow field behind the moving shock by acoustic waves and this information is sufficient to allow solution of the equations if the flow variables are averaged over the cross section of the duct. Thus, the analysis is quasi-one dimensional and, although it is too complex to be reproduced here, the essential features can be retained by making the one dimensional approximation at the onset. This simplification of Chester's work was first given by Whitham.

Since changes in pressure and velocity are carried by acoustic waves and changes in entropy are carried along particle paths, the appropriate equations to linearize are the characteristic equations (2). Then for small area variations the flow behind the travelling shock is perturbed about the initially uniform flow behind the undisturbed shock. This is denoted by the subscript (1). Thus

$$dp + \rho_1 c_1 \, du + \frac{\rho_1 c_1^2 u_1}{u_1 + c_1} \frac{dA}{A_1} = 0 \qquad \text{along } C+$$

$$dp - \rho_1 c_1 \, du + \frac{\rho_1 c_1^2 u_1}{u_1 + c_1} \frac{dA}{A_1} = 0 \qquad \text{along } C- \qquad (6)$$

$$dp - c_1^2 \, d\rho = 0 \qquad \text{along } S$$

and integrating along the respective characteristics

$$p - p_1 + \rho_1 c_1 (u - u_1) + \frac{\rho_1 c_1^2 u_1}{u_1 + c_1} \frac{A(x) - A_1}{A_1} = 2F[x - (u_1 + c_1)t]$$

$$p - p_1 - \rho_1 c_1 (u - u_1) + \frac{\rho_1 c_1^2 u_1}{u_1 - c_1} \frac{A(x) - A_1}{A_1} = 2G[x - (u_1 - c_1)t] \qquad (7)$$

$$p - p_1 - c_1^2 (\rho - \rho_1) = H[x - u_1 t]$$

where the arbitrary functions F, G and H express the fact that disturbances are carried along each of the three characteristic families. These disturbances, which are each generated in a different location in the duct, arrive simultaneously to produce a net change in density, pressure and particle velocity at the (arbitrary) point in the flow field which is under consideration. It can be seen from equations (7) that changes are also brought about by local area variations.

The functions F G and H are determined from the boundary conditions. Since the positive (C+) characteristics carry no disturbance in the initial flow far away from the shock, F must be identically zero. This means that for the linearized case (small area variations), the disturbances carried by the C+ characteristics are of second order and are therefore neglected in the analysis. Then with F=0, G and H can be determined from the boundary conditions at the shock i.e., the Rankine-Hugoniot equations (3).

For example, $G[x-(u_1-c_1)t]$ can be determined in the following way. Adding and subtracting the first two of equations (7) yields

$$p-p_1 = -\frac{\rho_1 c_1^2 u_1^2}{u_1^2-c_1^2}\,\frac{A(x)-A_1}{A_1} + G[x-(u_1-c_1)t] \qquad (8)$$

$$\rho_1 c_1 (u-u_1) = -\frac{\rho_1 c_1^3 u_1}{u_1^2-c_1^2}\,\frac{A(x)-A_1}{A_1} - G[x-(u_1-c_1)t]$$

Now, to first order at the shock ($x=Ut$)

$$p - p_1 = \frac{4\gamma p_0}{\gamma+1} M_0 (M - M_0) \qquad (9)$$

$$u - u_1 = \frac{2c_0}{\gamma+1}\left(1+\frac{1}{M_0^2}\right)(M - M_0)$$

where M_o is the initial undisturbed shock Mach number. Then eliminating $M-M_o$ from these relations

$$\rho_1 c_1 (u - u_1) = \frac{\rho_1 c_1}{\rho_0 c_0} \, \frac{1+\frac{1}{M_0^2}}{2M_0} (p - p_1)$$

$$= \frac{1+\frac{1}{M_0^2}}{2M_0} (p - p_1)$$

where use is made of equations (3) again. Then substituting equations (8) and simplifying

$$G\left(\frac{x}{k}\right) = \phi(M_0) \, \frac{\rho_1 c_1^2 u_1^2}{u_1^2 - c_1^2} \, \frac{A(x) - A_1}{A_1}$$

where

$$k = \frac{U}{U - (u_1 - c_1)}$$

$$\phi(M) = \frac{1 + \frac{1}{M^2} + (\gamma+1)\frac{\mu^2}{1-\mu^2}}{1 + 2\mu + \frac{1}{M^2}}$$

Thus finally

$$G\left[x-(u_1-c_1)t\right] = \tag{10}$$

$$\phi(M_0)\,\frac{\rho_1 c_1^2 u_1^2}{u_1^2-c_1^2}\;\frac{A\left(k\left[x-(u_1-c_1)t\right]\right)-A_1}{A_1}$$

The function $H(x-u_1t)$ can be determined in a similar way.

Then, if equation (8) is evaluated at the shock front where

$$x = Ut \quad , \quad A\left(k\left[x-(u_1-c_1)t\right]\right) = A(x)$$

and use is made of equations (3), (9) and (10), the final result is, after some simplification and dropping the subscripts

$$-\frac{\delta A}{A} = \frac{2M\,\delta M}{(M^2-1)\,k(M)}$$

which is just the CCW relation, equation (4).

The significance of the "characteristic rule" now becomes more evident. According to it, the first of equations (2) is approximately valid at the shock (x=Ut). Hence

$$\left(\frac{1}{U}\frac{\partial p}{\partial t}+\frac{\partial p}{\partial x}\right)+\rho c\left(\frac{1}{U}\frac{\partial u}{\partial t}+\frac{\partial u}{\partial x}\right)$$

$$+\frac{\rho c^2 u}{u+c}\,\frac{1}{A}\frac{dA}{dx} \approx 0$$

but in general

$$\left(\frac{1}{u+c}\frac{\partial p}{\partial t} + \frac{\partial p}{\partial x}\right) + \rho c\left(\frac{1}{u+c}\frac{\partial u}{\partial t} + \frac{\partial u}{\partial x}\right)$$

$$+ \frac{\rho c^2 u}{u+c}\frac{1}{A}\frac{dA}{dx} = 0$$

Therefore the rule applies if at the shock

$$\left(\frac{1}{U} - \frac{1}{u+c}\right)\left(\frac{\partial p}{\partial t} + \rho c\frac{\partial u}{\partial t}\right) \approx 0 \qquad (11)$$

But in the linearized case, differentiation of the first of equations (7) gives (with F=0)

$$\frac{\partial p}{\partial t} + \rho_1 c_1 \frac{\partial u}{\partial t} = 0$$

Hence equation (11) and, therefore, the CCW relation, is exactly correct in the linearized case. However, this does not explain why the methods works so well in the more general case where area variations are finite, although it is evident that equation (11) must be approximately true in that situation.

Chisnell also derived an equivalent form of the CCW relation on the basis of small area ~~variations and~~ variation of one dimensional steady flow. This analysis is straightforward and will not be presented here. However, since it is based on the steady flow relations, its validity is restricted to a region far away from the actual area variations. Since the final result is identical to Chester's, which is valid locally, Chisnell concluded that the average shock strength over the cross section does not vary after the area change, despite the fact that, in the actual case, multi-dimensional wave interactions due to reflected disturbances will continue to overtake the shock and alter it locally.

Chisnell's approach is significant because he then goes on to integrate the CCW relation, thereby extending it to finite area variations as an approximation. Written in terms of shock pressure ratio, it is demonstrated that equation (4) has an exact integral although the final result is rather complex. An obvious simplification is to consider the Chester function K(M) to be constant at some suitable average value. Then the integrated form of the CCW relation is

$$A^{K}(M^2-1) = \text{CONSTANT} \qquad (12)$$

which is then exact for very weak shocks ($K \to 0.5$) or very strong shocks ($K \to 0.394$). In the former case

$$M \sim 1/\sqrt{A}$$

a result which is well known from acoustic theory. For very weak shocks, then, it is expected that the CCW theory would give good results. In this case, the shock can be approximated as an acoustic wave (characteristic) which is, of course, just the essence of the "characteristic rule". Chester put it another way. In the acoustic limit, both the (weak) shock and the disturbances behind travel at the same speed. Therefore, these disturbances are unable to overtake the shock so that the only changes in shock strength come from area variations right at the shock front.

In his analysis, Chisnell reasoned that, for finite area variations, the disturbances in the flow field behind the shock are also finite and the use of the integrated form of the CCW relation is tantamount to neglecting their modifying effect altogether. However, he goes on to show, through a somewhat complicated approximate analysis, that for strong converging cylindrical and spherical shocks these disturbances, which are communicated to the shock by the positive characteristics, actually tend to nearly completely cancel each other - a rather remarkable and fortunate circumstance. Since there is no reason to suppose that the situation is not qualitatively different for nearly planar or moderate strength shocks, it may be concluded that the CCW theory is at least approximately correct for these cases.

To sum up, then, it appears that the CCW relation in either its differential or integrated form, can be applied with some degree of confidence to a wide variety of shock wave dynamics problems for which there is area variation alone. The theory is exact for small area variations or very weak shocks and approximately correct for finite area variations due to cancellation of reflected disturbances. The success of Whitham's "characteristic rule" in the general case then appears to be linked to the relative smallness of both factors in equation (11).

2.2 Extensions and Modifications of the CCW Theory

Thus far, only the effect of area changes on travelling shocks have been considered. Several investigators have examined the more general situation where mass, momentum and energy transfer may influence the shock motion as well. These provide further insight into the CCW theory.

Rosciszewski[45] performed an analysis somewhat different from Whitham's while retaining the mass, momentum and energy flux terms on the right side of equation (1). In this case, the characteristic equations are more compact written with the Riemann variables

$$P = \frac{2}{\gamma-1} c + u$$

$$Q = \frac{2}{\gamma-1} c - u$$

as dependant variables. Making use of the thermodynamic relation

$$T\,ds = dh - \frac{1}{\rho}\,dp = de + p\,d\left(\frac{1}{\rho}\right) \qquad (13)$$

as well as the perfect gas equation of state $p=\rho RT$ and the isentropic equation $c^2=\gamma p/\rho$, equations (1) can be transformed into

$$\frac{dP}{d\xi} - \frac{c}{\gamma R}\frac{ds}{d\xi} + uc\,\frac{\partial \ln A}{\partial x} = f_1 + f_2 + f_3 \equiv f(x,t) \qquad (14)$$

$$\frac{dQ}{d\eta} - \frac{c}{\gamma R}\frac{ds}{d\eta} + uc\,\frac{\partial \ln A}{\partial x} = f_1 - f_2 + f_3 \equiv g(x,t)$$

where as before

$$\frac{d}{d\xi} = \frac{\partial}{\partial t} + (u+c)\frac{\partial}{\partial x}\,, \quad \frac{d}{d\eta} = \frac{\partial}{\partial t} + (u-c)\frac{\partial}{\partial x}\,, \quad \frac{D}{Dt} = \frac{\partial}{\partial t} + u\frac{\partial}{\partial x}$$

are the directional derivatives in the respective characteristic directions. The situation is again shown in Figure (2.1) where the region of non-uniform shock propagation is taken to start at X=0. Now, Rosciszewski's method is to integrate the first of equations (14) along two neighbouring positive characteristics from the initial undisturbed region of flow (1) to the shock front (2). Then subtracting the two relations thus obtained and taking the limit as the characteristics are allowed to approach each other for the case where A=A(x) alone

$$dP_2 - dP_1 - d\int_1^2 \frac{c}{\gamma R}\,ds + \int_1^2 \frac{uc}{u+c}\,d\ln A = d\int_1^2 f\,d\xi$$

Applying Liebnitz' rule for differentials of integrals with variable limits and noting that all quantities in region (1) are constants for uniform flow ahead of the shock

$$dP_2 - \int_1^2 d\left(\frac{c}{\gamma R}\right) ds - \frac{c_2}{\gamma R}\,ds_2 + \int_1^2 d\left(\frac{uc}{u+c}\right) d\ln A$$

$$+ \frac{u_2 c_2}{u_2+c_2}\,d\ln A_2 = \int_1^2 df\,d\xi + f_2\,d\xi$$

and making use of the mean value theorem for integrals

$$dP_2 - (s_2 - s_1)\left(\frac{dc}{\gamma R}\right)_M - \frac{c_2}{\gamma R}\,ds_2$$
$$+ \ln\left(\frac{A_2}{A_1}\right)\left[d\left(\frac{uc}{u+c}\right)\right]_M + \frac{u_2 c_2}{u_2+c_2}\,d\ln A_2$$
$$= (\xi_2 - \xi_1)(df)_M + f_2\, d\xi_2$$

where the subscript (M) denotes mean values.
Now, for the linearized case where variations in both A and f are small all the terms in the above relation which contain mean values can be taken as second order and neglected. Then, dropping the subscripts

$$\left(\frac{dP}{dM} - \frac{c}{\gamma R}\frac{ds}{dM}\right)dM + \frac{uc}{u+c}\,d\ln A = \frac{f}{u+c}\,dx \qquad (15)$$

Oshima et al[22] arrived at the same result in a very similar way. Integration of (14) along a positive characteristic gives

$$\int_1^2 dP - \int_1^2 \frac{c}{\gamma R}\,ds + \int_1^2 \frac{uc}{u+c}\,d\ln A$$
$$= \int_1^2 \frac{f}{u+c}\,dx$$

Now differentiating with respect to X and again applying Liebnitz's rule yields

$$\frac{dP_2}{dx} - \frac{c_2}{\gamma R}\frac{ds_2}{dx} - \int_1^2 \frac{\partial}{\partial x}\left(\frac{c}{\gamma R}\right) ds + \frac{u_2 c_2}{u_2+c_2}\frac{d\ln A_2}{dx}$$

$$+ \int_1^2 \frac{\partial}{\partial x}\left(\frac{uc}{u+c}\right) d\ln A = \frac{f_2}{u_2+c_2} + \int_1^2 \frac{\partial}{\partial x}\left(\frac{f}{u+c}\right) dx$$

At this point, the authors simply state that the integral terms can be neglected in the linearized case without giving much justification as such. Although they go on to demonstrate that this in fact requires variations in area to be small, little is said about f at this stage of the analysis. However, from Rosciszewski's approach it can be seen immediately that variations in f should be small as well. Under these restrictions equation (15) is then obtained directly.

Now, by making use of the Rankine-Hugoniot relations (3) and equation (13) as well as

$$d\left(\frac{c^2}{\gamma R}\right) = \frac{2}{\gamma-1} c\,dc - \frac{dp}{\rho} \tag{16}$$

it can be shown in a straightforward way that at the shock

$$\frac{u+c}{uc}\left(\frac{dP}{dM} - \frac{c}{\gamma R}\frac{ds}{dM}\right) = \frac{2M}{(M^2-1)k(M)}$$

Therefore, equation (15) is

$$-\frac{dA}{A} = \frac{2M\,dM}{(M^2-1)\,k(M)} + \frac{f}{uc}\frac{dx}{dM}\,dM \qquad (17)$$

This, then, is the generalized form of the CCW relation. Clearly, its validity corresponds to that of the simpler case of area variations alone i.e., it is exact only for the linearized case where variations of A and f are small or the shock is very weak.

It is evident that a unique area-Mach number function ~~can not be obtained~~ by ~~integration of equation~~ ~~(17)~~ ~~despite~~ the fact that f(x,t) could be an implicit function of shock Mach number alone. This is so because the shock trajectory M(x) is not known in advance. Furthermore, the second of equations (14) offers no additional information since another unknown, η_1 is introduced.

Equation (17) also demonstrates that the effects of body forces and flux of mass, momentum and energy are equivalent to area changes. Furthermore, if A is fixed (dA=0), equation (17) can be integrated directly to give the shock trajectory if f(x,t) is specified as a function of either x or M. This approach has been employed successfully to describe shock wave attenuation in a uniformly perforated duct of constant cross section.[4,6] However, in such cases where variations in f(x,t) are finite, it is expected that equation (17) is only approximately correct for the same reasons that arose in the discussion of equation (4), namely the tendency of reflected waves generated by finite disturbances to cancel each other.

As a final note, it should be pointed out that Chester's perturbation solution is not quite correct as it is singular when the particle velocity behind the undisturbed shock is just sonic. This occurs for M=2.07 in air, for example. Friedman[57] recognized that this is a consequence of the linearization process itself by which the coefficients (u-c) are replaced by $(u_1 - c_1)$ in equations (6). For initially sonic flow, the disturbances on the negative characteristics resulting from small area changes then accumulate to finite proportions since they are stationary according to Chester's theory. In the actual case small disturbances will lead to values of (u-c) different from zero and are therefore carried away to spread out in the flow field.

This unrealistic buildup of small disturbances is remedied for the case of small area variations by linearizing all the terms in the equations of motion except those containing the coefficient (u-c). Since no difficulty is encountered along the positive characteristics or the particle paths, the arbitrary functions $G\{x-(u_1+c_1)t\}$, $H(x-u_1t)$ are retained as in Chester's theory. The solution is given in terms of a differential equation with (u-c) as dependant variable which can be integrated if the duct area variation is specified. It is shown that the solution reduces to Chester's when the initial particle velocity is far from the sonic condition. Although the details are not presented here, Friedman's analysis is noteworthy because it predicts the location and trajectory of secondary shocks which may form due to the confluence of negative characteristics in the flow field behind the incident shock wave. It should also be pointed out that the improvement of Chester's theory does not compromise any of the conclusions drawn from it in section 2.1 since Friedman's analysis is restricted to the linearized case of small area variations as well.

CHAPTER III

THE RAY-SHOCK THEORY

3.1 Formulation of the Theory

The ray-shock theory developed by Whitham[17] to describe the motion of a traveling curved shock is an approximate method which makes use of some concepts borrowed from the theory of geometrical acoustics. This is done by introducing a set of coordinates (α, β) where α represents the instantaneous shock shape and β the orthogonal trajectory of a given arbitrary point on the shock front. The latter are termed "rays" in analogy to those encountered in acoustic theory. Therefore successive positions of a moving curved shock are denoted by lines $\alpha = c_o t$ where c_o is the (constant) sound speed ahead of the shock. Thus the distance between successive shock positions α and $\alpha + d\alpha$ is $Md\alpha$. Similarly β may be chosen so that the distance between neighboring rays β and $\beta + d\beta$ is $Ad\beta$ where A is the local area bounded by the rays as shown in Figure 3.1. In the present case the flow is taken to be two-dimensional although Whitham demonstrated in a later paper[19] there is little difficulty in extending these concepts to three dimensions.

From the geometry of Figure 3.1 alone, Whitham was able to deduce that

$$\frac{\partial \theta}{\partial \beta} = \frac{1}{M}\frac{\partial A}{\partial \alpha}$$

$$\frac{\partial \theta}{\partial \alpha} = -\frac{1}{A}\frac{\partial M}{\partial \beta} \qquad (18)$$

where θ is the local inclination of the rays relative to a given direction (the x-axis, for example). Now, equations (18) contain the three dependant variables θ, M and A and Whitham reasoned that if a unique relation could be found between any two, these equations could, in principle, be solved directly for the shock positions at any instant.

Up to this point, the arguments have been purely geometric; therefore, the second relation must come from the dynamics of the shock motion. Clearly, the CCW Theory described in Chapter II provides just such a relation between A and M. Then, substitution of the general expression given by equation (17) into equations (18) and noting that $\partial/\partial x = \partial/M\partial\alpha$ yields

$$\frac{\partial \theta}{\partial \beta} + \frac{2A}{(M^2-1)k(M)}\frac{\partial M}{\partial \alpha} = \frac{Af}{uc}$$

$$\frac{\partial \theta}{\partial \alpha} + \frac{1}{A}\frac{\partial M}{\partial \beta} = 0 \qquad (19)$$

However, this approach does not appear to help much since despite the fact that the nonhomogeneous term f/uc may be an implicit function of M above, an explicit relation between A and M is still needed to solve the equations. On the other hand if the function f(x,t) describing the external mass, momentum and energy flux is zero or small enough to be neglected then A can be considered a function of M alone given by direct integration of the simpler form of the CCW relation equation (4).

$$A = F(M) = k\, e^{-\int \frac{2M\,dM}{(M^2-1)K(M)}} \tag{20}$$

Then equations (19) become

$$\frac{\partial\theta}{\partial\beta} - \frac{F'(M)}{A(M)}\frac{\partial M}{\partial\alpha} = 0 \tag{21}$$

$$\frac{\partial\theta}{\partial\alpha} - \frac{1}{A(M)}\frac{\partial M}{\partial\beta} = 0$$

According to the discussions of the CCW theory presented in Chapter II, it can be seen that the use of the CCW relation renders the ray-shock theory to be quite approximate for several reasons. First of all, it has been demonstrated that the CCW relation is approximate to begin with, and the use of the integrated form only increases the degree of approximation. More important, the rays are not streamlines although they do coincide with the streamlines just at the shock front but not behind. Therefore, in general, the function f(x,t) is not zero and one can only hope that it can be neglected. However, if, in a particular problem, only purely convective effects were considered, f(x,t) would be identically zero just at the shock.

In the more general situation where there are body forces, radiation or turbulent mixing, for example, this would not be the case.

Thus the ray-shock theory treats the rays as solid boundaries and ignores any mass, momentum or energy flux across them. Furthermore, the use of the integrated area-Mach number relation is equivalent to neglecting any reflected disturbances which may arise from area variations alone; although, as was noted earlier, this approximation may be justified for converging shocks. Also, the CCW relation is the result of an essentially one-dimensional theory. Fortunately, this limitation may be alleviated somewhat by the fact that the ray tubes can be made arbitrarily small.

Solution of the non-homogeneous equations is not entirely out of the question as was demonstrated by Oshima and his associates in their study of shock diffraction around a corner.[22] For this problem turbulent mixing across the ray tube boundaries was included by making use of the Prandtl mixing length hypothesis to compute the turbulent shear stress. While this analysis ignores mass and energy transport effects, it is a positive step towards a more general solution of the problem. The essence of the theory is that the effects of turbulent mixing are assumed to be small compared to those due to area changes so that equations (19) can be linearized. The zero order solution is then just the solution of the homogeneous equations (21). However, the non-homogeneous term in the first order equation is rather complicated, containing derivatives of M up to second order. In order to obtain a solution Oshima made a further assumption that all dependant variables are functions of a single similarity parameter β/α. The final result is then the sum of the zero and first order solutions.

Thus Oshima's solution is somewhat limited. In addition, introduction of the mixing length hypothesis brings a new unknown (the mixing length) into the problem which must be determined by experiment. Therefore the results are not generally applicable. In spite of its deficiencies, the method is valuable as it sheds some light on possible entensions to Whitham's analysis.

With the preceding remarks in mind, the ray-shock theory is formulated on the basis of the homogeneous equations (21) which are quasi-linear first order relations. Whitham showed that these could be conveniently solved by the method of characteristics. In characteristic form they are

$$\left(\frac{\partial}{\partial \alpha} \pm C \frac{\partial}{\partial \beta} \right) (\theta \pm \omega) = 0$$

where it can be shown that

$$C = \pm \frac{d\beta}{d\alpha} = \sqrt{-\frac{M}{A} \frac{dM}{dA}} \tag{22}$$

and

$$\omega = \int \frac{dM}{AC} \tag{23}$$

Therefore, along the respective characteristics $C^{\pm}$ the characteristic invariants are

$$\theta \pm \omega = \text{constant} \tag{24}$$

where the positive sign corresponds to the positive characteristics.

For the case of a simple wave where one family of characteristics originates in a region of uniform state, it is possible to deduce from equations (22), (23) and (24) that the other family of characteristics are straight lines in the (α, β) plane, and furthermore that θ and M are constant along them as well. This turns out to be a very convenient property as integration along the characteristics is greatly facilitated in this case. It appears that most cases it is easier to work in the (x, y) rather than the (α, β) plane and it is convenient to introduce the characteristic angle m which is defined as the angle between the characteristic and ray directions. From Figure (3.2) it is easily seen that

$$\tan m = \frac{A\,d\beta}{M\,d\alpha} = \frac{Ac}{M} \tag{25}$$

and the equations describing the characteristics in the physical plane are then

$$C_+ : \quad \frac{dy}{dx} = \tan(\theta + m) \tag{26}$$

$$C_- : \quad \frac{dy}{dx} = \tan(\theta - m)$$

Thus simple waves are straight lines in the (x, y) plane as well.

Now, in most problems the object is to determine the shock shape at various instants. From examination of Figure 3.2 it can be seen that this can be accomplished in several different ways i.e., by integration along characteristics, rays, or along the shock. Noting that the component of $M d\alpha$ along a C+ is $M d\alpha/\cos m$ and that the components of this quantity in the x and y directions respectively are $M \cos(\theta + m)\, d\alpha/\cos m$ and $M \sin(\theta + m)\, d\alpha/\cos m$. The coordinates of the shock front (X_s, Y_s) are

$$x_s = x_0 + \int_{\alpha_0}^{\alpha_s} \frac{M \cos(\theta + m)}{\cos m}\, d\alpha$$
$$y_s = y_0 + \int_{\alpha_0}^{\alpha_s} \frac{M \sin(\theta + m)}{\cos m}\, d\alpha \qquad (27)$$

where (X_0, Y_0) are the initial coordinates of the characteristic and α_0 is the corresponding time at which the point (X_s, Y_s) occupied the position (X_0, Y_0). Integrating along the shock and noting that $dx = -(A d\beta) \sin\theta$, $dy = (A d\beta) \cos\theta$,

$$x_s = \bar{x} - \int_{\bar{\beta}}^{\beta_s} A \sin\theta\, d\beta$$
$$y_s = \bar{y} + \int_{\bar{\beta}}^{\beta_s} A \cos\theta\, d\beta \qquad (28)$$

where $\bar{x}$, $\bar{y}$ and $\bar{\beta}$ are evaluated at the boundary along which the shock propagates.

Before turning to specific applications of the ray-shock theory, it is convenient to write out the expressions for certain parameters such as c, ω, etc. which will be used later. However, a difficulty arises when the CCW relation is substituted into equation (22) for $c(M)$ in that the expression is not readily integrated and Whitham gave the exact results only for the limiting cases where $K(M)$ approaches a constant value namely

$$M \rightarrow 1,\ K(M) \rightarrow 1/2\ ;\quad M \rightarrow \infty,\ K(M) \rightarrow .395$$

Neither of these cases is appropriate for the present problem therefore they will not be discussed further. Instead, since $K(M)$ is a slowly varying function of M over most of it's range (see Figure 2.2) an obvious simplification is to consider $K(M)$ a constant and use an average value in a given situation. It should be pointed out, however, that this simplification could lead to significant error if applied over a large shock Mach number interval, especially for $1 < M < 2$. Thus, this approach is not expected to yield good results for the diffraction of a moderate strength shock around a convex corner with large turning-angle, for example. For the present problem however, it will be shown later that the approximation is justified.

Then for $K(M) \simeq$ constant and defining $n = 2/K$. The following relations are easily derived

$$\frac{A(M)}{A_0} = \left(\frac{M^2-1}{M_0^2-1}\right)^{-\frac{1}{2}} \tag{29}$$

where A_0 is the area corresponding to the undisturbed shock Mach number M_0. For convenience, A_0 is taken to be unity so that the other parameters become

$$Ac = \sqrt{\frac{M^2-1}{n}}\,, \qquad A_0 = 1$$

$$c(M) = \frac{1}{\sqrt{n}}\,\frac{(M^2-1)}{(M_0^2-1)^{\frac{1}{2}}} \tag{30}$$

$$\omega(M) = \sqrt{n}\int_{M_0}^{M}\frac{dM}{\sqrt{M^2-1}}$$

$$= \ln\left(\frac{M+\sqrt{M^2-1}}{M_0+\sqrt{M_0^2-1}}\right)^{\sqrt{n}}$$

$$\tan m = \frac{1}{M}\sqrt{\frac{M^2-1}{n}}$$

In addition to these, for the case of a simple wave where the C- characteristics originate in a region where $M = M_0$, $\theta = \theta_0 = 0$

$$\theta(M) = \omega(M) = \ln\left(\frac{M+\sqrt{M^2-1}}{M_0+\sqrt{M_0^2-1}}\right)^{\sqrt{n}} \tag{31}$$

$$= \sqrt{n}\left(\cosh^{-1}M - \cosh^{-1}M_0\right)$$

3.2 Application to Shock Diffraction and Mach Reflection

Diffraction of an initially planar shock by both concave and convex corners has been examined by Whitham[17] in detail so the theory will be discussed only briefly here.

For the case of diffraction at a convex corner formed from the intersection of two planes, the simple wave situation discussed earlier exists and one family of characteristics is simply a fan composed of straight, radial lines centered at the corner. This is shown in Figure 3.3. Each characteristic carries a constant value of θ and M and corresponds to the appearance of acoustic waves in the physical plane which spread out and perform the modification of the shock. In fact, the characteristic lines are just the paths of the intersection of each acoustic wave with the shock. The path of the head characteristic is given by equation (30).

$$\tan m_0 = \frac{1}{M_0}\sqrt{\frac{M_0^2-1}{n}} \tag{32}$$

where M_0 is the undisturbed shock Mach number.

Now, the shock shape can be calculated by integration along characteristics (equation 27) and the shock (equation 28) or along rays instead. For the present work, the former method is chosen as it is simplest and the development for moderate strength shocks will be presented in section 3.3. For the diffraction of a very strong shock Whitham chose the latter method and found that the shock shape is given universally in terms of the similarity parameters $X/\alpha M_0$ and $Y/\alpha M_0$.

The approximate nature of the ray-shock theory is demonstrated by the fact that for a given shock Mach number there exists a limiting value of the turning angle θ_w, which corresponds to a wall shock Mach number M_w that is just unity.

$$\theta_{max} = \int_{M_0}^{1} \frac{dM}{Ac} \tag{33}$$

Beyond θ_{max}, no solution exists for a given M_0. This limitation can be quite restrictive at low initial shock Mach numbers. For example, at $M_0 = 1.2$, $\theta_{max} = 72.5$ according to Whitham's weak shock relations.

Experimental evidence indicates that neither equation (32) nor equation (33) is accurate for low or even moderate shock Mach numbers. For the diffraction problem illustrated in figure 3.3 the head of the expansion wave is (theoretically) cylindrical with a radius of $c_1 t$ and center located a distance $u_1 t$ from the corner, a result which is confirmed by experiment[58]. Therefore, it is a simple matter to show from (3) that theoretically[14,20]

$$\tan^2 m_0 = \frac{(M_0^2-1)\left[2+(\gamma-1)M_0^2\right]}{(\gamma+1)M_0^4} \tag{34}$$

From his experiments, Skews[20,29] demonstrated that equation (34) is indeed correct and that considerable error results if equation (32) is used for $M_0 < 3$. In fact, equations (32) and (34) do not converge to the same result until $M_0 \simeq 5$ as shown in Figure 3.4. These results imply that the ray-shock theory will likely not accurately predict the characteristic angle m (equation (30)) at any arbitrary location on the diffracted shock as well. This fact is particularly important when constructing the wave diagram for the present problem and will be discussed later in section 3.4.

Skews experiments further show that equation (33) is unrealistic. Schlieren photography[20] demonstrates that a finite shock strength is observed at $M_0 = 1.2$ for all corner angles tested (up to nearly 180^0) while the theory breaks down at $\theta = 72.5^0$ as noted above. Skews concludes that in general the ray-shock theory is adequate for all shock Mach numbers if the corner angle is less than about 30^0. For large corner angles, good agreement with the theory is observed only for $M_0 > 3$. These results graphically illustrate the approximate nature of the ray-shock theory in general.

The case of shock diffraction by a simple concave corner usually corresponds to the well known phenomenon of Mach reflection. However, if the corner angle exceeds a certain critical value (which depends on the undisturbed shock Mach number M_0 and is usually relatively large) regular reflection may be observed. The Mach configuration is characterized by the confluence of three shocks: The incident, reflected and the so called "Mach stem". The point of confluence, which is often referred to as the "triple point", lies some distance away from the wall and experimental evidence indicates that, for the two-dimensional case which is being considered here, the triple point follows a straight line path from the corner. For subsonic particle velocity behind the incident shock, the reflected shock has a somewhat cylindrical shape which allows it to propagate upstream as well as downstream. Otherwise, the reflected shock will face downstream with a straight segment attached to the corner. The Mach stem, which extends from the triple point to the wall, is usually taken to be straight although experiments have shown that this is not necessarily the case, particularly in the region surrounding the triple point. Since part of the gas ahead of the advancing shock wave system is processed by two shocks (incident and reflected) and part by only one shock (the Mach stem) a slip line forms in the flow field behind the Mach configuration. The situation is shown diagramatically in Figure 3.5.

Analysis of the Mach reflection configuration by the ray-shock theory is relatively simple if it is assumed that both the incident shock and Mach stem are straight over their entire length. Application of the ray-shock theory, however, precludes the acquisition of any information concerning the reflected shock. Now the triple point is just the "shock-shock" in Whitham's parlance and from his analysis it was shown that the shock-shock velocity $C = \Delta\beta/\Delta\alpha$ in the (α, β) plane is

$$C^2 = -\frac{M^2 - M_0^2}{A^2 - A_0^2} \tag{35}$$

where M_0, A_0 and M, A refer to the incident shock and Mach stem respectively. Now from the geometry given in Figure (3.5), if $\beta=0$ is taken to represent the wall and time is measured from the instant at which the incident shock reaches the corner, the coordinates of the triple point are (α, β) so that the angle χ representing the path of the triple point is given by

$$\tan\chi = \beta A/M\alpha = \frac{AC}{M}$$

From this Whitham was able to deduce that

$$\tan\chi = \frac{A}{A_0}\sqrt{\frac{1-(M_0/M)^2}{1-(A/A_0)^2}} \tag{36}$$

$$\tan\Theta = \frac{\sqrt{(M^2 - M_0^2)[1-(A/A_0)^2]}}{M_0 + M(A/A_0)} \tag{37}$$

Thus by making use of the CCW relation between area and shock Mach number these equations can be solved to give χ and M for a given corner angle θ and incident shock Mach number M_0.

Calculations were carried out by Whitham using the strong shock relation equivalent to equation (29) and it was found that the predicted values of the triple point locus angle χ were somewhat greater than those given by the conventional three shock theory. Both theories show that χ decreases rapidly as θ is increased.

Again, the approximate nature of the ray-shock theory is revealed by comparison of the above relations with experimental results. Milton[33], using a fairly accurate approximation to the Chester function K(M), compared the ray-shock theory to a compendium of experimental results for M_0 = 1.51 and 1.42 which is reproduced in Figures 3.6 and 3.7. From these, it can be seen that the ray-shock theory tends to overestimate χ somewhat for deflection angles θ greater than around 20^0. However, for lower θ the agreement is not good at all for M_0 = 1.51 and fair for M_0 = 2.42. The experiments correctly show that as θ approaches zero and the reflected shock strength diminishes to that of an acoustic wave, χ approaches the value given by the acoustic relation (34). The ray-shock theory however is seen to underestimate this value by about 50% and 20% for M_0 = 1.51 and 2.42 respectively. This error undoubtably results from the inability of the ray-shock theory to correctly predict the (acoustic) characteristic angle m as was noted earlier in the discussion of equation (32). Thus it is concluded that the ray-shock theory does not accurately predict the triple point locus angle χ for moderate to weak incident shock strengths.

Fortunately the situation is better with regard to the stem shock Mach number M as demonstrated in Figure 3.8 which again shows the result of Milton's calculations. From these results it can be concluded from equation (37) that for moderate strength shocks the ray-shock theory yields an acceptable estimate of the stem shock Mach number if the corner angle is not too large.

In view of the above discussion it is evident that the ray-shock theory should be applied cautiously to shock diffraction and reflection problems particularly if the shock Mach number is less than about 3.0. In spite of this, the evidence suggests that under certain conditions the ray-shock theory may lead to acceptable results. In the next section it will be reasoned that the present problem falls into this category.

3.3 Application to the Present Problem

Before proceeding with the details of the mathematical analysis it is worth considering again the nature of the problem. In this way the limitations of the ray-shock theory as they apply to the present problem can be better understood.

The situation is depicted in Figure 3.9 which shows an initially planar shock wave propagating down a channel having a uniform rectangular cross section of height h. At the location x = 0 the shock encounters a slit of width ℓ and is subsequently diffracted around the edge of the slit. The channel wall is assumed to be very thin so that the corner angle is essentially 360^0 and viscous effects do not play a large role in the formation of the fluid jet which emerges from the slit at some angle θj. Upon encountering the downstream edge of the slit the diffracted shock is reflected and unless the incident shock strength is very great, the Mach configuration will occur which then propagates downstream along with the expansion wave generated by the initial diffraction process. As noted in Chapter I, multiple reflections will occur within the slit ~~until the~~ fluid jet is fully formed.

Now, the presence of the upper wall at y = h plays a fundamental role in the subsequent motion. If no wall were present the disturbance produced by the slit would continue to propagate along the traveling shock essentially unchanged and the motion would eventually become self-similar once the fluid jet from the slit is fully developed and the incident shock is far away. The Mach stem which is in contact with the lower wall would then propagate at a uniform velocity indefinitely. However, if the upper wall is present, the disturbance reflects from it and eventually returns again to the lower wall where it then modifies the Mach stem. Thus in this case, the Mach stem undergoes a decleration in finite jumps, the frequency of which depends on the channel height h and the incident shock Mach number M_0. This behavious continues until the disturbance is so diffused by multiple reflections and viscous action that the attenuation process becomes essentially continuous but very gradual i.e., asymptotic.

For the present investigation, only the wave motion within the duct or in the immediate vicinity of the slit will be considered. Attenuation will be focused primarily on the internal shock attenuation and viscous effects will not be considered so that it is expected that the analysis will adequately describe only the initial stages of the attenuation process. This limitation is not considered restrictive since only this phase of the process is of practical interest.

With these concepts in mind, the ray-shock theory can now be employed to describe the attenuation process. As noted in previous sections the theory itself is quite approximate. Nevertheless, it should, at the very least, provide a qualitative description of the wave interaction phenomena.

According to the theory the initial diffraction of the incident shock wave corresponds to a simple wave in the (α, β) plane and the positive characteristics are straight lines centered at the upstream edge of the slit which is taken as the origin of coordinates. In the physical plane the C+ characteristics are also linear with slopes given by equation (26). As noted in section 3.1, local shock Mach number M and ray orientation θ are constant along each C+ in this case. This means that the local shock Mach number and inclination of the wave approaching the downstream edge of the slit is always the same regardless of the slit width ℓ. Thus the stem shock Mach number just downstream of the slit is also independent of ℓ, i.e., the initial attenuation does not depend on the slit width. However, the attenuation rate further downstream does depend on the slit width since this is governed by the wave interactions. Increasing the slit width tends to shift upstream the point where the head of the reflected expansion wave arrives at the lower wall and thus contributes to greater attenuation rates. This fact will become more obvious after construction of the wave diagram. The important point is that according to the ray-shock theory the slit width ℓ provides only a secondary effect on the overall shock attenuation.

At this point some remarks concerning the expected accuracy of the ray-shock analysis of the present problem are in order. The theory is applied in the following rather straight forward way. The relations appropriate to the diffracted shock can be solved directly for M and θ

along any of the C+ characteristics indicated in Figure 3.9. In particular, the solution is sought along the positive characteristic which coincides with the X axis as this gives the local M and θ just prior to the Mach reflection process at the downstream edge of the slit. Since the Mach stem after reflection must be normal to the wall at its foot, the effective corner angle is just the θ found previously. This information is then sufficient to allow solution of the Mach reflection relations for the stem shock Mach number. The subsequent wave interactions are found by construction of the wave diagram.

Now, it was noted in the previous section that for moderate strength shocks the ray-shock theory yields acceptable predictions of the stem shock Mach number if the corner angle is not too large. For the present problem, most of the diffraction occurs outside the duct therefore it appears that this condition can be met since only the internal flow will be considered. That the internal portion of the shock does not become excessively curved for moderate strength shocks can also be deduced from the diffraction equations. This is not the case for very strong incident shocks, however. Unfortunately, the situation is not as optimistic with regard to the triple point locus angle χ or the characteristic angle m. For moderate strength shocks neither parameter is expected to be predicted accurately. However, the former fortunately does not enter into the initial attenuation calculation and the latter can always be computed from the acoustic relation, Eq. (34). Thus it appears that the ray-shock theory can be applied to the present problem with some degree of confidence despite the fact that only moderate strength shocks will be considered. In addition, the Chester function K(M) can probably be taken as a constant since large variations in M are not expected to exist along that portion of the diffracted shock which remains inside the duct.

As noted above, the mathematical analysis is straightforward. Time is measured from the instant the undisturbed shock reaches the upstream edge of the slit so that $\alpha = 0$ there. The subscript (*) is used to denote conditions at that location on the diffracted shock which just comes into contact with the downstream edge of the slit i.e., $\alpha = \alpha^*$ at that instant. Since the simple wave conditions hold along the C+ characteristics (M, θ and m are constant along them) integration of equations (27) gives directly

$$x = M \frac{\cos(\theta + m)}{\cos m} \alpha$$

$$y = M \frac{\sin(\theta + m)}{\cos m} \alpha$$

In particular, the solution is sought along the characteristic which coincides with the X axis, hence setting y = 0 yields

$$\theta_* = - m(M_*) \qquad (38)$$

and setting $X = \ell$ at $\alpha = \alpha^*$. The other relation gives

$$\frac{\ell}{\alpha_*} = \frac{M_*}{\cos m(M_*)}$$

and making use of equation (30) for $K(M)$ = constant

$$\frac{\ell}{\alpha_*} = \sqrt{\frac{(n+1)M_*^2 - 1}{n}} \tag{39}$$

Since α^* is unknown this equation can not be solved for M^* just at the downstream edge of the slit. However, another relation between α^* and M^* ~~is~~ obtained by integrating along the shock. Since the undisturbed portion of the incident shock travels a distance $X^* = M_0\alpha^*$ when contact is just made with the downstream edge, equation (28) gives (taking $\beta = 0$ where $M = M_0$)

$$\frac{\ell}{\alpha_* M_0} = 1 - \frac{1}{M_0\alpha_*}\int_0^{\beta_*} A \sin\Theta \, d\beta \tag{40}$$

Now along any C+ characteristic $c = \beta/\alpha$ so $d\beta = \alpha^* dc$ along the shock at $t = t^*$. Hence

$$A\,d\beta = \alpha_* A\,dc$$

and if $K(M)$ is assumed to be constant at some suitable average value making use of equations (29) and (30) leads to

$$A\,d\beta = \frac{n+1}{\sqrt{n}}\,\alpha_*\,\frac{M\,dM}{\sqrt{M^2-1}}$$

so that equation (40) is

$$\frac{l}{\alpha_* M_0} = 1 - \frac{n+1}{\sqrt{n}\,M_0}\int_{M_0}^{M_*}\frac{M}{\sqrt{M^2-1}}\,\mathrm{Sin}\,\theta\,dM$$

Again noting that the simple wave conditions hold, θ is eliminated by making use of equation (31). Making the substitution

$$Z = \mathrm{Cosh}^{-1} M$$

The above relation becomes

$$\frac{l}{\alpha_* M_0} = 1 - \frac{n+1}{\sqrt{n}\,M_0}\,\mathrm{Cos}\,\sqrt{n}\,Z_0\int_{Z_0}^{Z_*}\mathrm{Sin}\,\sqrt{n}\,Z\,\mathrm{Cosh}\,Z\,dZ$$

$$+ \frac{n+1}{\sqrt{n}\,M_0}\,\mathrm{Sin}\,\sqrt{n}\,Z_0\int_{Z_0}^{Z_*}\mathrm{Cos}\,\sqrt{n}\,Z\,\mathrm{Cosh}\,Z\,dZ$$

Integration by parts and simplification gives the final result

$$\frac{l}{\alpha_*} = \sqrt{\frac{M_{*0}^2-1}{n}}\,\mathrm{Sin}\,\phi_* + M_*\,\mathrm{Cos}\,\phi_* \qquad (41)$$

where

$$\phi_*(M_0, M_*) = \sqrt{n}\, \ln\left(\frac{M_0 + \sqrt{M_0^2 - 1}}{M_* + \sqrt{M_*^2 - 1}}\right)$$

Therefore equating (39) and (41) leads to a single equation for M*

$$\sqrt{\frac{M_*^2 - 1}{n}}\, \sin\left[\sqrt{n}\, \ln\left(\frac{M_0 + \sqrt{M_0^2 - 1}}{M_* + \sqrt{M_*^2 - 1}}\right)\right]$$

$$+ M_* \cos\left[\sqrt{n}\, \ln\left(\frac{M_0 + \sqrt{M_0^2 - 1}}{M_* + \sqrt{M_*^2 - 1}}\right)\right] - \sqrt{\frac{(n+1)M_*^2 - 1}{n}} = 0 \qquad (42)$$

Since this is a rather complicated transcendental equation it is best solved by iteration. At the same time the iteration for n = 2/K can be conveniently included. However, it turns out that M* has a double root so that the usual techniques (such as regula falsi or the secant method) do not converge well. This difficulty can be easily overcome when it is realized that under the conditions of a double root the solution of F(M*) = 0 is also given by solution of

$$\frac{d}{dM_*} F(M_*) = 0$$

Therefore, the equation to be solved is

$$[\text{illegible}]$$

$$[\text{illegible}] \qquad (43)$$

$$-2(\gamma-1)M_* \sqrt{\frac{M_*^2-1}{(\gamma+1)M_*^2-1}}\left(M_*+\sqrt{M_*^2-1}\right) = 0$$

and this equation is easily solved for M^* by conventional iteration methods. Once M^* is computed, θ^* is calculated from equation (31). The shape of the diffracted shock could be computed for any instant of time by a similar approach.

Once M^* and θ^* are known, the Mach reflection equations can be solved for the stem shock Mach number M. The idealized situation which is taken to represent the local conditions just at the downstream edge of the slit is shown in Figure 3.10. Such a representation appears to be justified by the fact that the effect of the diffracted shock curvature can be later accounted for by construction of the wave diagram. Thus Figure 3.10 is taken to represent the actual situation just at the instant reflection begins and is the correct one locally. The calculation of M is therefore not compromised provided it is kept in mind that M corresponds to the stem shock Mach number at its foot.

Again taking $K(M)$ to be constant at some average value and recalling that $\theta^* = -m(M^*)$ equation (30) gives

$$\tan\theta_* = -\tan m(M_*) = \frac{-1}{M_*}\sqrt{\frac{M_*^2-1}{M}}$$

and equation (29) is

$$\frac{A_y}{A} = \left(\frac{M_y^2-1}{M_i^2-1}\right)^{-\frac{1}{2}}$$

Therefore if both these relations are substituted into equation (37) a single equation is obtained M alone. The result is

$$\left(M^2 - M_i^2\right)\left[1 - \left(\frac{M_i^2-1}{M^2-1}\right)^n\right] - \frac{M_i^2-1}{n_1}\left[1 + \frac{n}{n_i}\left(\frac{M_y^2-1}{M_i^2-1}\right)^{\frac{n}{2}}\right] = 0 \qquad (44)$$

As before, this equation can be solved by iteration for M and the iteration for n = 2/K is easily incorporated into the scheme.

This completes the solution for the initial attenuation of the incident shock wave. As noted earlier, M will remain constant (neglecting viscous attenuation) until the expansion wave reflects from the upper wall and returns to the lower wall to further attenuate the shock. However, arrival of the reflected shock in a similar manner a short time later tends to undo any gain in attenuation. The solution for M given by equation (44) is then likely to provide a good estimate of the stem shock Mach number for some distance downstream of the slit. How good this approximation is depends upon the wave interactions themselves. These are examined via a wave diagram, the details of which are discussed in the next section.

3.4 The Wave Diagram

Construction of the wave diagram is important in the present problem because this is virtually the only convenient way by which the wave interactions can be analyzed. Using this method the additional attenuation of the shock some distance downstream of the slit can be estimated. It should be realized, however, that since the characteristic relations come from the ray-shock theory, the method is quite approximate for the reasons discussed earlier. The fact that the flow field behind the travelling shock is neglected in the analysis becomes quite evident during the construction. Only the intersection of the expansion wave and the reflected shock with the main shock is considered and the wave diagram is nothing more than the computed trajectories of these points. The trajectory of the triple point is, of course, the "shock-shock" described by Whitham and its role in the wave diagram is exactly analagous to that of a shock wave in the more familiar case of unsteady one-dimensional gas flow. In other words, the shock-shock represents a discontinuity, not only to the physical flow field but to the characteristics as well. The change in the characteristic invariants as the characteristics cross the shock-shock is then described by the Mach reflection relations given in the last two sections.

A sketch of the wave diagram for the internal flow in the present problem is shown in Figure 3.11. From this it can be seen that there are four types of interactions to be considered. These are (1) crossing of characteristics of opposite family, (2) reflection of characteristics from a solid boundary, (3) crossing of the shock-shock characteristics of either family and (4) shock-shock reflection from a solid boundary.

The first two cases are easily handled in the usual way by making use of the characteristic invariants

$$\begin{aligned} P &= \Theta + \omega = \text{CONSTANT ALONG } C+ \\ Q &= \Theta - \omega = \text{CONSTANT ALONG } C- \end{aligned} \qquad (45)$$

Usually, two of the four variables in the relations are known so it is a simple matter to solve for the other two. For the case of crossing characteristics, P and Q are usually known.

For reflection of characteristics from a solid boundary the characteristic invariant along the incident characteristic is known as is the wall direction θ_w. Hence adding equations (45)

$$P + Q = 2\,\Theta_w$$

at the point of reflection. For the present problem since $\theta = 0$ along either wall,

$$Q = -P \qquad \begin{cases} y = 0 \\ y = h \end{cases} \qquad (46)$$

Interactions involving shock-shocks are more complicated as the characteristic invariant P or Q changes discontinuously across them. Thus the characteristic slopes downstream of the shock-shock are unknown, since θ and M are unknown there. However, if $\Delta\theta$ across the shock-shock is chosen, the Mach reflection relations can be used to compute M so it is possible to develop an iteration scheme if another relation between M and θ can be found.

Milton[33] has suggested such a scheme. Consider the case where two neighbouring C- characteristics cross the shock-shock as illustrated in Figure (3.11). It is assumed that the solution for the first interaction (1) has already been completed so that M_1, θ_1, M_1' and θ_1' are known where primes indicate quantities downstream of the shock-shock. Also, it is assumed that M_2 and θ_2 are known on the upstream side of the neighbouring interaction (2) either by computation or interpolation of the characteristic net. It is desired to find θ_2', M_2'.

Now, downstream of the shock-shock the Mach stem, which is assumed to be locally straight, will have a different orientation on characteristics 1' and 2'. Thus the effect of the characteristic intersections with the shock-shock is to bring about a curvature of the Mach stem. Since the characteristic mesh is finite, the curved Mach stem is represented by a series of straight line segments connected together. The point of connection appropriate to two neighbouring characteristics then follows some path in the flow field. Furthermore, since it is characteristics themselves which carry the disturbances, it is logical to assume that for a finite characteristic mesh this path, called a contiguity line, is simply the average of the two neighbouring characteristic slopes.

For the case under consideration (C- characteristics) the contiguity direction is (relative to the X axis)

$$\psi = \frac{1}{2}\left[(\theta_1' - \mu_1') - (\theta_2' - \mu_2')\right]$$

Equating the components of the two shock velocities in this direction gives

$$\frac{M_1' \, d\alpha}{\cos(\psi - \theta_1')} = \frac{M_2' \, d\alpha}{\cos(\psi - \theta_2')}$$

hence for C- characteristics

$$\frac{M_2'}{M_1'} = \frac{\cos \frac{1}{2}(\theta_1' - \theta_2' - \mu_1' - \mu_2')}{\cos \frac{1}{2}(\theta_2' - \theta_1' - \mu_2' - \mu_1')} \qquad (47)$$

The iteration is simple. Choose $\Delta\theta_2 = \theta_2' - \theta_2$ and compute M_2' from the Mach reflection relations. This value is compared with that computed from equation (47) and if they don't agree, a new $\Delta\theta$ is assumed.

For the case where positive characteristics cross the shock-shock it is a simple matter to derive the analogous relation to equation (47)

$$\frac{M_2'}{M_1'} = \frac{\cos\frac{1}{2}(\theta_1' - \theta_2' + m_1' + m_2')}{\cos\frac{1}{2}(\theta_2' - \theta_1' + m_1' + m_2')} \qquad (48)$$

It should be pointed out that there is no difficulty evaluating the very first interaction 1-1' since θ_1' is known in that case to be equal to $\theta_w = 0$ as the Mach stem is taken to be straight and normal to the wall initially. The same holds true after reflection of the shock-shock from either wall.

Shock-shock reflection from a solid boundary is easily handled when it is recognized that the incident shock and Mach stems simply interchange positions in the three shock configuration. In this case since the new Mach stem is again normal to the wall, the $\Delta\theta$ for the shock-shock reflection is then θ_2', the Mach stem orientation just prior to the reflection process. The "incident" shock Mach number is M_2'. This information is sufficient to allow determination of the new stem shock Mach number from the Mach reflection equations.

From the above relations the wave diagram is then constructed step by step. To start it, the simple wave corresponding to the initial shock diffraction through the slit is constructed by arbitrarily choosing suitable values of M between M_0 and M*. Since Q is known from the upstream conditions, P and θ can then be computed for each of the chosen C+ characteristics. Also, the initial stem shock

Mach number is known from the analytical solution so the initial shock-shock trajectory is also known.

Since the wave diagram construction involves iteration at the shock-shock points, it is perhaps easiest to use graphical methods for all the calculations. For such purposes curves of χ vs. $\Delta\theta$, and M/M_0 vs. $\Delta\theta$ constructed from the ray-shock theory and are presented in Figures (3.12) and (3.13) for various incident shock Mach numbers M_0. Also, it was found convenient to use graphs instead of numerical computation of the characteristic angle m(M) and ω(M). These are shown in Figures (3.4) and (3.14). The latter was calculated for $M_0 = 1.4$ which was the incident shock Mach number chosen for the wave diagram construction. It was noted earlier, however, that the ray-shock theory does not appear to predict the shock-shock angle χ very accurately. Thus the actual values given by Figures (3.12) were not used for the wave diagram construction; they were corrected by an empirical relation. The exact form of this relation will be given later in Chapter V, after the experimental results have been discussed.

CHAPTER IV

EXPERIMENTS

4.1 Experimental Apparatus

A simple air/air shock tube with a square cross section 2.06 X 2.06 inches was employed for all tests. This apparatus was constructed from seamless structural steel tubing with a 1/4 inch wall thickness and consisted of a driver section five feet long followed by a driven section of equal length which was in turn followed by a shorter test section in which all measurements were performed. The comparatively long driver section was chosen to ensure that neither the contact surface nor the expansion wave originating at the diaphragm would enter the test section until long after the events of interest had been completed. Mylar plastic sheets of 1, 2 and 5 mil thicknesses were used as the diaphragm material. A schematic of the shock tube facility is presented in Figure 4.1.

Tests were performed with the driven section both at atmospheric conditions and in partial vacuum so two different test sections capable of permitting schlieren viewing were built. The first (designated "A") was constructed by simply milling away a 5 inch segment on two opposite walls of a 17.5 inch length of tube to expose the interior. Plexiglass plates 1/2 inch thick were then clamped over the opening, being sealed with rubber gaskets. These were extended well above the slit in order to preserve the two-dimensional nature of the external flow field. A 0.275 inch slit was milled in one of the remaining walls and externally chamferred at 30^0 to simulate a thin wall tube. In this way the structural integrity of the test section was not compromised. A schematic of test section A is given in Figure 4.2 (a).

The second test section (designated "B") was constructed in a similar manner to also provide a 5 inch view of the internal flow field. However, in this case the entire segment of the tube was enclosed so that it could be evacuated. In addition, the upper wall (which contains the slit) was constructed of removable flanges so that the slit width could be varied. A 10^0 external slit chamfer was used in this case. Ordinary plate glass side walls were used for schlieren viewing. The shock tube was extended 20 inches past the test section so that pressure measurements well downstream of the slit could be performed. The details are shown in Figure 4.2 (b).

Photographic studies were carried out in both test sections using a time delayed spark schlieren optical system which was triggered by a pressure transducer located just upstream of the test section. The trigger pulse was divided so that a pulse was also sent simultaneously to trigger an osilloscope beam. In addition, the output pulse from the capacitive time delay unit was divided so that one high voltage pulse was sent to fire the spark unit and another was sent to the vertical input terminals of the oscilloscope. In this way the actual time delay was measured. The high voltage (11 kv) spark was used as a light source for a conventional double mirror schlieren optical system using 48 1/2 inch focal length mirrors. The system magnification was roughly 80% and all photographs were recorded on 3000 ASA Polaroid Film (Type 47).

The pressure measurements were accomplished with "home made" piezoelectric pressure transducers utilizing a 1/4 inch barium titanate piezo-element bonded by silver epoxy to a zinc rod which serves to delay reflection of acoustic waves from the end of the element. The entire element-rod combination is encased in rubber to minimize the effects of mechanical vibration and housed in a 1/2 inch threaded brass tube.* This gauge was found to have a poor rise time and short time constant but the output was sufficiently high to allow it's use as a shock detector. For this reason, no charge amplifier was used in conjunction with this type of gauge.

Shock velocity measurements were performed by employing the transducers in groups of three with the first transducer used to trigger an oscilloscope (Tektronix Model 555) beam.

---

*The transducers were designed and constructed by Prof. R. Knystautas of the Shock Wave Physics Group of the Department of Mechanical Engineering and the author is indebted to him for the loan of these devices.

The following two gauges were connected to the input terminals of the oscilloscope vertical deflection plates. Knowing the transducer spacing and the oscilloscope time scale, shock velocities were easily computed from the oscilloscope traces which were recorded on Polaroid film. For the present tests, trigger transducers were always located 2 inches upstream of the first pickup transducer and a transducer spacing of 4 inches was employed for all shock velocity measurements.

4.2 Experimental Procedure

All tests were performed with air as the working fluid. Compressed air was supplied from a storage tank filled by a reciprocating compressor. In the 55-310 psig driver pressure range shock Mach numbers between 1.17 and 1.67 were obtained with the driven section at atmospheric pressure. In order to obtain higher shock Mach numbers the driver section was evacuated with a vacuum pump to pressures as low as 29.2 inches Hg (vacuum) and driver pressures up to 100 psig were simultaneously employed. This procedure yielded shock Mach numbers as high as 2.44. Higher shock Mach numbers were not attempted as the air density was too low to yield satisfactory schlieren photographs.

Although the shock tube was fitted with a double diaphragm system to control the breaking pressure all tests were performed with a single diaphragm i.e., the shock tube was carefully filled until the diaphragm suddenly burst. This procedure was found to be quite satisfactory if the driver was filled slowly enough. At low diaphragm pressure ratios where a small change produces a relatively large change in shock Mach number, the diaphragms were found to break consistantly, at very nearly the same driver pressure. The variation was almost unnoticeable on the driver pressure gauge which was calibrated in 10 psi increments. Some inconsistency (±12 psi) was observed at driver pressures of 300 psig however, this variation does not lead to a significant change in shock Mach number ($\Delta M = \pm .015$ theoretically) in this range.

Test section A was used exclusively for photographic purposes in the shock Mach number range 1.17-1.67. Since only one photograph was obtained from each firing of the shock tube, the photographic history of the shock-slit interaction was pieced together by employing a successively greater spark delay for each run. Also, since consistent diaphragm bursting pressures were obtained, the incident shock velocity was not measured with transducers for each run. Instead, this was deduced from the photographs since the time delay was measured. Thus good repeatability was essential for consistent results. This aspect of the tests will be discussed more fully in the next section.

Both photographic and pressure measurements were performed with test section B which was used in the shock Mach number range 1.28-2.44. For the photographic survey, exactly the same test procedure described above was employed.

It was observed from the photographic results that only approximately one half cycle of the wave motion downstream of the slit was obtained using the full 2 inch channel. Therefore one series of tests was performed with the removable flanges containing the slit mounted further into the channel to give h = 0.68 inches. For a 0.35 inch slit photographs of nearly one full cycle of the motion were subsequently obtained. In order to preserve the same upstream flow conditions as before, it was necessary to extend the new channel wall far upstream. However, when this test section was used for shock velocity measurements alone, measurements were performed both upstream and downstream of the slit. In this case, for each shock Mach number-slit width combination five identical runs were performed and the results were averaged. Altogether, four slit widths ranging from 0.068-1.250 inches were tested. In addition, tests were conducted with no slit i.e., a straight uniform tube in order to determine the magnitude of viscous attenuation alone. The location of both the upstream and downstream edges of the slit relative to the fixed transducer stations was not the same for each slit width so the appropriate dimensions are tabulated in Figure 4.3.

4.3 Some Observations Concerning the Tests

It was pointed out in the previous section that repeatability of the test conditions was essential for the successful acquisition of consistent experimental results. Consider first the shock velocity measurements. A typical oscilloscope trace is shown in Figure 4.4 which was obtained for an incident shock Mach number of 1.67 and a 1 1/4 inch slit. The lower beam corresponds to the incident shock which according to Figure 4.3 was measured between stations 6.44 and 2.44 inches upstream of the slit. The attenuated shock (upper beam) velocity was measured between stations 19.18 and 23.18 inches downstream of the slit. The maximum observed variation in incident shock Mach number was about ±4% from the average of five runs and in most cases the variation was ±2% or less. Furthermore, the variations were observed to be fairly symmetric about the mean so that these levels were considered to be acceptable. This was borne out by the observation that variations in the ratio of attenuated to incident shock Mach number were ±1% and again fairly symmetric about the mean for five runs. Thus although the maximum observed (average) attenuation was only about 6% for any of the tests, it is felt that the results are reasonably accurate.

Repeatability was considered to be more crucial for the photographic tests since the incident shock Mach number was measured from successive photographs. This was possible because an undisturbed portion of the incident shock remains visible until the expansion wave reaches the wall opposite the slit. The shock speed measurement can be done in two ways knowing the time difference between successive photographs. The first is done by measuring the change in the location of the undisturbed segment of the shock between any two photographs. However, since the location of the slit is known relative to the time delay trigger transducer, the shock speed can alternately be computed by dividing the distance between the undisturbed shock segment and the trigger transducer by the overall time delay for each photograph.

In the course of the tests, anomalies in the time delay of the order 2-3 microseconds were observed. Since the relative time delay between successive photographs was as low as 10 microseconds, use of the first method described above could lead to considerable error in computed shock speed. This error becomes more significant for higher incident shock Mach numbers. However, since the lowest absolute time delay used for the tests was about 100 microseconds, the second method is considerably more accurate and was adopted. Using this method, the variation in shock Mach number for $M_0 = 1.41$ (average) was found to be approximately ±2% for example.

It should be realized however, that when computing various parameters such as triple point trajectories and expansion wave velocity, for example, the calculations are subject to the larger errors described above. This is so because time is measured relative to the instant the shock arrives at the upstream edge of the slit. In most cases, this condition was not observed directly so that this time had to be estimated from the (more accurately) computed incident shock speed. Fortunately, as the events proceed, the possible 2-3 microsecond error becomes less significant. For example, at $M_0 = 1.41$ the events are observable for about 85 microseconds after the shock passes the slit so the maximum estimated error is about 3% at this time.

Due to the relative roughness of the shock tube walls outside of the 5 inch region of observation it was necessary to investigate the natural shock attenuation due to viscous boundary layer effects alone. The shock tube had been so calibrated during previous studies and the results are presented in Figure 4.5 for shock Mach numbers between 1.4 and 1.85. The measurements encompass the region between 70 and 110 inches from the diaphragm. For the present tests, the region of interest is nearly the same therefore these results are directly applicable. From the figure, it can be seen that the shock attenuation is practically negligible in the shock Mach number range tested. These results are in general accord with the findings of Glass, et.al.[59] for which no attenuation was found for shock Mach numbers below 1.7. In the terminology of these authors, only a "formation decrement" exists in that a diaphragm pressure ratio greater than the theoretical value is required to generate a shock of given strength.

Although for the present tests shock Mach numbers as high as 2.44 were employed, this was done with an evacuated driven section so that it is presumed that due to the much lower density, viscous attenuation was not significant. The data in Figure 4.5 was obtained with an atmospheric driven section.

In spite of some of the difficulties noted above, the experimental results are considered to be reasonably accurate and consistant.

CHAPTER V

RESULTS AND DISCUSSION

5.1 Photographic History of the Shock-Slit Interaction

In this section a qualitative description of the shock-slit interaction process is provided from the photographic study described briefly in Chapter IV. This part of the analysis yields valuable information regarding the nature of the shock attenuation process and other associated phenomena.

A sequence of sixteen schlieren photographs depicting the shock-slit interaction for an incident shock Mach number of 1.41 and a slit width of 0.275 inches is presented in Figure 5.1. Numbers on the left side of the photographs give the time delay in microseconds relative to the instant the shock passes the spark lamp trigger transducer 2.875 inches ahead of the slit. The field of view is roughly 1 3/4 X 3 1/4 inches in the two inch channel.

From the photographs it can be seen that the incident shock is quite plane. In accordance with the discussion that has been given in Section 1.2 interpretation of the photographs is straightforward. Photographs (b) and (c) depict the diffraction of the shock through the slit and the subsequent generation of a nearly cylindrical expansion wave (dark region) which moves transversely across the shock. In (d) collision of the diffracting shock with the downstream edge of the slit and the generation of a nearly cylindrical reflected shock is shown. Spreading of these waves into the flow field is illustrated in (e) through (i). As explained in Section 1.2, the reflected shock takes on a Mach configuration and the slip line emanating from the triple point is visible in the photographs.

The development of the fluid jet emerging from the slit is the main feature to be observed in photographs (j) through (p). A rather large vortex accompanies the jet formation and as anticipated, the jet is inclined to the duct axis. In this case the jet pressure ratio exceeds the critical value so that choking occurs. This corresponds to the mixed flow (regime (ii)) discussed in Section 1.2. In the immediate vicinity of the slit the flow is subsonic, the free streamlines from the edges of the slit exhibiting considerable curvature. The shear layer on both sides of the jet boundary is quite pronounced. The jet appears to be fairly well established roughly 100μs. after arrival of the incident shock wave.

Figure 5.1 clearly demonstrates the attenuation mechanism. The effect of the expansion wave is to induce a small amount of shock curvature which is indicative of retardation. This is offset somewhat by the reflected shock which follows closely behind and terminates the expansion. The net effect is a ~~reduction in shock strength~~ as the Mach stem lags behind the undisturbed segment of the incident shock. Thus the attenuated portion of the shock exhibits significant curvature and the Mach stem is normal to the wall only at its foot. Clearly, the attenuation process will be gradual since the energy loss through the slit is communicated to the shock by transverse waves and a finite time is required for these waves to process the incident shock. Additional attenuation will result from multiple reflection of the transverse waves from the duct walls so that the attenuation rate is then controlled by the wall spacing. Continual spreading of the expansion wave will also contribute to a gradual attenuation process.

A similar but less extensive study of the sequence of events is presented in Figures 5.2 through 5.5 for shock Mach numbers between 1.17 and 1.67. In these cases the particle velocity behind the incident shock is subsonic so the internal wave motion is similar to that described above. The jet structure is controlled by the pressure ratio across the slit which is (theoretically) subcritical for M_0 less than 1.21. Thus in Figure 5.2 the jet is entirely subsonic.

For the other cases choking is theoretically possible. It is interesting to observe in Figures 5.3 through 5.5

that although the flow is initially subsonic the cylindrical expansion wave accelerates the fluid near the slit to sonic velocity and a Prandtl-Meyer expansion is established at the upstream edge of the slit. In this way a small patch of supersonic flow is established. Eventually, however, for $M_0 = 1.45$ the reflected shock passes through this region and the flow becomes subsonic near the slit again. For the higher shock Mach numbers the reflected shock has difficulty penetrating the supersonic patch and tends to bend around it.

The reason for this sudden weakening of the jet is not immediately obvious although a possible explanation is that it is due to the arrival in the test section of the contact surface separating the shocked and expanded flows generated by the rupture of the shock tube diaphragm. However, a simple calculation shows that this contact surface is still far upstream at this time. It turns out that this peculiarity is, in fact, a result of wave reflections from the wall opposite the slit (see Figure 5.12). Apparently the re-reflected shock "pumps" itself through the supersonic patch. Although this phenomenon is not observed in Figures 5.4 and 5.5 no definite conclusions can be drawn as the tests were terminated prior to the arrival of the reflected waves from the opposite wall (see Figure 5.4 (d)).

As might be anticipated on purely intuitive grounds the photographic results show that the inclination of the fluid jet decreases as shock Mach number increases. A similar behaviour is observed for the jet development time.

In order to examine the jet structure more closely, additional tests were performed with a greater optical magnification for a field of view encompassing only the immediate vicinity of the slit. The results are shown in Figures 5.6 and 5.7 for shock Mach numbers of 1.45 and 1.55 respectively. These clearly show the choking effects and the modifications to the jet structure attributed to re-reflected waves.

It was noted in Section 1.2 that when the particle velocity behind the incident shock is supersonic, a Prandtl-Meyer expansion will be established at the upstream edge of the slit so that the fluid jet is entirely supersonic. Furthermore, the expansion wave and reflected shock are unable to propagate upstream against the supersonic stream and remain essentially attached to their respective points of origin. This situation is shown in Figure 5.8 which depicts the shock-slit interaction for $M_0 = 2.14$.

Actually, the reflected shock is observed to be slightly detached from the edge of the slit possibly due to a slight bluntness of the edge (0.03 inches approximately). Inside the duct the reflected shock has a straight segment characteristic of supersonic wedge flows which joins smoothly to the cylindrical segment which propagates transversely. The slip line originating at the triple point of the reflected shock is particularly evident in these photographs.

The structure of the emerging fluid jet is seen to be quite complex due to reflection from the jet boundary of the external portion of the reflected shock. The subsequently formed expansion wave eventually reflects again to form an oblique shock in the jet. A similar behavior is observed for the expansion wave originating from the blunt lip of the downstream edge of the slit.

In the last few frames of Figure 5.8 the arrival of the reflected shock from the opposite wall is seen to result in a regular re-reflection. The point of contact moves upstream so it appears that these waves will eventually reach the slit and modify the structure of the jet to some extent.

Figure 5.9 shows the shock-slit interaction for the highest Mach number tested, $M_0 = 2.44$. Due to the low density in the test section the quality of the photographs is poor, however, the essential features can be seen.

The jet structure for the supersonic case is shown in greater detail in Figures 5.10 and 5.11, for $M_0 = 2.14$ and 2.33 respectively, due to the greater optical magnification employed. The bluntness of the downstream edge of the slit and the subsequent detachment of the reflected shock is more evident in these photographs. The oblique shock formation in the external jet is also very clearly demonstrated. It is also interesting to observe the contact surface (curved white line) separating the shocked and expanded gases as the incident shock diffracts through the slit.

The final phase of the photographic study [illegible] with an examination of the wave reflection process following the shock as it progresses down the duct. The results are presented in Figure 5.12 for a channel width of 0.68 inches, a slit width of 0.34 inches and an incident shock Mach number of 1.4. Unfortunately, the gasket seals at the edges of the flanges forming the upper walls proved to be inadequate and some extraneous waves due to leakage are visible in the photographs. However, these do not appear to seriously compromise the qualitative features of the flow.

In Figure 5.12(a) and (b) the diffraction and reflection processes are shown as before. Figures 5.12(c), (d) and (e) show the transverse and upstream propagation of the expansion wave and reflected shock as well as the subsequent reflection of these waves from the opposite wall. In (d) the head of the reflected expansion has traveled about half way back to the lower wall while in (e) the reflected shock occupies about the same position although the triple point is just arriving at the upper wall. It is interesting to note that at this time, which is taken to be the completion of one half cycle of the motion, the attenuated shock is again nearly plane.

The rest of the sequence depicts the continued re-reflection of the transverse waves. Photograph (h) shows the situation after one complete cycle of the motion as the triple point has just returned to the wall containing the slit. The last frame shows about one and a half cycles of the motion.

The effect of the wave reflections upon the jet structure can be discerned in the last few photographs in the sequence. Re-reflection of the secondary shock from the upper wall is seen to be regular with two points of contact propagating in opposite directions. That moving upstream is forced or "pumped" through the flow surrounding the slit. In addition, several segments of the reflected shock then merge to form what would appear to be a fairly strong secondary shock which tends to move slowly upstream. This process is quite evident in the last two frames near the right hand edge of the photographs.

Clearly, the effect of the multiple reflections from the walls of the duct is to further attenuate the incident shock wave. As the shock moves through the duct, these transverse waves continually sweep across it so that the shock Mach number at either wall tends to be altered in a cyclic fashion. However, as the motion progresses the head of the expansion wave tends to outrun the reflected shock so that the cyclic motion goes out of phase and the attenuation becomes more continuous although gradually weaker. This aspect of the attenuation process will be shown more clearly by the wave diagram which illustrates the wave motion on the shock. This will be presented later in Section 5.5.

To summarize, then, the attenuation mechanism has been demonstrated by the photographic study. The initial attenuation of the incident shock results from the diffraction process through the slit although this effect is reduced by the subsequent reflection at the downstream edge. Thus the initial attenuation is expected to be relatively weak. Furthermore, the additional attenuation which takes place as the shock progresses down the duct will be gradual, since the energy loss through the slit is communicated to the shock by transverse waves which require a certain period of time to process the shock. In addition, the transverse waves spread out behind the shock so that their effect becomes less concentrated. The wall spacing rather than the slit width therefore tends to control the attenuation rate.

Finally, the effect of shock Mach number on the external flow field has been illustrated. Depending on the pressure ratio, the fluid jet escaping through the slit may be purely subsonic, mixed sub and supersonic or purely supersonic. The inclination of the jet is seen to depend on shock Mach number.

From the photographic study that has been presented it is possible to measure various parometers associated with the shock-slit interaction. The results of such measurements will be discussed in the following two sections.

5.2 EXTERNAL FLOW FIELD MEASUREMENTS

In this section the various parameters which describe the fluid jet emerging from the slit are presented. From the photographs presented in Section 5.1 it is possible to measure the jet angle, contraction ratio and the time required for the jet to become established at the slit. These are compared with approximate theoretical predictions given by various authors. In addition, it is possible to construct a wave diagram depicting the jet structure for the case where the flow behind the incident shock is initially supersonic. This is done by the method of characteristics making use of an approximate theory for the shape of the detached shock at the downstream edge of the slit.

The jet angle variation with shock Mach number is presented in Figure 5.13 and as noted in the last section θ_j decreases as M increases. This behavior is to be expected since as the local particle velocity ahead of the slit increases it becomes increasingly difficult to turn the flow through the slit. This, then, is an inertia or Reynolds number effect.

For shock Mach numbers up to about 1.6 the measured jet angle appears to be predicted fairly well by an approximate theory due to Troshin[5].

$$\theta_j = \cos^{-1}(V/V_j) \tag{49}$$

where V is the particle velocity approaching the upstream edge of the slit and V_j is the ultimate velocity achieved by the jet after expansion into the surrounding fluid. Now, equation (49) is derived from compressible hodograph theory under the assumption that the slit is very small so that the momentum of the escaping jet is small compared to that of the approaching stream. Furthermore, Troshin assumed the flow to be subsonic everywhere so extension of his theory into the supercritical regime is questionable. However, since the derivation is based solely on momentum principles this does not seem to compromise the generality of equation (49). The difficulty arises from the fact that the jet does not ultimately achieve a uniform velocity when the pressure ratio is supercritical. Rather, the jet overexpands and a repetitive unsymmetrical, cellular structure appears and V_j has little significance in this context. In fact, ~~the maximum~~ velocity that appears in the jet interior will far exceed V_j which is computed from the pressure ratio alone. Thus, equation (49) is not expected to be accurate in the supercritical regime and this conjecture is verified by the experimental results.

Figure 5.14 shows the measured jet contraction ratio which is defined as the ratio of the minimum flow area of the jet to the area of the slit. Again, Troshin[5] gives a solution for subcritical flow (M<1.21 in air) although the theory is much too complex to be given here. For supersonic particle velocity behind the incident shock wave (M>2.07 in air) a Prandtl-Meyer expansion exists at the upstream edge of the slit so that in this case there is no contraction of the jet as such. However, since the jet passes through the slit obliquely there is an effective reduction in flow area. This is shown theoretically in Figure 5.14 by a solid line which is terminated at M = 2.07 since this is the theoretical lower limit for which supersonic flow can exist.

According to Figure 5.14 the contraction ratio (theoretically) increases with increasing shock Mach number in both the subcritical and supersonic flow regimes. For the former case this behaviour is similar to that observed in simple orifice flows for which compressible contraction ratios are always observed to be greater than incompressible ones so long as the flow is subcritical. This is due to the fact that pressure forces (~~due to~~ expansion) predominate over inertia or viscous forces which is again, a Reynolds number effect. In the supersonic flow regime it is clear that the Prandtl-Meyer expansion will turn the jet more towards the normal to the duct axis as shock Mach number increases so therefore the contraction ratio must increase. Despite this, the overall inclincation of the jet decreases slightly, as shown in Figure 5.13. In this discussion, the effect of the detached shock at the downstream edge of the slit has been ignored as such effects are likely small except, perhaps, when the supersonic Mach number approaching the downstream edge is very close to unity.

The experimental results show good agreement with theory in the supersonic flow regime. In the subcritical flow regime there is only one data point although it does tend to support the trend predicted by Troshin's theory. In the mixed flow regime, for which there is no theory available, the experimental results indicate that the contraction ratio decreases steadily as shock Mach number increases. This behaviour suggests a Reynolds number effect i.e., in this regime inertia forces predominate so that the flow can not be easily turned to pass through the slit.

Measurement of the jet development time from the photographs is a somewhat subjective process. For this purpose, the jet was taken to be fully developed when the flow pattern in the immediate vicinity of the slit ceases to change significantly with time. Since the objective of this part of the tests is to observe the pressure adjustment at the mouth of the slit, changes in the jet structure due to wave reflections from the opposite wall are not considered. Thus, in Figure (5.1) the jet is taken to be established at about 100μs. after arrival of the incident shock at the upstream edge.

The experimental results are given in Figure 5.15 and are compared to theoretical predictions based on a theory developed by Rudinger[7] for the pressure adjustment when a shock reflects from an open end of a duct. The theory is essentially acoustic so it applies mainly to weak shocks. For the present case the opening (slit) is transverse to the incident shock while

Rudinger examined the situation where the opening is normal to the direction of motion of the incident shock. He found that the theoretical pressure adjustment is asymptotic although essentially complete in a time $t=4\tau$ where τ is the time required for an acoustic wave to traverse the flow through the opening. Since this time could vary considerably throughout the adjustment process, use of an average value is recommended.

Despite the obvious limitations, Rudinger's theory is applied to the present problem as a rough approximation. For the emerging jet, the time required for an acoustic wave to transverse the jet is easily computed if the jet is assumed to be uniform and straight near the slit although inclined to the axis of the tube. This assumption is likely to be quite crude in the subcritical and mixed flow regimes when there is considerable contraction of the jet as it emerges from the slit. The result, which is derived in Appendix A, is

$$\frac{C_0\tau}{l} = \frac{1}{2}\left\{\frac{C_0/C_1}{1+M_1} + \frac{C_0/C}{1-M^2}\left[\sqrt{1-M^2\sin^2\theta_j} - M\cos\theta_j\right]\right\} \qquad (50)$$

The line $t=4\tau$ is plotted in Figure 5.15 and it can be seen that the measured values are greater than the theoretical predictions by a nearly constant factor of about six. In addition, the pressure adjustment at the slit is about four times longer at $M = 1.17$ than it is at $M = 2.44$. This behaviour is attributed to a decrease in jet angle and an increase in particle velocity as shock Mach number increases. Thus, despite some rather crude assumptions, the Rudinger theory does predict the right trends for the jet development process.

An example of the computation of the structure of the emerging fluid jet is presented in Figure 5.16 for $M=2.33$. In this case, the particle velocity behind the incident shock is supersonic and the jet structure is also entirely supersonic. The calculation is based on the method of characteristics for two-dimensional steady flow and the details are given in Appendix B. The most difficult part of the calculation is the determination of the shape and stand-off distance of the detached shock and this is overcome by employing an approximate theory given by Moeckel[6] for which the shock shape is assumed to be hyperbolic. The result is presented in Figure 5.16 and is seen to compare favourably with the experimental results given in Figure 5.11 for the same shock Mach number. Especially noteworthy is the oblique shock formation due to reflection of expansion waves from the jet boundary. The approximate analysis appears to predict this formation rather well.

In principle, one could extend Troshin's work to include a calculation of the jet boundary for purely subcritical flow.

However, the analysis is rather complex, involving infinite series of ratios of hypergeometric functions which apparently converge very slowly if at all. Thus the method does not appear to be attractive. Furthermore, extension of the theory into the transonic (mixed flow) regime is also a rather formidable task and will not be considered here.

The present discussion concerning measurements of the external flow field is concluded with an examination of the diffracted portion of the incident shock which passes through the slit and then continues to expand as time progresses. It was noted from the photographs that the diffracted shock remains nearly cylindrical in shape within the present period of observation. The radius and center of this cylindrical shock can be easily determined from the photographs by a simple geometric construction and plotted out. Now, Whitham[17] found that for strong diffracting shocks the shock expands uniformly with time so that the quantities $x/\alpha M$ and $Y/\alpha M$ are similarity coordinates. For the present case, similar results are obtained as shown in Figure 5.17 which give the diffracted shock radius $r/\alpha M$ and center $X/\alpha M$ measured relative to the upstream edge of the slit. A single, smooth curve for both quantities is obtained. It can be seen that the diffracted shock is weak, expanding uniformly with a speed close to the sound speed behind the incident shock. At the same time the center of the diffracted wave moves slowly downstream at a uniform rate. The reason for this behaviour is not clear but it is probably related to the development process for the emerging fluid jet.

The results that have been presented in this section show that the various parameters associated with the fluid jet emerging from the slit are not predicted especially well by the theory that has been given. The jet angle is described well by Troshin's theory only for weaker incident shocks and the jet development turns out to be roughly six times longer than predicted by a somewhat crude use of Rudinger's theory. Both, however, predict the proper trends, Fortunately, the jet contraction ratio appears to follow the theoretical prediction except in the mixed flow regime for which there is no theory presently available.

5.3 INTERNAL FLOW FIELD MEASUREMENTS

The various parameters that describe the internal wave motion associated with the shock attenuation process will now be considered. From the photographs that have been presented in Section 5.1 measurements of the transverse wave motion can be performed to provide a quantitative analysis that complements the qualitative description that has been presented earlier.

It was pointed out in Chapter I that the motion of the expansion wave is ideally self-similar when viewed in a coordinate system which is fixed to the upstream edge of the slit. This notion is confirmed by the experimental data that is presented in Figure 5.18 which shows the expansion wave radii measured from the photographs. These results were obtained in two ways. First, several points on each wave were measured and the average from several photographs plotted in the similarity coordinates $X/\alpha M$, $Y/\alpha M$. These points are shown by the symbols on the figure. At the same time the expansion wave radius and center can be easily determined from a simple geometric construction. The former are shown by solid lines and the wave centers by the symbols on the positive X-axis.

The data shows that the expansion wave is essentially pseudostationary as all the data for a given shock Mach number fall onto a single curve characteristic of that Mach number.

The curve is very nearly cylindrical in shape so that the expansion wave spreads out uniformly with time. For supersonic particle velocities the wave can not propagate upstream and is therefore joined to the edge of the slit by a straight segment inclined at the local Mach angle. The expansion wave center is also convected downstream with a uniform speed.

Ideally, the expansion wave radius r_e and center coordinate X_e are given by $r_e = c_1 t$ and $X_e = u_1 t$ where c_1 and u_1 are the sound speed and particle velocity behind the undisturbed shock. These relationships are confirmed by the experimental results which are summarized in Figure 5.19. The agreement between theory and experiment is quite good.

Similar results are obtained for the reflected shock wave which are shown in Figures 5.20 and 5.21. In this case, the coordinate system is now fixed at the downstream edge of the slit. As for the expansion wave, the wave shape is nearly cylindrical except near the intersection with the incident shock wave. However, for $M_0 > 1.67$ the appearance of the supersonic "patch" tends to destroy the self-similar motion.

Figure 5.21 shows that the reflected shock spreads out at a rate that is not too different from the acoustic velocity c_1. This does not necessarily imply that the reflected shock is weak, however since it is advancing into a flow which is directed towards itself by the preceeding expansion wave. Interestingly, the shock center is convected downstream at a speed roughly equal to that for the expansion wave, i.e., at the velocity u_1.

According to the ray-shock theory the locus of the point of intersection between the expansion wave and the incident shock is a straight line, the slope being the tangent of the characteristic angle m_0. This fact is confirmed by the experimental results presented in Figure 5.22 and 5.23 for respective shock Mach numbers of 1.41 and 2.41. Similarly, the triple point trajectories taken from the same photographs are found to be linear as well. While it is well known that the path is straight for simple Mach reflection it is not clear why this should be so in the present case where the incident shock is somewhat curved. The photographic results do indicate, however, that the degree of curvature is not too large in the present case and perhaps this explains why a linear path is observed.

According to the discussion given in Section 3.2 it is expected that the characteristic angle m would be best predicted theoretically by the acoustic relation, equation (34), rather than the ray-shock theory, equation (32). Examination of Figure 5.24, which present the present experimental measurements, demonstrates that this is indeed the case and confirms the measurements previously given by Skews[20,29].

Similarly, the variation in the triple point locus angle χ with incident shock Mach number is presented in Figure 5.25 which shows that χ varies only slightly over the range of the tests. The values predicted by the ray-shock theory are also presented and as might be anticipated the theory considerably underestimates χ. This discrepency is attributed not only to the deficiencies of the ray-shock theory discussed in Chapters II and III but to the significant shock curvature near the triple point as well which is not accounted for in the theory. In spite of this, the theory does correctly predict that the variations in χ are small.

The simple three-shock theory can also be employed to predict χ but unfortunately, the error turns out roughly the same as for the ray-shock theory which is again attributed to shock curvature.

Examination of the photographs reveals that once the triple point has moved well away from the wall, the triple point lies roughly half way between the break in the Mach stem and the break in the incident shock (due to the expansion wave). This suggests the simple empirical relation

$$\chi = (\chi' + m_0)/2 \qquad (51)$$

where χ' is the value given by the ray-shock theory (or alternately by the simple three-shock theory) and m_0 is given by the acoustic relation, equation (34). From Figure 5.25 it can be seen that equation (51) fits the experimental data fairly well except at low shock Mach numbers. In the absence of a better theory, the only recourse seems to be to employ equation (51) for the construction of the wave diagram. Although the method is somewhat crude, the experimental results suggest it should lead to acceptable results.

In this section the pseudo-stationary nature of the transverse wave motion accompanying the attenuation process has been demonstrated from the experimental results. Both the sonic intersection and triple point paths have been shown to be linear, the former well predicted by acoustic theory. The failure of the ray-shock theory to accurately describe the triple point locus angle necessitates the implementation of an empirical relation in its place.

5.4 Attenuation of the Shock Wave

In Section 5.1 it was demonstrated that the attenuation of the incident shock proceeds in two phases. There is an initial attenuation due to the diffraction and reflection processes as the shock passes over the slit which results in a Mach stem shock velocity that is lower than the incident wave speed. The Mach stem then proceeds along the wall at a uniform speed until the second phase of the attenuation process begins. This occurs when the transverse waves reflect from the back wall opposite the slit and return to modify the Mach stem velocity again. This process is continued indefinitely as the wave systems undergo successive reflections from the walls of the duct. In this section the wave speed measurements corresponding to these two phases of the attenuation process will be examined and discussed.

The first phase of the attenuation process which is associated with the initial shock-slit interaction can be measured directly from the photographs presented in Section 5.1. According to the discussion that was given there this initial attenuation is expected to be weak since most of the shock diffraction occurs outside the duct and because of the compensating effect of the reflection process at the downstream edge of the slit. As noted previously, the energy loss associated with the mass flux through the slit is communicated to the shock via a transversely propagating expansion wave and a finite time is required for its full effect to be felt at the shock front.

Measurements were performed from the photographs in two ways. First, distance and time were measured relative to one photograph, usually the first showing the attenuated wave. However, the wave speeds obtained in this way did not yield good results so an alternate method was adopted. The time at which the shock reaches the downstream edge of the slit was estimated (from the measured incident shock speed and neglecting shock curvature) and used as a reference time for the calculations. The attenuated wave speed was then obtained from measurement of the distance traveled by the Mach stem from the downstream edge of the slit. In some cases this procedure led to wave speeds greater than the incident wave speed so the data was discarded in such occurrances. The average wave speed for each series of photographs was then plotted as a single point. Generally, the average was computed from at least three separate photographs although for $M_0 = 1.67$ only one photograph yielded acceptable results.

The results of the measurements are presented in Figure 5.26 from which it can be seen that the agreement with theory is quite good despite the fact that measurement from the photographs is not especially accurate. As anticipated, the initial attenuation is relatively weak, ranging between 3% and 7% over the range of the tests. Intuitively it is expected that the greatest attenuation would occur for the highest shock Mach numbers since the diffraction effects are relatively greater in that case. The experimental results show that this notion is indeed correct.

It should be pointed out that the experimental data presented in Figure 5.26 correspond to two different slit widths. For $M_0 \leq 1.67$ a slit width of 0.275 inches was employed while for the greater shock Mach numbers a slit width of 0.375 inches was used, an increase of 35%. However, as was pointed out in Sections 1.2 and 3.3 the diffraction process is self-similar since no characteristic length enters the problem initially. Thus, as is also revealed by the ray-shock theory, the diffracted shock Mach number approaching the downstream edge of the slit is the same for all slit widths for a given incident shock Mach number (M and θ are constant along each of the ray-shock characteristics). Therefore, it is not surprising to see no discernable effect of slit width in the results given in Figure 5.26 although it is recognized that more extensive testing is required for conclusive evidence.

As explained in Chapter IV, attenuated wave speeds were also measured with pressure transducers roughly two feet downstream of the slit in order to examine the effect of wave reflections on the attenuation rate. In this case the attenuation is therefore expected to be greater than that measured from the photographs although not significantly so because of the gradual nature of this phase of the attenuation process.

Results are shown in Figure 5.27 for slit widths between 0.07 and 1.25 inches. As anticipated, the theoretical curve, which does not take into account the increased attenuation due to wave reflections, still adequately describes the observed attenuation. Thus the effect of wave reflections appears to be slight at this point of measurement. However, the results do show a small tendency towards increased attenuation as slit width is increased. This is shown more clearly in Figure 5.28 where the ratio of attenuated to incident shock Mach number is given. For an incident shock Mach number of about 1.3 increasing the slit width by a factor of about eleven from 0.068 to 0.75 inches increases the attenuation by only about half, from 4% to 6%. For higher shock Mach numbers this effect is even smaller. This behavior is attributed to the fact that increasing the slit width actually tends to increase the number of wave reflections that occur. This will be shown more clearly in the next section when the wave diagram for the transverse wave motion is presented and discussed in detail.

From the results that have been presented so far it can only be concluded that the increased attenuation due to reflections and the corresponding effect of slit width is relatively small within the scope of the present tests. Naturally, it is to be expected that the theoretical predictions according to the ray-shock theory would not agree as well with experimental measurements performed at much larger distances downstream of the slit. However, such measurements are probably outside the range of practical interest.

Curiously, the experimental results presented in Figure 5.28 for the higher shock Mach numbers show a slightly lower attenuation rate than that measured from the photographs, when in fact the opposite is to be expected. The reason for this is not immediately evident although a possible explanation lies with experimental error. At the higher wave speeds the distance measured from the oscilloscope traces becomes correspondingly smaller and the susceptibility to experimental error increases. Moreover, the quantity that is being measured (the attenuation) is of the same order of magnitude as the errors that might be expected from this type of measurement. However, as noted earlier, the experimental results do appear to be fairly consistant. For the lower shock Mach numbers the anticipated slight increase in shock attenuation downstream of the slit is in fact observed.

Another and perhaps more speculative explanation is that the number of cycles of the transverse wave motion changes as incident shock Mach number is increased, although Figures 5.24 and 5.25 suggest that such changes would be small over most of the range of the present tests. Since the measurements were performed at a fixed location for each series of tests it is possible that the measurements corresponding to two different shock Mach numbers also correspond to somewhat different phases of the transverse motion. This then, might explain the unexpected positive slope of the experimental results in Figure 5.28.

Results are also shown for the case where there is no slit in the side wall so that the effect of viscous attenuation alone could be estimated. For the lower shock Mach numbers some attenuation is observed although it is generally smaller than that observed with an open slit. Some data scatter is present and this gives some idea of possible experimental errors. At higher shock Mach numbers almost no attenuation is observed and this is attributed to low ambient air density in the test section.

For the largest slit width tested, $\ell = 1.25$ inches, the tests were prematurely terminated at moderate shock strengths due to a sudden degradation of transducer output likely resulting from deterioration of the piezo-element.

Generally, the results of this section confirm the intuitive expectation that the shock attenuation due to a single slit is both weak and gradual. Within the scope of the tests the effect of slit width is secondary and the experimental results are therefore adequately described by the ray-shock theory.

5.5 The Wave Diagram and Stability of the Attenuated Shock Wave

The wave diagram illustrating the transverse wave motion on the shock front was constructed for the case $M_0 = 1.4$, $\ell = 0.35$ inches, $b = 0.68$ inches according to the method of characteristics appropriate to the ray-shock theory as outlined in Section 3.4. This case corresponds directly to that shown in the photographs of Figure 5.12 and the completed wave diagram is presented in Figure 5.29. In the figure all distances are made nondimensional with respect to the channel width of 0.68 inches and about two and a half cycles of the theoretical shock motion are shown.

According to the ray-shock theory the cylindrical expansion wave which is generated when the shock diffracts through the slit corresponds to a simple wave originating at the upstream edge of the slit. For construction purposes, five finite elements were used to initially represent the essentially continuous wave. These are shown as light solid lines on the diagram. Only the internal motion is of interest here hence that part of the simple wave which corresponds to the external shock diffraction is omitted from the diagram.

Collision of the diffracted shock with the downstream edge of the slit generates a reflected shock and the accompanying phenomenon of Mach reflection. This corresponds to the generation of a shock-shock originating from the downstream edge of the slit and its subsequent trajectory on the wave diagram is shown as a heavy solid line. In accordance with the principles outlined in Section 3.4 the history of the kinematic waves is then worked out. The results of the calculations are summarized in Table 5.1.

From the wave diagram it can be seen that the expansion wave reflects from the upper wall and then interacts with the shock-shock to modify it as it propagates towards the wall. The effect of this interaction is to cause the shock-shock trajectory to curve towards the upper wall slightly. The shock-shock then reflects and again meets the expansion wave which by this time has reflected from the lower wall. The reflection processes then continue in a more or less cyclic manner. However, it can be seen that as the shock proceeds down the duct the expansion wave spreads out more and more until it becomes indistinct not only on the wave diagram but in the schlieren photographs of Figure 5.12 as well. At the same time the head of the expansion wave is seen to "outrun" the shock-shock so that the motion goes out of phase and the attenuation process becomes more diffused and gradual. Although the schlieren photographs of Figure 5.12 show only a little more than about one complete cycle of the motion this is sufficient to allow experimental measurement of the shock-shock trajectory. On the wave diagram the experimental points are shown by circles and it can be seen that the shock-shock trajectory is predicted quite well by the ray-shock theory. Only one point exhibits appreciable error and this is likely due to significant experimental variation in the incident shock speed. It should be recalled, however, that the empirical relation, equation (51) rather than the ray-shock relation is employed to compute the shock-shock locus angle χ. In addition, the acoustic relation, equation (34), must be used to compute the characteristic slopes otherwise the wave diagram will be in considerable error from the start. For the present case the shock-shock path is observed to be fairly straight over the range of the calculations. Even when the head of the expansion wave overtakes the shock-shock after roughly two cycles of the motion, the subsequent change in the trajectory is small, at least theoretically.

The effect of slit width on the attenuation rate can also be deduced from the wave diagram. From the slopes of the shock-shock trajectory as well as the characteristics it can be seen that increasing the slit width tends to increase the number of reflections of the expansion wave and therefore tends to increase the shock attenuation rate. This is so because an increase in slit width tends to move the point where the head of the reflected expansion reaches the lower wall (point 15) further upstream i.e., closer to the slit. The same is seen to be true for the additional reflections (points 26, 37, 48) and the above conclusion thus follows.

The cyclic nature of the transverse wave motion is illustrated by plotting out the theoretical variation in shock Mach number along both walls of the duct. This data which is taken from Table 5.1 is presented in Figure 5.30. From these results the attenuation mechanism is clearly demonstrated as it is observed that the peak shock Mach number for each cycle is slowly decreasing along both walls. The spreading of the expansion wave and the subsequent change in phase of the motion is also evident in this figure.

It is also interesting to note from the data at the lower wall that the effect of the expansion wave is to weaken the shock-shock initially when the motion of the two waves is more or less opposed. However, later on at roughly X/h = 10 the motion of both waves is in the same direction and the shock-shock tends to be reinforced somewhat. Thus the transverse wave interactions are analogous to "beating" phenomenon that is observed when linear waves of different frequencies are superimposed. However, in this case the amplitude of the motion must slowly decrease.

From the completed wave diagram it is possible to trace in the theoretical shock shape with the aid of the tabulated results. These are shown on the wave diagram, Figure 5.29, as solid lines sketched into the flow field. In the figure, the initial Mach stem curvature due to any characteristics which may be generated by the initial interaction between the expansion wave and the shock-shock is ignored. Thus the Mach stem is taken to be straight initially.

It can be seen from the diagram that the initial effect of the expansion wave is to induce a significant amount of curvature in the incident shock wave which is almost immediately counterbalanced by the arrival of the shock-shock. Owing to the reflection of the expansion wave from the upper wall a small degree of curvature is retained, however. This is amplified by re-reflection of the expansion wave from the lower wall and then reduced again by the shock-shock which has returned after reflection from the upper wall. Thus the shock curvature tends to increase and decrease alternately in a cyclic manner which is related to the frequency of the reflections of the transverse waves from the walls of the duct.

In addition, it can be seen from the wave diagram that the effect of the transverse wave motion is to also reverse the shock curvature periodically. This effect is readily discerned from the schlieren photographs in Figure 5.12 as well.

The accuracy of the wave diagram can be further checked by comparing the theoretical shock shape to that obtained experimentally. This was done by blowing up the schlieren photographs of Figure 5.12 by roughly four times and sketching the photographic results into the appropriate location on the wave diagram. These results are shown as dotted lines in Figure 5.29 from which it can be seen that the agreement between theory and experiment is reasonably good. Both the sense and the degree of curvature appear to be fairly well predicted by the wave diagram over the first complete cycle of the motion. Since no experimental results were obtained for the subsequent cycles of the motion no further conclusions regarding the accuracy of the wave diagram can be drawn.

In addition to the information described above the wave diagram also demonstrates that the traveling shock is stable i.e., perturbations in the wave form tend to decrease as the shock advances along the duct after passing over the slit. This is easily shown by measuring the theoretical total perturbation in the wave form directly from the wave diagram. For this purpose the total perturbation is taken to be the maximum (horizontal) distance between any two points on the shock wave at a given instant. The sense of the curvature is disregarded so that the total perturbation is always taken to be a positive quantity.

The results of measurements from the wave diagram are presented in Figure 5.31. It can be seen that, as anticipated from the previous discussions, the total perturbation varies in a cyclic manner. Clearly, the shock is stable since the perturbation amplitude decreases as the shock moves down the duct. The experimental results obtained by measurement from the schlieren photographs in Figure 5.12 are also included on the figure. From these it can be seen that the wave diagram underestimates the perturbation amplitude somewhat for the first half cycle of the motion and overestimates for the rest. Thus the experimental results indicate that the shock tends to a planar form much more rapidly then the wave diagram suggests. However, as noted earlier, the wave diagram does appear to give the proper frequency of the motion at least within the range of the experimental tests.

Some qualitative insight into the stability mechanism is provided by the wave diagram. It is the expansion wave which induces the greatest curvature in the shock wave and the Mach reflection process (or shock-shock) which tends to counteract its effect. Clearly, the expansion wave spreads out as time progresses so the induced curvature tends to decrease. Since the shock is confined by the duct walls, the total perturbation produced by the expansion wave must therefore tend to decrease as the shock moves down the duct. The spacing between the duct walls controls the frequency with which the transverse waves move across the shock front hence this parameter also determines the rate at which the shock will approach a planar form. It is evident that if no back wall were present the shock front would never achieve a plane form and the perturbation would continue to grow indefinitely.

Stability of initially planar shock-waves has been studied theoretically by Freeman[60,61] for the case where a shock traveling in a uniform duct encounters a small change in cross sectional area. By extending a linear theory due to Lighthill and Chester, Freeman was able to deduce that the perturbation in wave form is inversely proportional to the 3/2 power of the distance traveled by the shock. The theory is valid however, only far away from the origin of the disturbances which are assumed to undergo a large number of reflections from the walls.

Lapworth[62] has investigated experimentally the stability of shocks perturbed by "roof top" obstacles placed on the sidewalls of a shock tube and concluded that the 3/2 power law is approximately correct in that case. Examination of Figure 5.31 indicates that the present experimental results appear to be adequately described by the 3/2 power law as well although the amount of the data is insufficient to allow one to draw any definite conclusions. However, it was noted by Lapworth that the magnitude of the perturbations predicted by Freeman's theory were significantly greater than those actually observed.

In view of the above discussion regarding the wave diagram for the present problem it is not surprising to find that Freeman's stability theory predicts cyclic variations in the shock front perturbation. However, according to the theory the perturbation should periodically approach zero although the data presented in Figure 5.31 suggest that this in fact does not occur in the present case. According to the wave motion described by the wave diagram it is virtually impossible for this to occur although the perturbation can theoretically become relatively small. Lapworth arrived at a similar conclusion from his experimental results. It must be recalled though that the experiments show only the first few cycles of the motion and the theory really does not apply so close to the origin of the disturbances.

As a final comment regarding the shock wave stability it should be pointed out that Freeman's analysis is quite approximate and rather complicated as well. For many practical problems construction of the wave diagram may be a preferable alternative despite its complexity and apparent inaccuracy in predicting the perturbation amplitude.

In summary, for the single case illustrated, it has been demonstrated that the wave diagram constructed according to the principles of the ray-shock theory not only provides valuable insight into the shock attenuation mechanism but yields some quantitative information as well. The shock-shock trajectory for the first cycle of the wave motion is predicted reasonably well although the perturbations to the wave front are generally overestimated. Stability of the attenuated shock wave is also readily demonstrated by this technique.

5.6 Concluding Remarks

Attenuation of an initially planar shock wave has been examined for incident shock Mach numbers between 1.17 and 2.44 and for slit widths between 0.068 and 1.25 inches. Experimental measurements have been performed via spark schlieren photography and using pressure transducers to measure shock velocity. Theoretical considerations have been based on Whithams ray-shock theory. Within the scope of the present investigation the main results are summarized and conclusions drawn:

(1) The photographic history of the shock-slit interaction demonstrates the attenuation mechanism-diffraction of the shock through the slit and a subsequent Mach reflection. The transverse waves thus generated are nearly cylindrical and pseudo-stationary in their respective time frames.

(2) Attenuation of the incident shock by a single slit is relatively weak. The greatest decrease in shock Mach number observed for the present tests was about 7% and occurred for the largest slit width. The additional attenuation due to transverse wave reflections is also very gradual so that the ray-shock theory adequately predicts the attenuated wave speed even some distance downstream of the slit.

(3) The tendency for the initial shock attenuation to be independant of slit width according to the ray-shock

theory is observed in practice. Although increasing the slit width produces a small increase in shock attenuation some distance downstream from the slit, this effect is attributed to transverse wave reflections which are not accounted for by the theory. Thus the most efficient attenuation would be produced by a series of closely spaced narrow slits.

(4) The external flow field is characterized by the appearance of a fluid jet which is established at the mouth of the slit and the character of this jet is observed to depend on the pressure ratio across the slit. Steady flow is established roughly six times longer than predicted by an approximate theory.

(5) A wave diagram constructed according to the ray-shock theory is observed to faithfully describe the transverse wave motion on the attenuating shock. The cyclic nature of this wave motion is clearly demonstrated. However, the success of the wave diagram technique in predicting the shock-shock trajectory is based on an empirical relation for the triple point locus angle χ.

(6) Stability of the attenuating shock is clearly demonstrated by the wave diagram technique. Perturbations on the shock front are also observed to possess a cyclic nature although the perturbation amplitude steadily decreases as the shock moves down the duct.

The experimentally observed perturbation is found to decrease much more rapidly than predicted by the wave diagram.

(7) The photographic study clearly shows the formation of a nearly plane secondary shock in the flow field which originates in the vicinity of the slit and propagates upstream against the main flow. This shock is observed to be produced by coalescence of the components of transverse wave reflections.

Although the present investigation may be regarded as successful in achieving the stated objectives of defining and describing theoretically the attenuation process, what has been presented here is by no means a complete examination of the problem. Considerations for future work should include an investigation of shock attenuation for much stronger shock waves which are more likely to be encountered in actual practice. An experimental study of the attenuation produced by a series of closely spaced slits is also called for.

Improvement of the theoretical aspects of the problem are called for although it is recognized that this task is a rather formidable one. From what has been discussed in Chapters II and III it can be seen that extension of the CCW and ray-shock theories is at best a difficult job. At the same time it can be seen that due to its complexity and approximate nature elimination of the wave diagram via improvement of the theoretical technique is desirable.

Finally, a theoretical description in the transonic regime for the fluid jet emerging from the slit is needed. At present, there seems to be many difficulties to be overcome regarding such an extension of compressible hodograph theory. At the same time, an extension of Rudinger's work on the transition from unsteady to steady flow conditions is required for an adequate description of the present problem.

REFERENCES

1. Strehlow, R.E., "Unconfined Vapor Cloud Explosions - An Overview", Fourteenth Symposium (International) on Combustion, The Combustion Institute, 1972.

2. "LNG Supertanker: Hazardous Visitor", Technology Review, Massachussetts Institute of Technology, March/April 1974. John I. Mattill, Editor.

3. "Investigation Into The Hazards Connected with Storage And Transport Of LNG, Working Program 1974", Technologisch Laboratorium, Rijswijk, Netherlands, 1974.

4. Wu, J.H.T., Ostrowski, P.P. and Lee, P., "Shock Diffraction By A Chamfered Slit In A Shock Tube", Proceedings of the Fourth Canadian Congress of Applied Mechanics, Montreal, Canada, 1973.

5. Troshin, V., "Gas Flow Through An Opening In A Channel Wall", PMM Journal of Applied Mathematics and Mechanics 23, 1959.

6. Moeckel, W.E., "Approximate Method For Predicting Form And Location Of Detached Shock Waves Ahead Of Plane Or Axially Symmetrical Bodies", NACA TN 1921, 1949.

7. Rudinger, G., "The Reflection Of Pressure Waves Of Finite Amplitude From An Open End Of A Duct", Journal of Fluid Mechanics 3, 1957.

8. Baker, W.F., Explosions In Air, University of Texas Press, Austin and London, 1973.

9. Lighthill, M.J., "The Diffraction Of Blast I", Proceedings of the Royal Society of London, Series A, 198, 1949.

10. Lighthill, M.J., "The Diffraction Of Blast II", Proceedings of the Royal Society of London, Series A, 200, 1950.

11. Ludloff, H.F. and Friedman, M.B., "Aerodynamics Of Blast-Diffraction Of Blast Around Finite Corners", Journal of the Aeronautical Sciences, 22, No.1, 1955.

12. Ludloff, H.F. and Friedman, M.B., "Difference Solution Of Shock Diffraction Problems", Journal of the Aeronautical Sciences, 22, No. 2, 1955.

13. Rusanov, V.V., "The Calculation Of The Interaction Of Non-Stationary Shock Waves And Obstacles", N.R.C. (Canada) Technical Translation TT-1027, 1962.

14. Gururaja, J. and Deckker, B.E.L., "Numerical Solution Of Flows Behind Shock Waves In Non-Uniform Regions", Proceedings of the Institution of Mechanical Engineers, 184, Pt. 3G, 1969-70.

15. Belotserkovskii, O.M. and Ghushkin, P.I., "The Numerical Solution Of Problems In Gas Dynamics", Basic Developments In Fluid Mechanics, Academic Press, New York and London, 1965, M. Holt, Editor.

16. Pack, D.C., "The Reflexion And Diffraction Of Shock Waves", Journal of Fluid Mechanics, 18, 1963.

17. Whitham, G.B., "A New Approach To Problems Of Shock Wave Dynamics, Part I, Two Dimensional Problems", Journal of Fluid Mechanics, 2, 1957.

18. Whitham, G.B., "On The Propagation Of Shock Waves Through Regions Of Non-Uniform Area Or Flow", Journal of Fluid Mechanics, 4, 1958.

19. Whitham, G.B., "A New Approach To Problems Of Shock Wave Dynamics, Part II, Three Dimensional Problems", Journal of Fluid Mechanics, 5, 1959.

20. Skews, B.W., "The Shape Of A Diffracting Shock Wave", Journal of Fluid Mechanics, 29, 1967.

21. Skews, B.W., "Shock Diffraction On Rounded Corners", Third Australian Conference on Hydraulics and Fluid Mechanics, The Institution of Engineers, Australia, 1968.

22, Oshima, K., Sugaya, K., Yamamoto, M. and Totoki, T., "Diffraction Of A Plane Shock Around A Corner", Institute of Space and Aeronautical Science, University of Tokyo, Report No. 393, 1965.

23. Oshima, K., "Propagation Of Spatially Non-Uniform Shock Waves", Institute of Space and Aeronautical Science, University of Tokyo, Report No. 397, 1965.

24. Miles, J.W., "A Note On Shock-Shock Diffraction", Journal of Fluid Mechanics, 22, 1965.

25. Chisnell, R.F., "A Note On Whitham's Rule", Journal of Fluid Mechanics, 22, 1965.

26. Bryson, A.E. and Gross, R.W.F., "Diffraction Of Strong Shocks By Cones, Cylinders And Spheres", Journal of Fluid Mechanics, 10, 1961.

27. Knystautas, R. and Lee, J.H., "Experiments On The Stability Of Converging Cylindrical Detonations", Combustion and Flame, 16, 1971.

28. Setchell, R.E., Storm, E. and Sturtevant, B., "An Investigation Of Shock Strengthening In A Conical Conveyant Channel", Journal of Fluid Mechanics, 56, 1972.

29. Skews, B.W., "The Shape Of A Shock Wave In Regular Reflection From A Wedge", Canadian Aeronautics and Space Institute Transactions, 5, No. 1, 1972.

30. Skews, B.W., "Shock Wave Shaping", A.I.A.A. Journal, 10, No. 6, 1972.

31. Lau, J. and MacLeod, D., "Electrical Shock Tube With Curved End Wall", Canadian Aeronautics and Space Institute Transactions, 5, No. 1, 1972.

32. Milton, B.E. and Archer, R.D., "Generation Of Implosions By Area Change In A Shock Tube", A.I.A.A. Journal, 7, No. 4, 1969.

33. Milton, B.E., "Shock Wave Motion And Focusing In Area Contractions", Ph.D. Thesis, University of New South Wales, Australia, 1971.

34. Milton, B.E. and Archer, R.D., "Pressure And Temperature Rise In A Logrithmic Spiral Contraction", <u>Shock Tube Research</u>, Chapman and Hall, London, 1971. J.L. Stollery, A.G. Gaydon and P.R. Owen, Editors.

35. Wu, J.H.T., Archer, R.D. and Molder, S.M., "Shock Propagation In A Two Dimensional Logrithmic Spiral Contraction", <u>Recent Developments in Shock Tube Research</u>, Stanford University Press, Stanford, Cal., 1973. D. Bershader and W. Griffith, Editors.

36. Courant, R. and Friedrichs, K.O., <u>Supersonic Flow And Shock Waves</u>, Interscience, New York, 1948.

37. Polachek, H. and Seeger, R.J., "Shock Wave Interaction", Fundamentals Of Gasdynamics, Section E, Princeton University Press, 1958. H. Emmons, Editor.

38. Schelkin, K.I. and Troshin, Ya K., Gasdynamics Of Combustion, Mono Book Corp. Baltimore, 1965.

39. Kawamura, R. and Saito, H., "Reflection Of Shock Waves-1, Pseudo-Stationary Case", Journal of the Physical Society of Japan, 11, No. 5, 1956.

40. Sternberg, J., "Triple Shock Wave Intersections", Physics of Fluids, 2, No. 2, 1959.

41. Molder, S., "Reflection Of Curved Shocks", Seventh Congress of the International Council of Aeronautical Sciences, Rome, Italy, 1970.

42. Deckker, B.E.L. and Gururaja, J., "An Investigation Of Shock Wave Behavior In Ducts With A Gradual Or Sudden Enlargement In Cross Sectional Area", Proceedings of the Institution of Mechanical Engineers, 184, Pt. 3G, 1969-70.

43. Mirels, H., "Source Distribution Method For Unsteady One Dimensional Flows With Small Mass, Momentum And Heat Addition And Small Area Variation", NASA Memo 5-4-59E, 1959.

44. Mirels, H. and Mullen, J.F., "Shock Bounded Self-Similar Flows With Volumetric Mass, Momentum And Energy Addition", Report No. TDR 69/2230-01/TR-2 Aerospace Corp. El Segundo, Cal., 1962.

45. Rosciszewski, J., "Calculations Of The Notion Of Non-Uniform Shock Waves", Journal of Fluid Mechanics, 8, 1961.

46. Wu, J.H.T. and Ostrowski, P.P., "Shock Attenuation In A Perforated Duct", Shock Tube Research, Chapman and Hall, London, 1971. J.L. Stollery, A.G. Gaydon and P.R. Owen, Editors.

47. Szumowski, A.P., "Attenuation Of A Shock Wave Along A Perforated Tube", Shock Tube Research, Chapman and Hall, London, 1971. J.L. Stollery, A.G. Gaydon and P.R. Owen, Editors.

48. Dosanjh, D.S., "Interaction Of Grids With Travelling Shock Waves", NACA TN 3680, 1956.

49. Dresner, L. and Chester, C.K., "Attenuation Of Shocks In Tubes By Orifice Plates", Oak Ridge National Laboratory Report ORNL TM-1750, 1967.

50. Davies, P. and Dwyer, M.J.' "A Simple Theory For Pressure Pulses In Exhaust Systems", Proceedings of the Institution of Mechanical Engineers, 179, Pt. 1, No. 10, 1964-65.

51. Deckker, B.E.L. and Male, D.H., "Unsteady Flow In A Branched Duct", Proceedings of the Institution of Mechanical Engineers, 182, Pt. 3H, 1967-68.

52. Deckker, B.E.L. and Male, D.H., "Fluid Dynamic Aspects Of Unsteady Flow In Branched Ducts", Proceedings of the Institution of Mechanical Engineers, 182, Pt. 3H, 1967-68.

53. Chester, W., "The Quasi-Cylindrical Shock Tube", Phil. Mag. 45, 1954.

54. Chisnell, R.F., "The Motion Of A Shock Wave In A Channell With Applications To Cylindrical And Spherical Shock Waves", Journal of Fluid Mechanics, 2, 1957.

55. Chester, W., "The Propagation Of Shock Waves Along Ducts Of Varying Cross Section", Advances in Applied Mechanics, 6, 1960.

56. Honda, M., Takayama, K. and Onodera, O., "Study On The Motion Of Shock Waves Propagating Along Perforated Ducts", Institute of High Speed Mechanics, Tohoku University, Report No. 272, Sendai, Japan, 1974.

57. Friedman, M.P., "An Improved Perturbation Theory For Shock Waves Propagating Through Non-Uniform Regions", Journal of Fluid Mechanics, 8, 1960.

58. Wu, J.H.T. and Ostrowski, P.P., "Shock Interaction With A Narrow Slit", Canadian Aeronautics and Space Institute Transactions, 5, No. 1, 1972.

59. Glass, I.I., Martin, W., and Patterson, G.N., "A Theoretical and Experimental Study Of The Shock Tube", University of Toronto Institute of Aerophysics Report No. 2, 1953.

60. Freeman, N.C., "A Theory Of The Stability Of Plane Shock Waves", Proceedings of The Royal Society of London, Series A, 228, 1955.

61. Freeman, N.C., "On The Stability Of Plane Shock Waves", Journal of Fluid Mechanics, 2, 1957.

62. Lapworth, K.C., "An Experimental Investigation Of The Stability Of Plane Shock Waves", Journal of Fluid Mechanics, 6, 1959.

Appendix A

Idealized estimate of the average time required for a sound wave to traverse the flow through the slit.

According to Rudinger's approximate theory[7] the jet development time is proportional to the time required for a sound wave to traverse the flow in the vicinity of the slit. An average value between the initial and final flow configurations is recommended and this is computed on the basis of an idealized representation of the actual flow conditions.

For an incident shock Mach number M the Mach number, pressure and sound speed M_1, p_1, C_1 behind it are known from the Rankine-Hugoniot equations in terms of the ambient conditions (subscript 0). Now initially, before the jet is formed the speed of a sound wave is simply $u_1 + c_1$ so the time required for the wave to traverse a slit of width ℓ is

$$\frac{C_0 t}{\ell} = \frac{C_0/C_1}{1+M_1} \tag{A1}$$

An idealized representation of the flow conditions after the jet is formed is shown in figure (A1). For the purposes of this calculation the jet is assumed to be locally uniform with some velocity V and straight while inclined to the duct axis at some angle θ_j. If c is the local sound speed then from the figure

$$c^2t^2 = (Vt \sin\theta_j)^2 + (\ell - Vt\cos\theta_j)^2$$

and solving for t

$$t = \frac{\sqrt{V^2\cos^2\theta_j + C^2 - V^2} - V\cos\theta_j}{C^2 - V^2}$$

Then simplifying this further and introducing the local Mach number M = V/c

$$\frac{C_o t}{\ell} = \frac{C_o/C}{1-M^2}\left[\sqrt{1-M^2\sin^2\theta_j} - M\cos\theta_j\right] \qquad \text{(A2)}$$

Then the average time is

$$\frac{C_o \bar{t}}{\ell} \equiv \frac{C_o \tau}{\ell}$$

$$= \frac{1}{2}\left\{\frac{C_o/C_1}{1+M_1} + \frac{C_o/C}{1-M^2}\left[\sqrt{1-M^2\sin^2\theta_j} - M\cos\theta_j\right]\right\} \qquad \text{(A3)}$$

Once the local Mach number at the slit is established the calculation of t is straight forward.

Appendix B

Calculation of the external jet structure for $M = 2.33$ and a slit width of 3/8 inches.

The supersonic flow field in the immediate vicinity of the slit is sketched in Figure B1. Due to a slight bluntness (0.03 in.) and oblique flow direction, the stationary portion of the shock stands off a distance L from the downstream edge of the slit. Since the particle velocity is supersonic, a Prandtl-Meyer expansion stands at the upstream edge of the slit and at the shoulder of the downstream edge as well. The external portion of the detached shock reflects from the boundary of the emerging fluid jet and gives rise to a decidedly unsymmetrical and complex jet structure. The purpose of this section is to show that once the stand off distance L and the shock shape can be estimated from an approximate theory due to Moeckel[6], the jet structure can be easily computed by the method of characteristics.

The details of Moeckel's theory are not given here although it is based on the fact that the shape of detached shock waves are somewhat insensitive to the actual shape of the body that causes them. Then the shock shape is assumed to be hyperbolic so that for a given free stream Mach number M it is given by

$$\beta y' = \sqrt{x'^2 - x_0'^2} \qquad \text{(B1)}$$

$$\beta = \sqrt{M^2 - 1}$$

and X_0' is the distance from the wave vertex to the intersection of its asymptotes as shown in the figure. Application of a simplified continuity relation leads to an expression for X_0 which is conveniently plotted versus M by the author. The shock standoff distance L is determined from a simple geometric argument based on the experimental evidence that the body sonic point is often very close to a sharp shoulder. It is found that

$$\frac{L}{y_*'} = \cot \theta_d(M) \qquad \text{(B2)}$$

where y_*' is the coordinate of the body sonic point (shoulder) and θ_d' is the detachment angle corresponding to M. Therefore if the Mach number M approaching the downstream edge of the slit is known the shock shape can be easily constructed from equations (B1) and (B2) with X_0 given from Moeckel's data. It should be pointed out that equation (B1) is considered to be valid only up to the shock sonic point. This is determined by assuming the sonic line is straight in the case of sharp shouldered bodies. However, for the present case equation (B1) is extended beyond the sonic point to the jet boundary as a further approximation.

Now since L is not known in advance M is not known either. In other words, the Mach line from the upstream edge of the slit which just intersects the X' axis at $X' = X_0'$ is not known beforehand. It can, however, be found by iteration. Choose an X", y" coordinate system fixed at the upstream edge of the slit. The equation of the Mach lines (which are C+ characteristics) is

$$y'' = -x'' \tan(\theta - \mu)$$

also

$$L = (x'' - \ell)\sec\theta = y''\csc\theta \tag{B3}$$

Therefore, eliminating y''

$$\frac{x''}{\ell} = \frac{\tan\theta}{\tan\theta + \tan(\theta - \mu)} \tag{B4}$$

The iteration is carried out by assuming a value for θ. Since the Mach number and flow direction ($\theta = 0$) are known ahead of the Prandtl-Meyer expansion, this immediately gives a trial value of M from which $(\theta - \mu)$ and then X''/ℓ is computed. Then L/ℓ is given by (B3) and compared to the value given by (B2). The iteration is continued until these two values agree.

A detailed calculation is presented for an incident shock Mach number $M = 2.33$, $p_0 = 0.95$ psia and $\ell = 3/8$ inches. Denoting the flow variables behind the undisturbed shock by the subscript (1) it is easily found by straight forward calculation that

$$M_1 = 1.13\,;\quad p_1/p_0 = 6.17\,,\quad p_{t_1}/p_0 = 13.63$$

If the flow conditions downstream of the Prandtl-Meyer expansion are given the subscript (j) then again straightforward calculation gives

$$M_j = 2.36 \; , \; \theta_j = 33.59^\circ \; , \; p_j = p_0$$

and iteration of equations (B2), (B3) and (B4) gives with $b/\ell = 0.08$

$$M = 2.02 \; , \; \theta = 25.0^\circ \; , \; L/\ell = 0.169 \; , \; \theta_d = 23.25^\circ$$

where the latter value is taken from appropriate tables. Furthermore, from Moeckel's data (Figure 3 of his report)

$$\frac{x_0'}{y_*'} = \frac{x_0'}{b \cos\theta} = 18.6$$

so $X_0'/\ell = 1.350$. Therefore from (B1) the equation of the shock is

$$\left(\frac{x'}{\ell}\right)^2 = 3.080\left(\frac{y'}{\ell}\right)^2 + 1.823 \qquad \text{(B5)}$$

The next step is to compute the strength of the Prandtl-Meyer expansion at the shoulder of the downstream edge of the slit. Along the stagnation streamline ahead of the detached shock $M_x = M = 2.02$ and from the normal shock tables $p_{ty}/p_{tx} = .7115$, $p_y/p_x = 4.594$ hence downstream of the shock

p_{ty} = 9.21 psia, p_y = 4.364 psia. Now according to the approximate theory the head of the expansion wave is the sonic line M = 1 and the pressure there is p^* = .52828 (9.21) = 4.87 psia. At the tail of the expansion wave the pressure is ambient, p_0. Hence the pressure ratio across the expansion wave is p^*/p_0 = 5.122 and the Mach number M_t at the tail of the expansion is easily computed since the stagnation pressure is known.

$$M_t = 2.138 \;,\; \mu_t = 27.89^\circ \;,\; \nu_t = 30.14^\circ$$

At the shoulder Moeckel's analysis assumes that the flow inclination is θ_d relative to the "free stream" ($\theta = 25^0$) hence

$$\theta_* = 23.25 + 25 = 48.25^\circ$$

$$\theta_t = \theta_* - \Delta\nu = 48.25 - 30.14 = 18.11^\circ$$

which is the initial slope of the jet boundary downstream of the shoulder; the flow does not follow the surface of the wedge forming the downstream edge of the slit. The wave diagram is calculated on the basis of the characteristic relations

$$C+: \quad \frac{dy}{dx} = \tan(\theta - \mu) \;, \quad P = \theta + \nu = \text{CONSTANT}$$

$$C-: \quad \frac{dy}{dx} = \tan(\theta + \mu) \;, \quad Q = -\theta + \nu = \text{CONSTANT} \qquad \text{(B6)}$$

$$\theta = \frac{P - Q}{2} \;, \quad \nu = \frac{P + Q}{2}$$

and the diagram is started by using five elements to represent the expansion wave which is a C- family according to the chosen coordinate system. For convenience M is chosen for each element and using the same procedure as was done to compute θ_t, the flow angle θ for each characteristic can be easily determined. Then from equations (B6) Q is known along each of the characteristics.

During the course of the construction of the diagram several different types of interactions must be considered. First consider the reflection of the detached shock from the jet boundary. Since the shock shape is known beforehand the point of reflection can be found graphically. Then the slope of the shock can be computed from differentiation of equation (B5). It is found that the shock angle $\phi = 70.06^0$ relative to the (x, y) coordinate system by transforming the coordinates. However, the Mach number and flow direction ahead of the shock are $M_j = 2.36$, $\theta_j = 33.59^0$ so the effective shock angle is $\theta_s = 36.47^0$ and from the oblique shock charts the flow deflection $\delta = 13.0^0$ and Mach number downstream of the shock is M = 1.83. This is denoted by point 6 on the diagram, Figure (5.16). As before, the pressure ratio across the reflected expansion wave is easily computed and this gives the new jet boundary Mach number $M_{14} = 2.313$.

Three elements are used to represent the reflected expansion wave which is a C+ family. As before, M is chosen for each element and the characteristic invariant P is found for each in the same manner as before.

Fortunately, almost the entire portion of the wave diagram that has been worked out corresponds to isentropic flow and the characteristic mesh is simple to construct in that case since P and Q are known on each of the respective characteristics. θ and ν (and hence M and μ) are computed immediately from equations (B6) and the mesh is constructed using the average slope between successive points.

Reflection of characteristics from the jet boundary is also easily handled as θ is known from the previous steps. Hence either P and θ or Q and θ are known in equations (B6) and it is a simple matter to solve for the remaining two variables.

Both expansion waves eventually reflect from the jet boundary as compression waves and ultimately converge to form oblique shock waves. This merging of characteristics is handled in the usual approximate way; the slope of the shock is taken to be the average of the slopes of the two merging characteristics. In the present case both shocks formed in this manner are seen to reflect from the jet boundary again (as expansion waves) shortly after their formation. Thus as a first approximation they may be considered weak so that the change in the characteristic invariants across them may be neglected.

The completed wave diagram showing the first "cell" of the emerging jet is shown in Figure (5.16). In spite of the many approximations employed for the construction, it surprisingly seems to give a fairly faithful picture of the actual flow field observed from schlieren photography. The pertinent parameters associated with each point shown on the diagram is presented in Table (B1) which is self-explanatory.

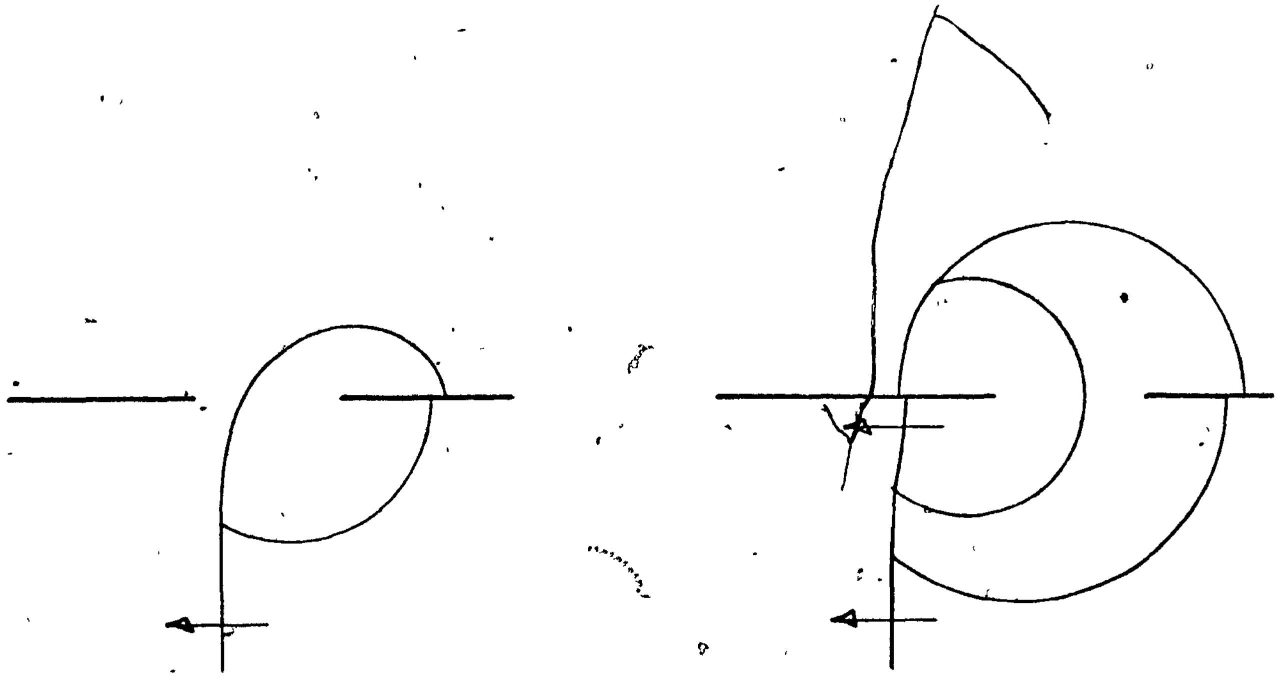

(a) DIFFRACTION

(b) DIFFRACTION AND MACH REFLECTION

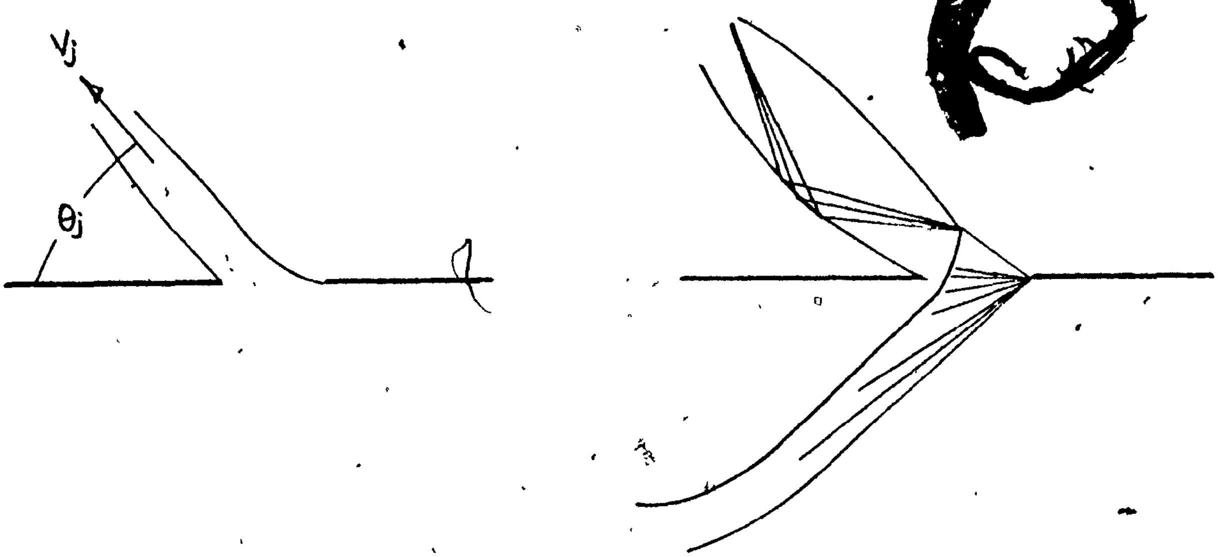

(c) STEADY STATE CONFIGURATION (SUBSONIC FLOW)

(d) STEADY STATE CONFIGURATION (SUPERSONIC FLOW)

FIGURE 1.1: THE SHOCK-SLIT INTERACTION

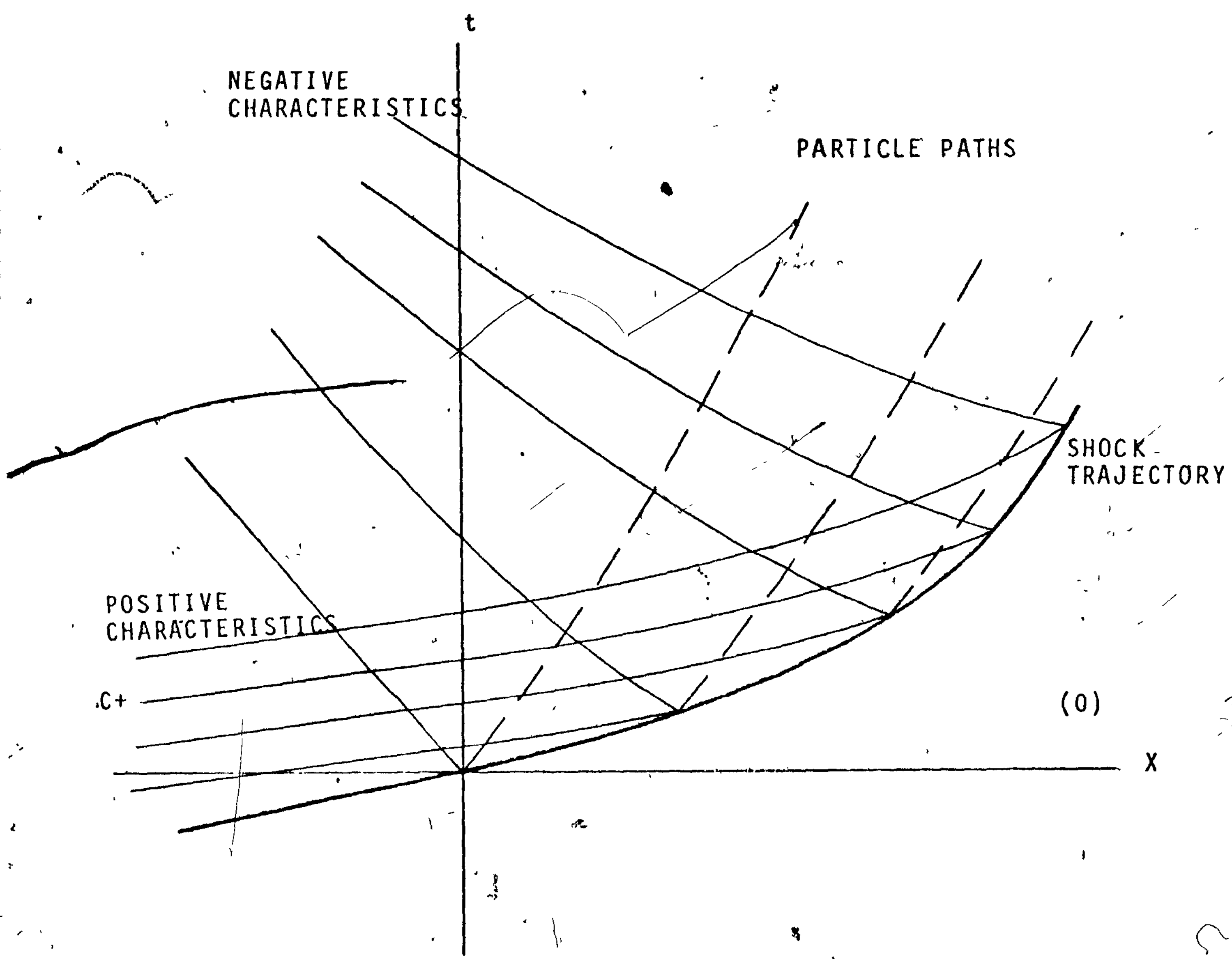

FIGURE 2.1: NON-UNIFORM SHOCK PROPAGATION IN THE x-t PLANE FOR SUBSONIC PARTICLE VELOCITY BEHIND THE UNDISTURBED SHOCK

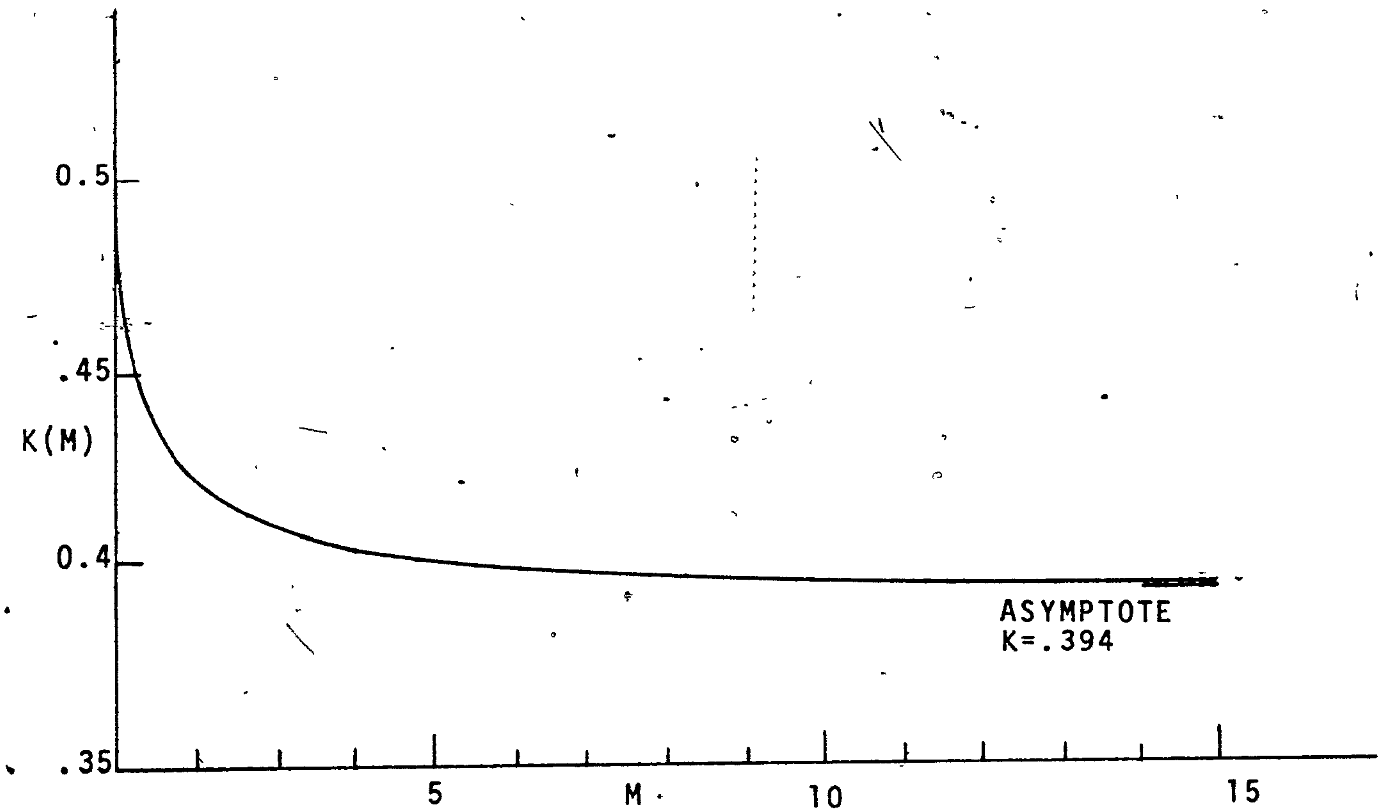

FIGURE 2.2: THE CHESTER FUNCTION K(M)

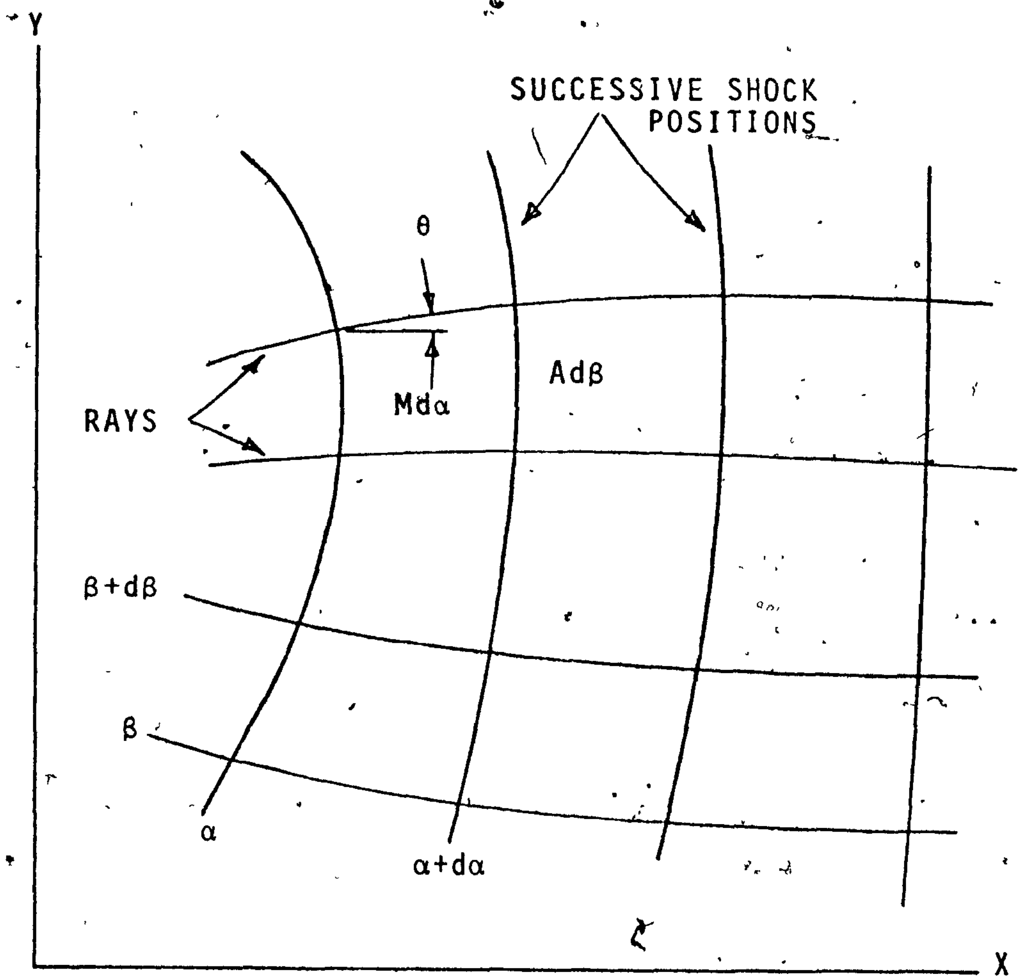

FIGURE 3.1: ORTHOGONAL RAY-SHOCK GRID FOR A TRAVELLING CURVED SHOCK

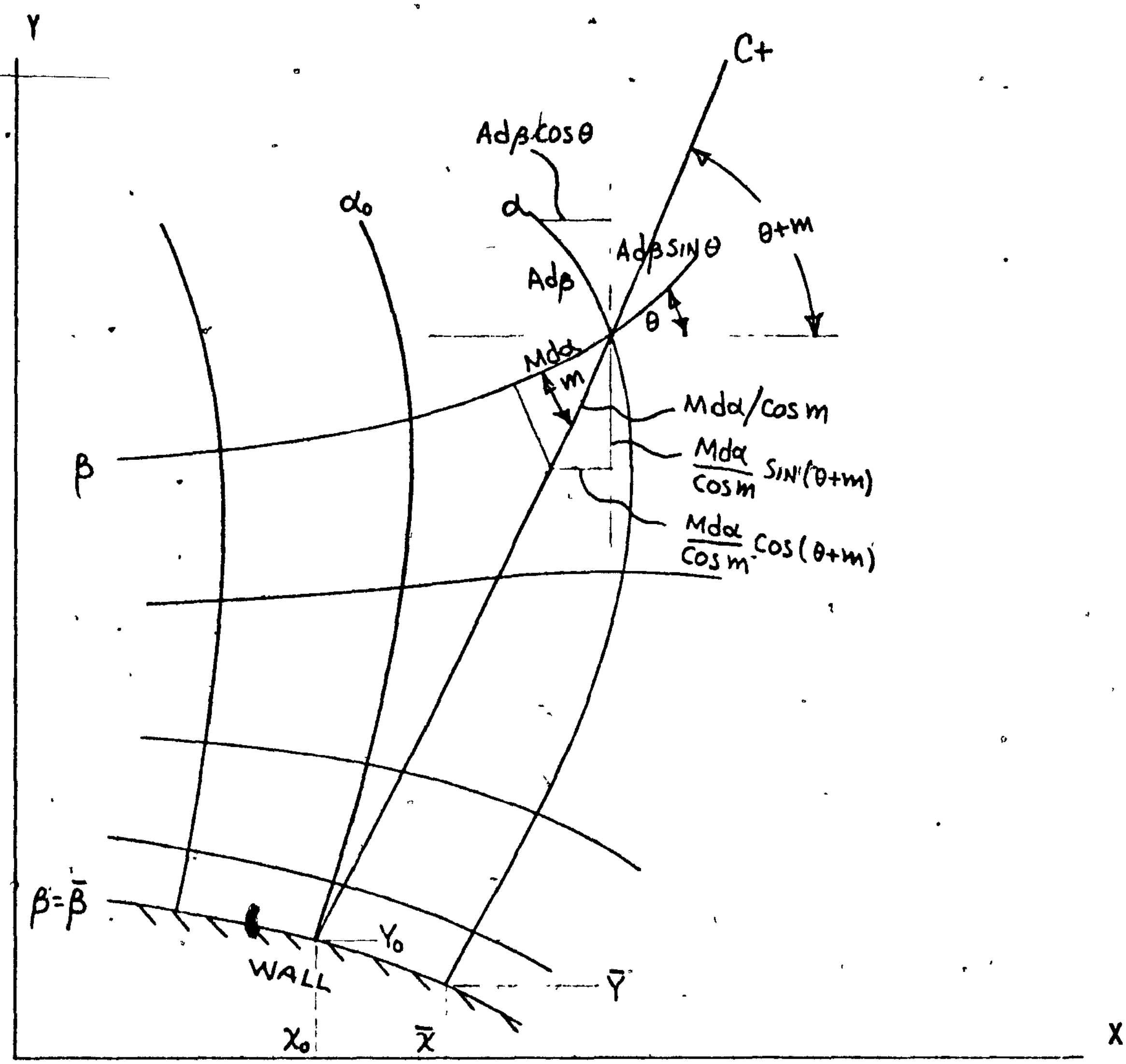

FIGURE 3.2: CHARACTERISTIC COORDINATES IN THE x-y PLANE

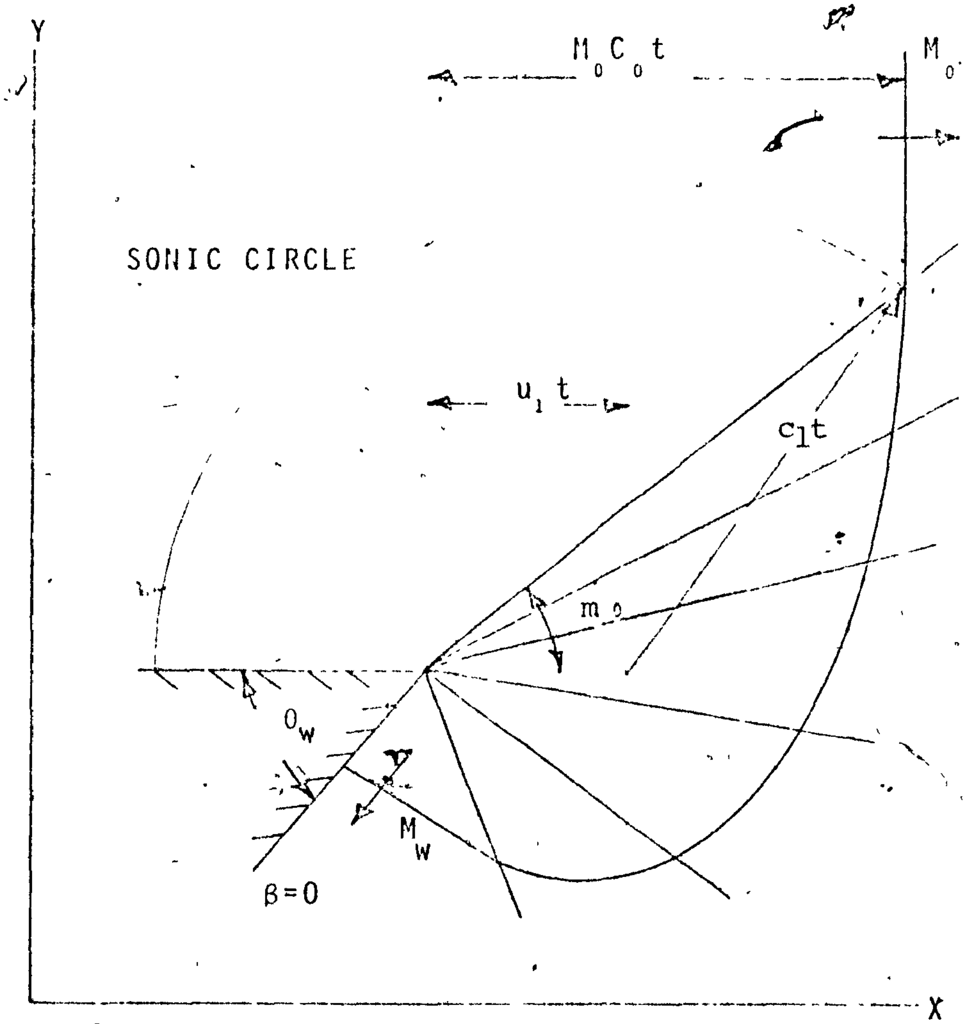

FIGURE 3.3: SHOCK DIFFRACTION AT A CONVEX CORNER. THE CASE FOR SUBSONIC PARTICLE VELOCITY BEHIND THE UNDISTURBED SHOCK IS SHOWN.

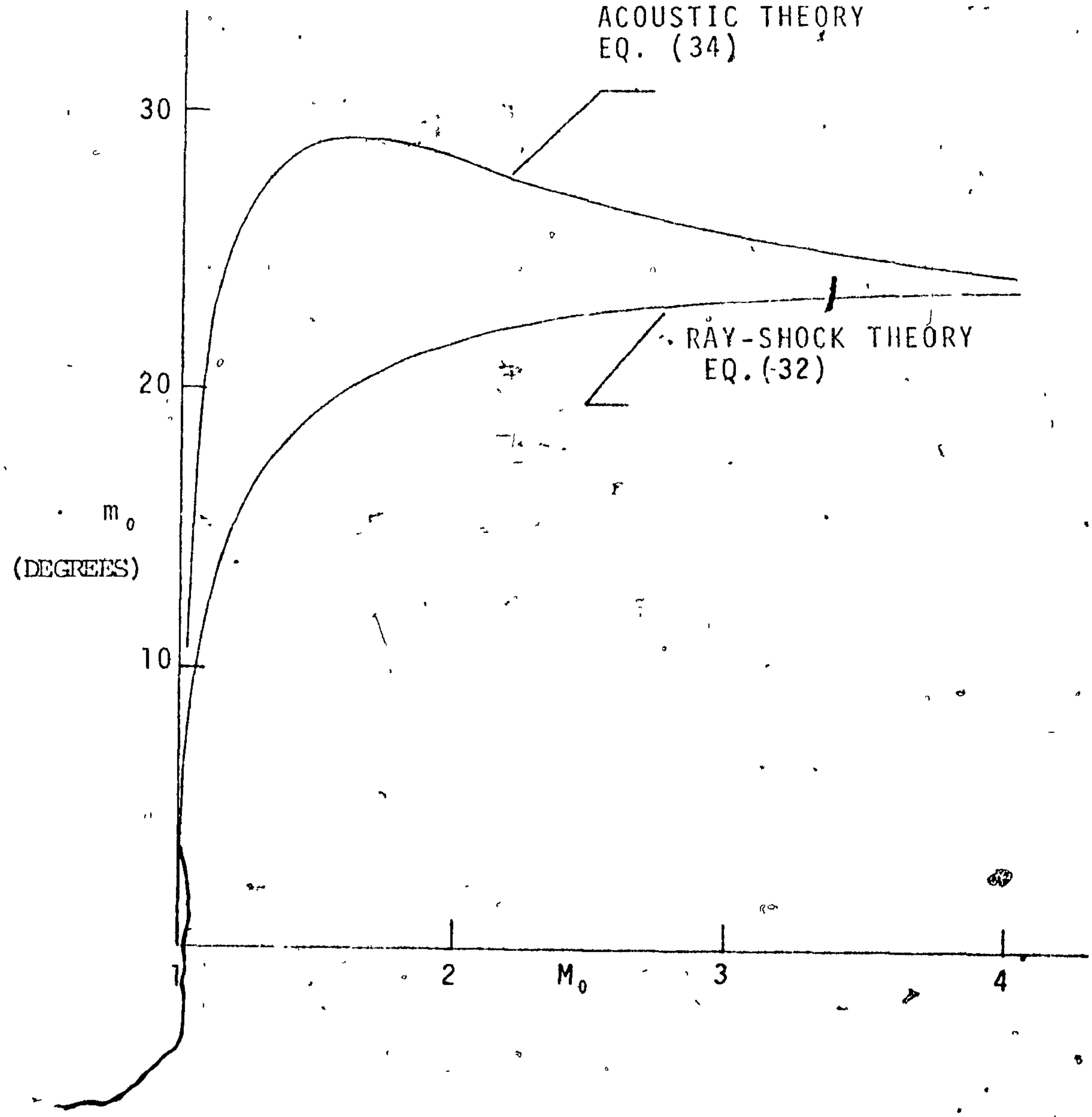

FIGURE 3.4: THE CHARACTERISTIC ANGLE m_0.

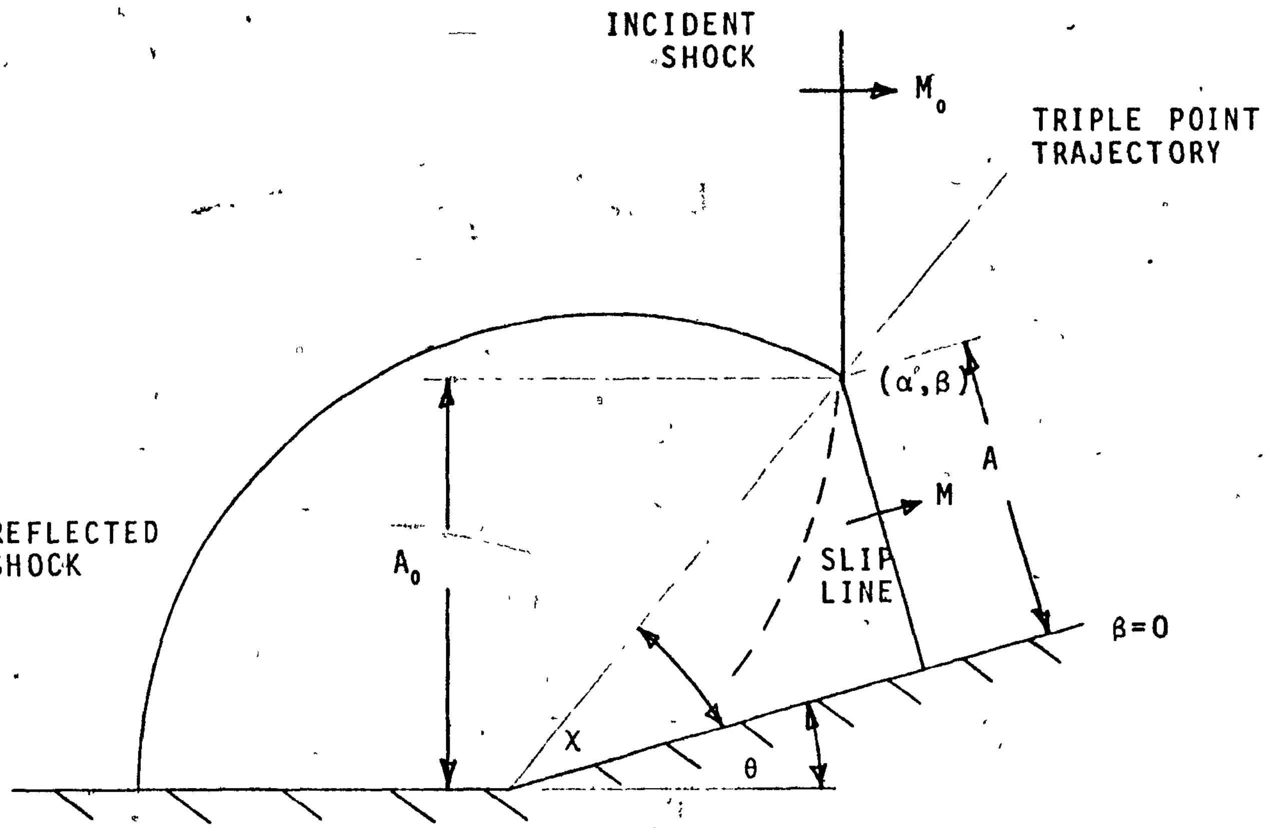

FIGURE 3.5: IDEALIZED MACH REFLECTION CONFIGURATION FOR SUBSONIC PARTICLE VELOCITY BEHIND THE INCIDENT SHOCK.

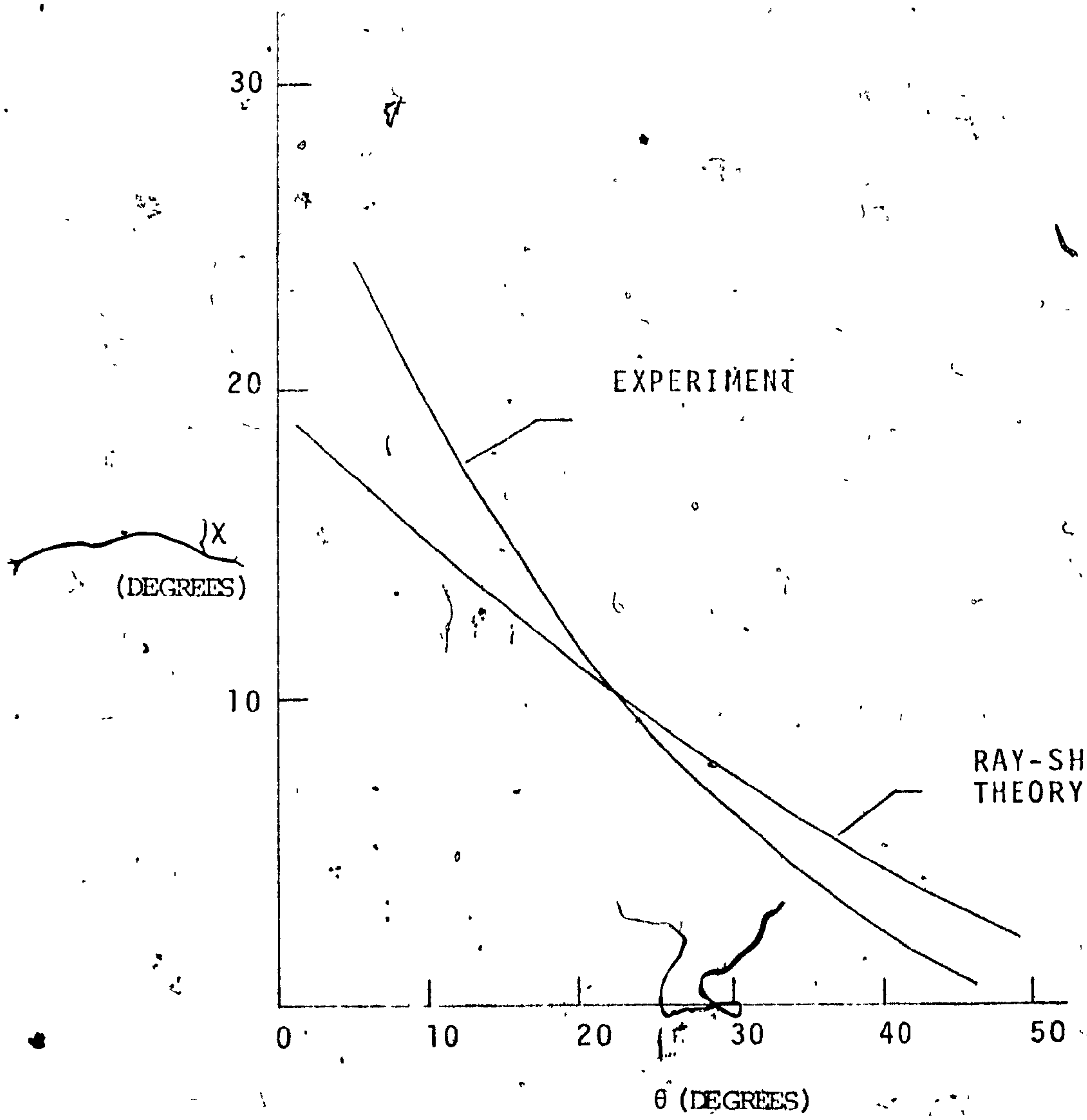

FIGURE 3.6: TRIPLE POINT LOCUS FOR M_0 = 1.51 TAKEN FROM MILTON[33].

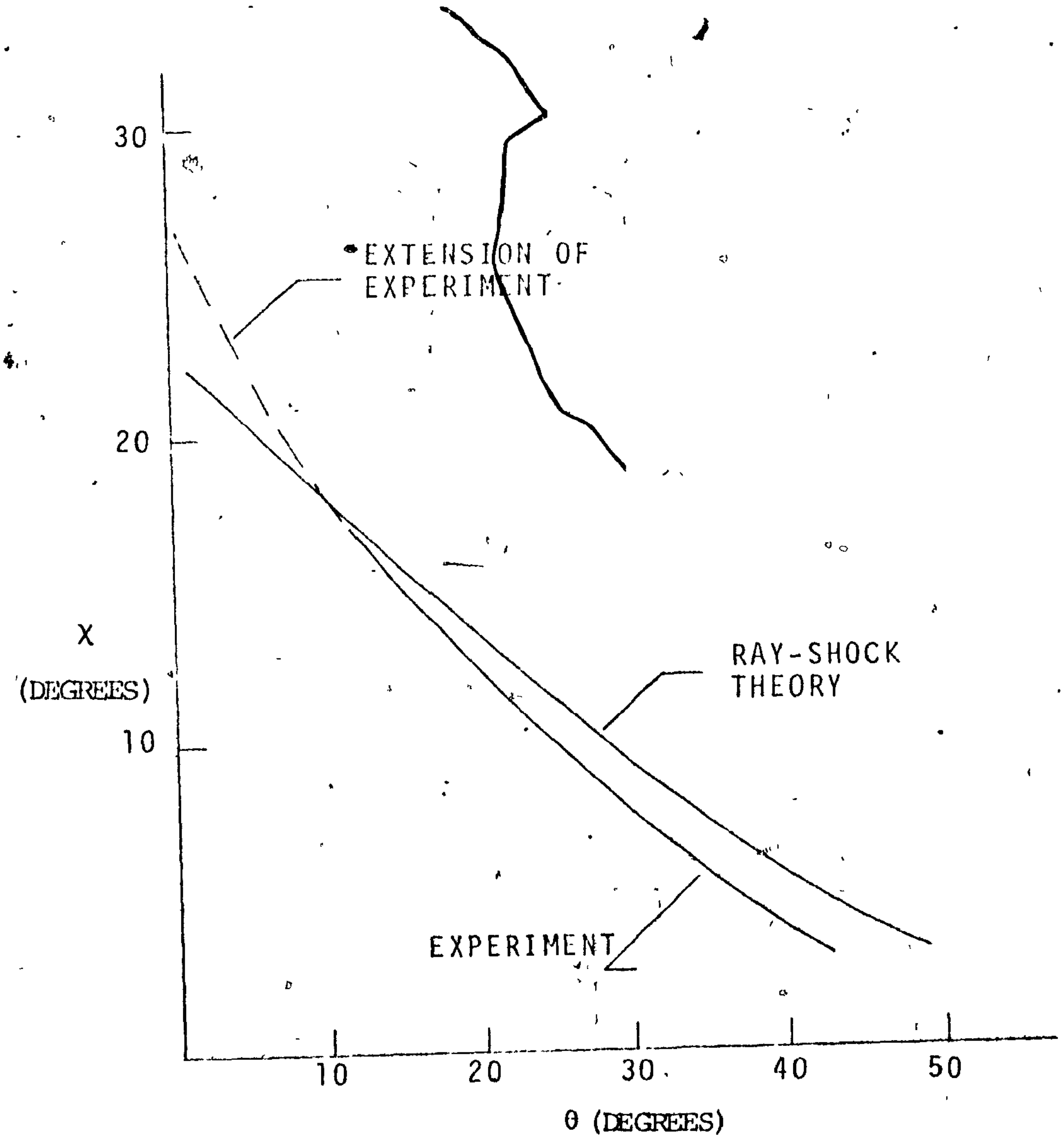

FIGURE 3.7: TRIPLE POINT LOCUS FOR $M_0 = 2.42$ TAKEN FROM MILTON[33].

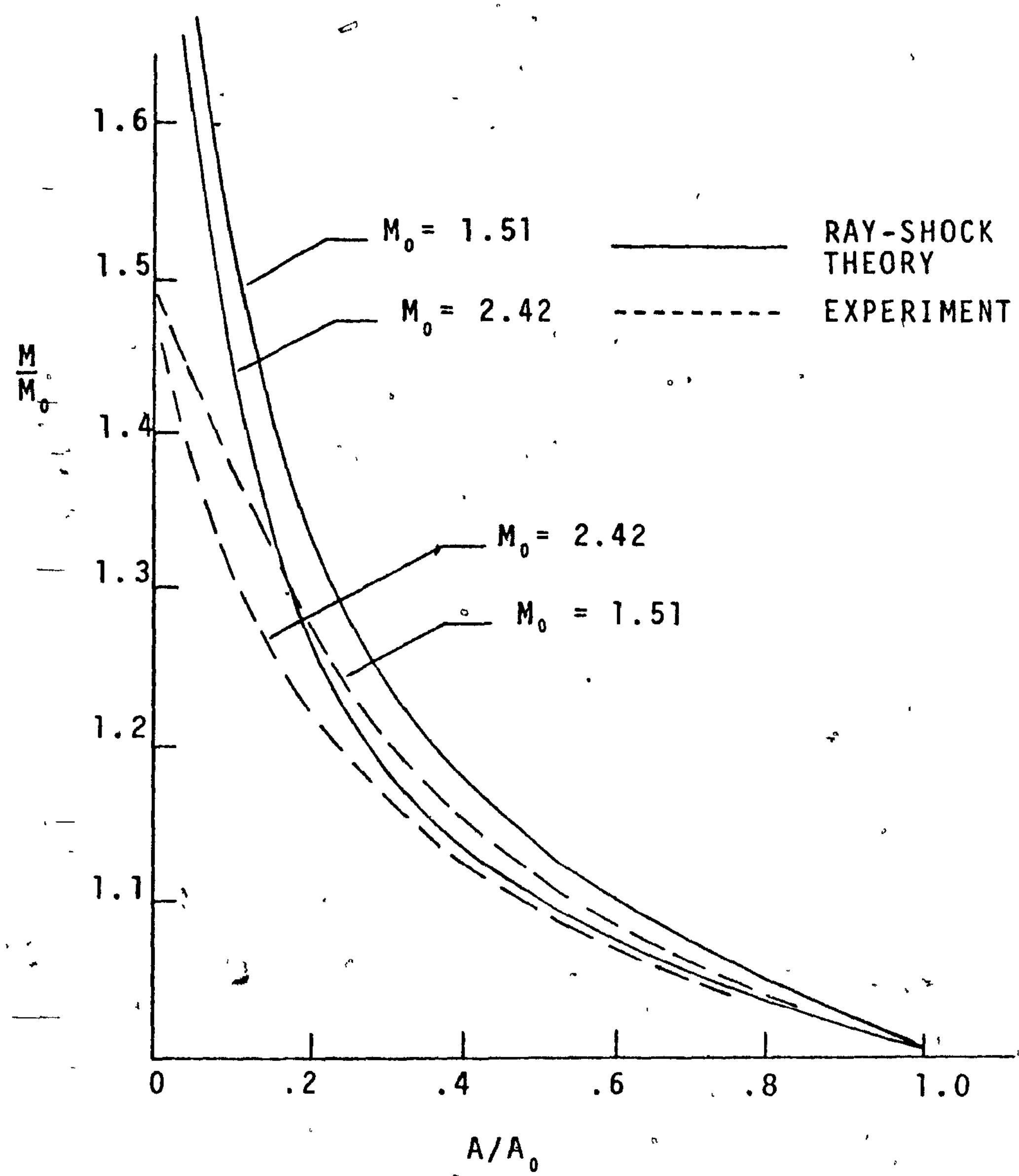

FIGURE 3.8: STEM SHOCK MACH NUMBER VERSUS STEM AREA RATIO. TAKEN FROM MILTON[33].

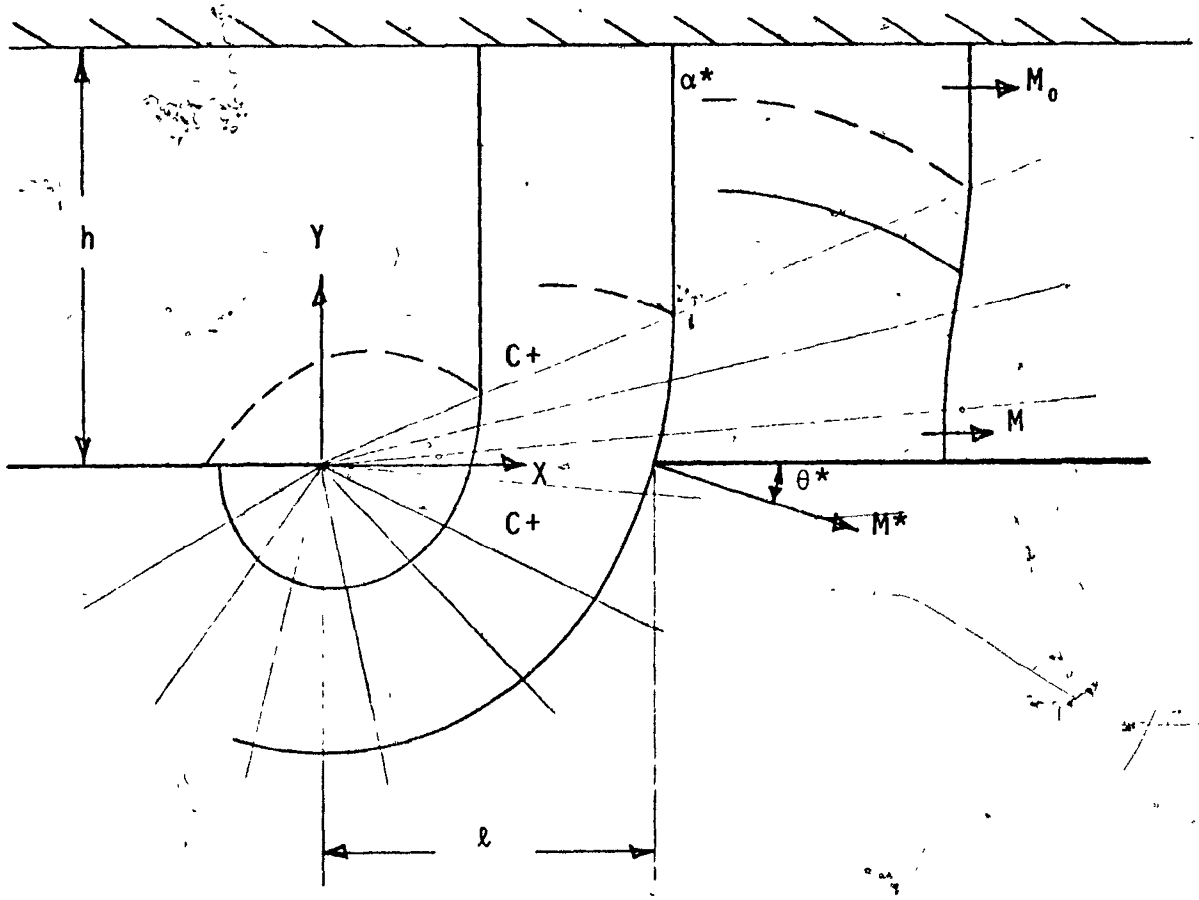

FIGURE 3.9: WAVE CONFIGURATIONS FOR SHOCK ATTENUATION IN A RECTANGULAR CHANNEL WITH A SLIT IN ONE WALL. EXPANSION WAVES ARE INDICATED BY BROKEN LINES.

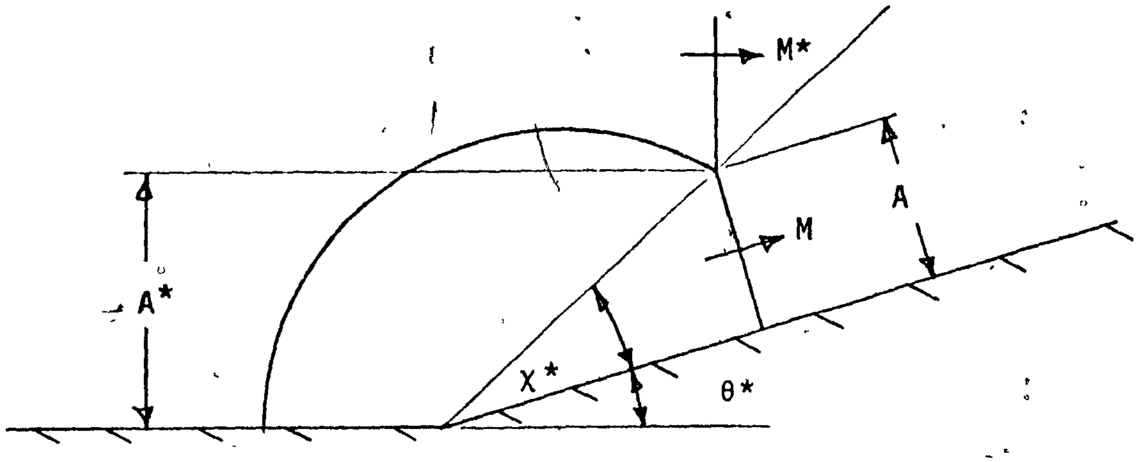

FIGURE 3.10: IDEALIZED REPRESENTATION OF THE MACH REFLECTION PROCESS AT THE DOWNSTREAM EDGE OF THE SLIT

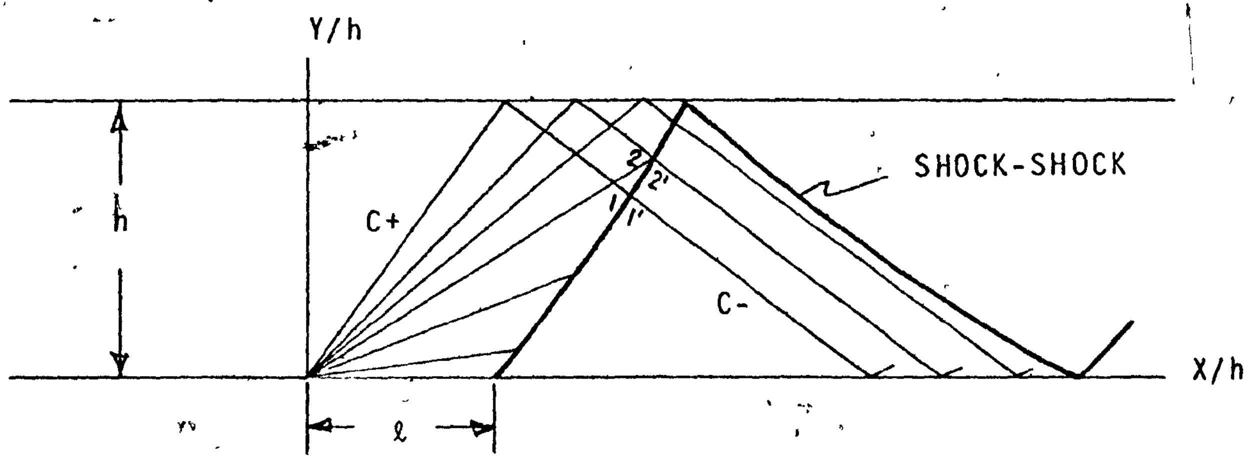

FIGURE 3.11: WAVE DIAGRAM SKETCH FOR THE PRESENT PROBLEM SHOWING ONE CYCLE OF THE MOTIØN

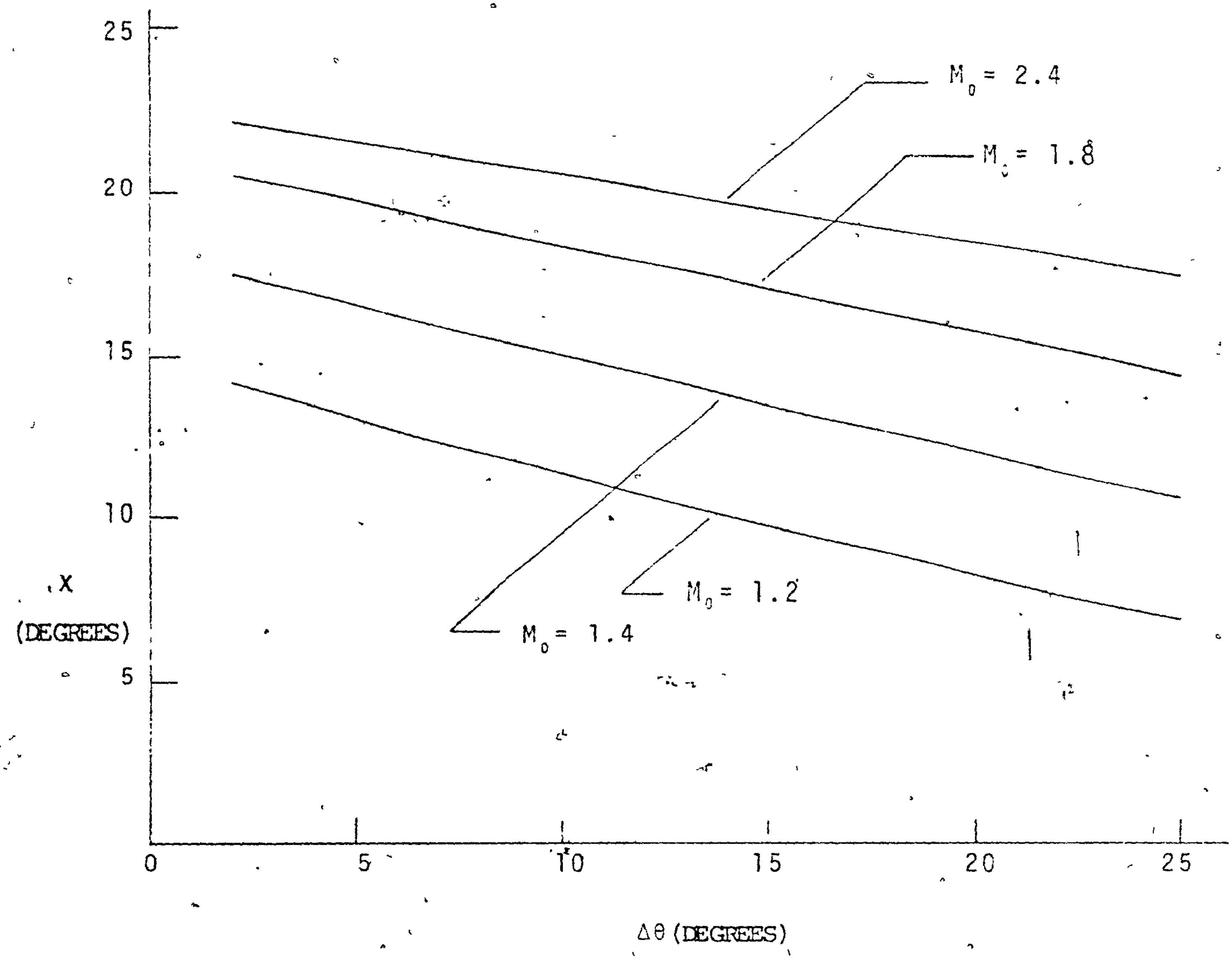

FIGURE 3.12: TRIPLE POINT LOCUS ANGLE χ VERSUS DEFLECTION ANGLE $\Delta\theta$ ACCORDING TO THE RAY-SHOCK THEORY (EQUATION 36).

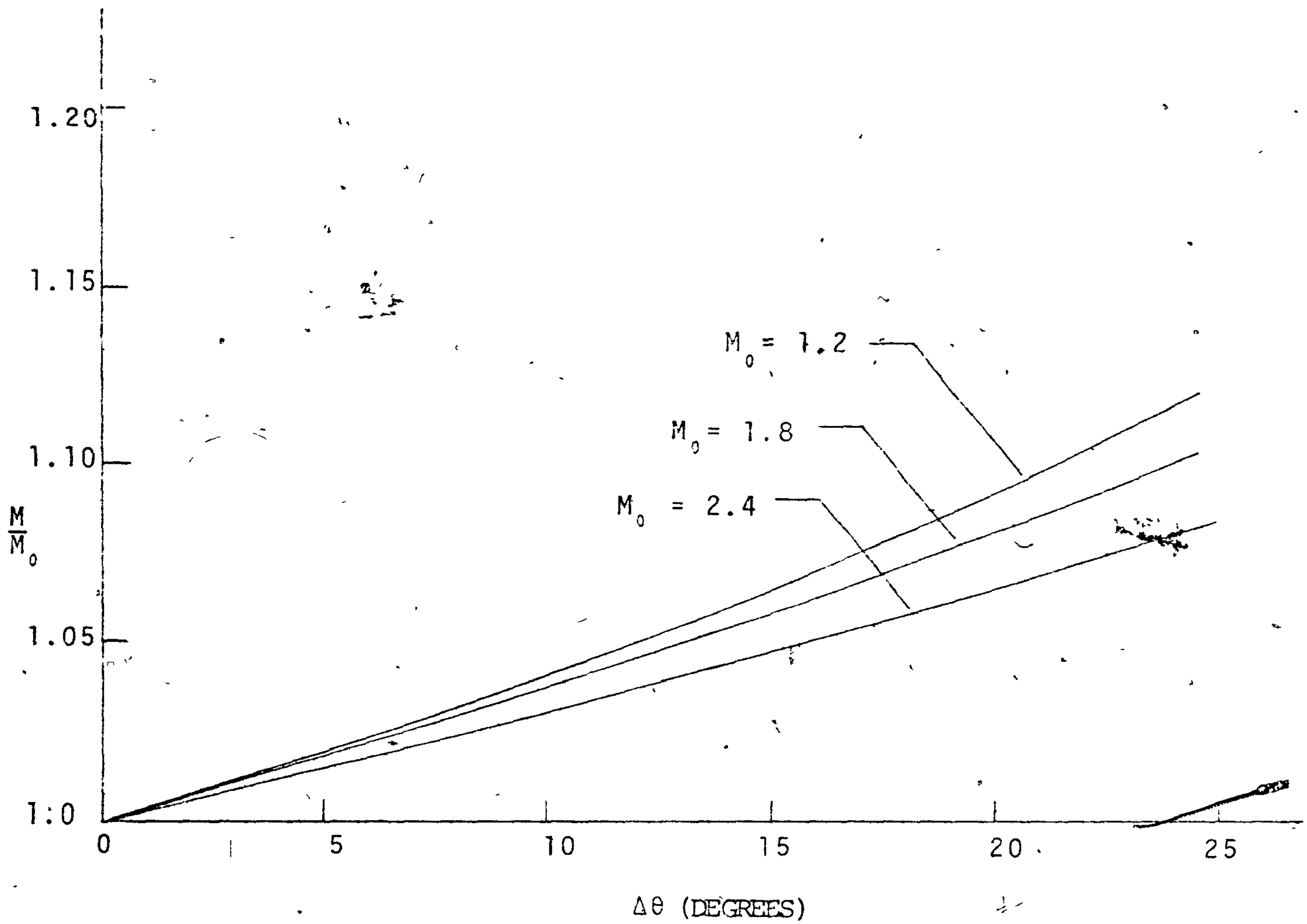

FIGURE 3.13: STEM SHOCK MACH NUMBER VERSUS DEFLECTION ANGLE Δθ ACCORDING TO THE RAY-SHOCK THEORY (EQUATION 37).

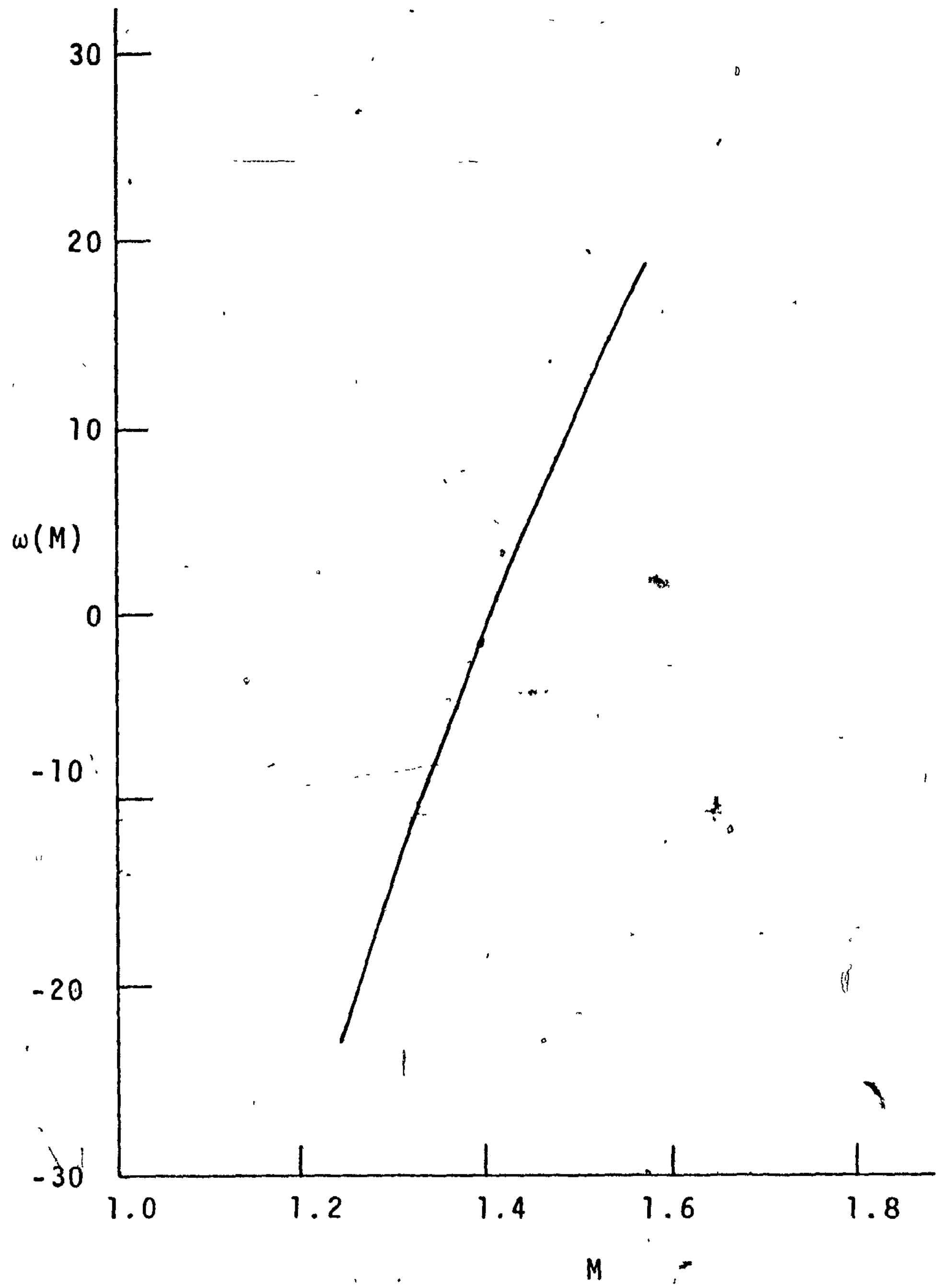

FIGURE 3.14: THE FUNCTION $\omega(M)$ IN DEGREES FOR $M_0 = 1.4$ ACCORDING TO THE RAY-SHOCK THEORY (EQUATION 30)

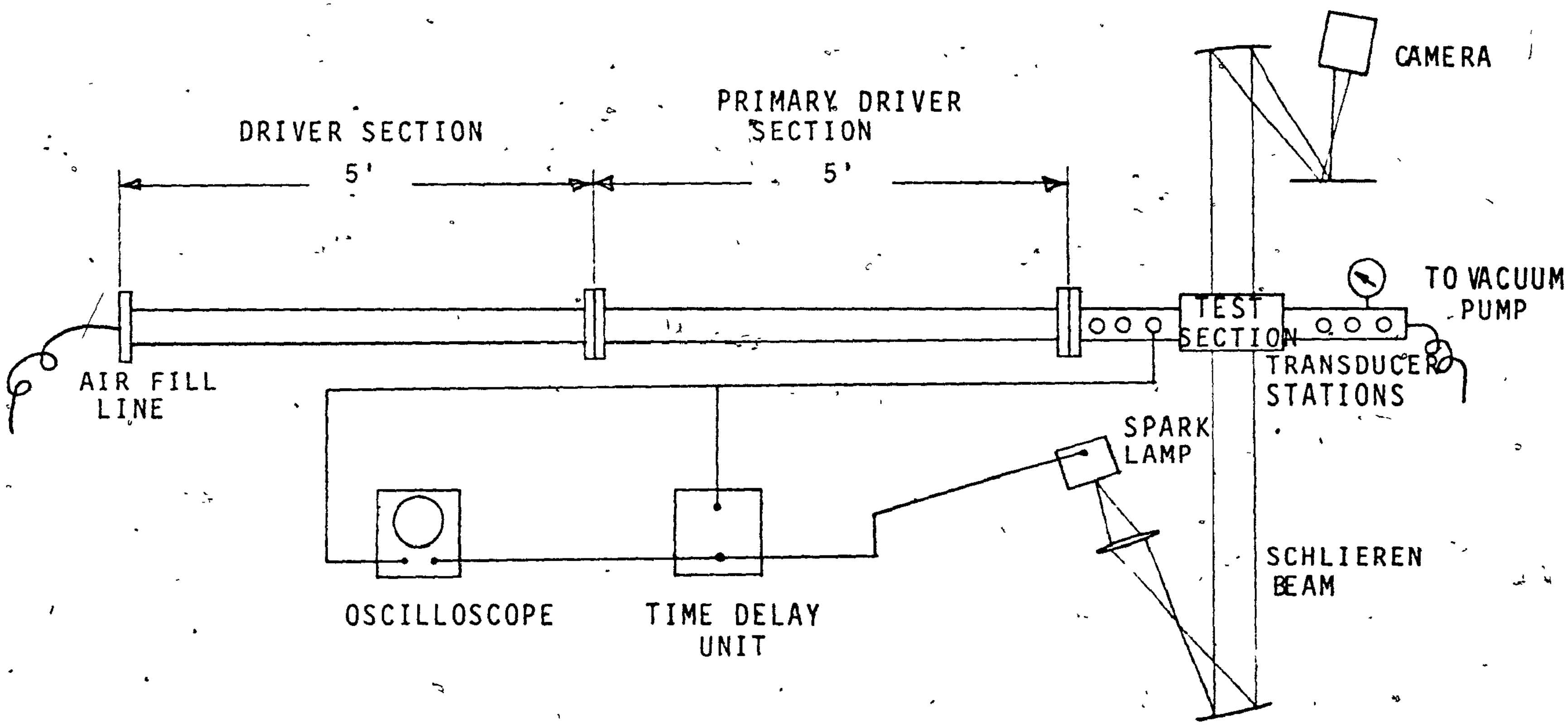

FIGURE 4.1: SCHEMATIC OF 2X2 INCH SHOCK TUBE AND ANCILLARY EQUIPMENT

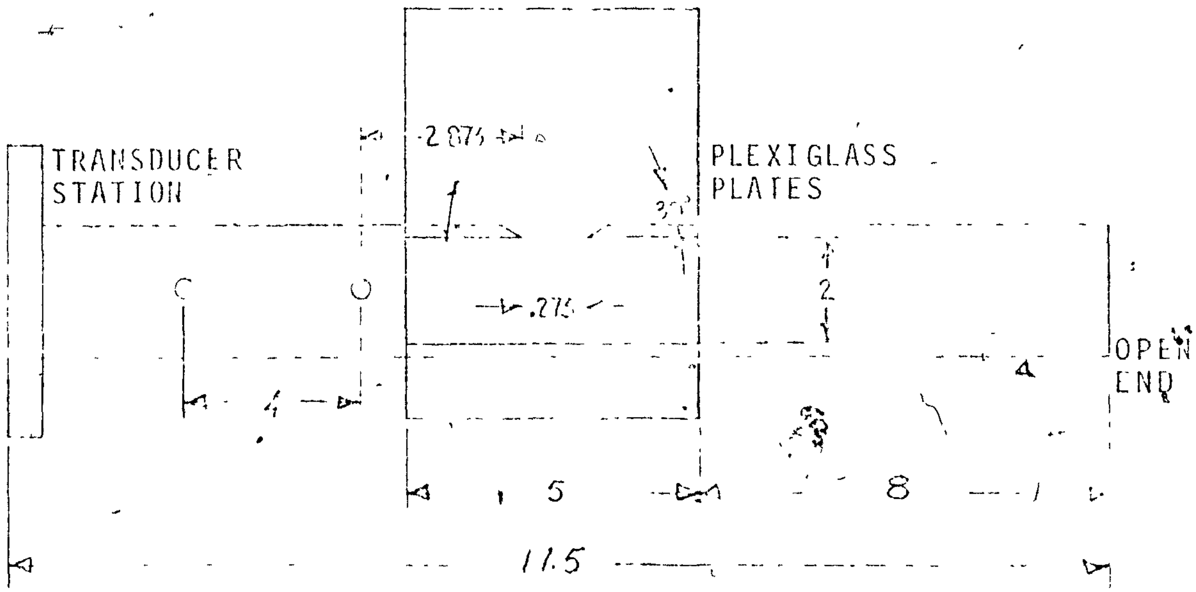

(a) TEST SECTION "A"

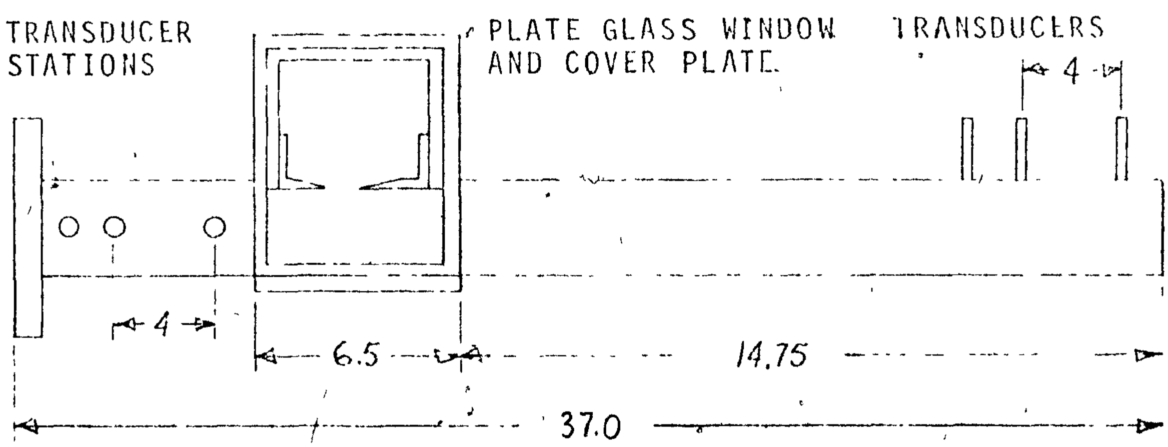

(b) TEST SECTION "B"

FIGURE 4.2: TEST SECTION SCHEMATICS. ALL DIMENSIONS IN INCHES.

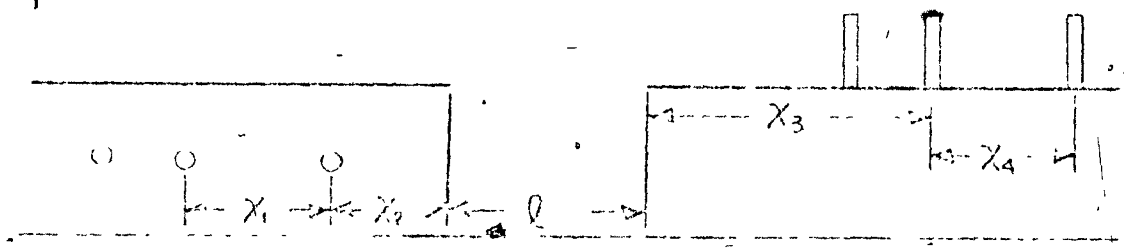

TEST SECTION	ℓ	x_1	x_2	x_3	x_4	h	ℓ/h
B	0	——	4.0	——	4.0	2	0
B	.068	2.624	4.0	20.183	4.0	2	.034
B	.250	2.442	4.0	20.183	4.0	2	.125
B	.750	2.442	4.0	19.683	4.0	2	.375
B	1.250	2.442	4.0	19.183	4.0	2	.625
A	.275	2.875	4.0	——	——	2	.138
B	.375	3.375	4.0	——	——	2	.138
B	.350	2.692	4.0	——	——	.680	.515

FIGURE 4.3: TEST CONDITIONS; ALL DIMENSIONS GIVEN IN INCHES.

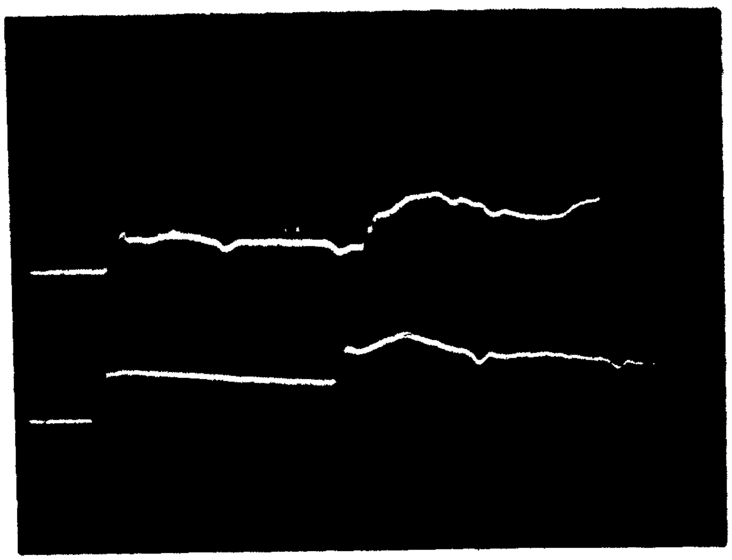

FIGURE 4.4: A TYPICAL OSCILLOGRAPH RECORD FOR M_0 = 1.67 AND = 1.25 INCHES. THE TIME SCALE IS 50 s/DIVISION.

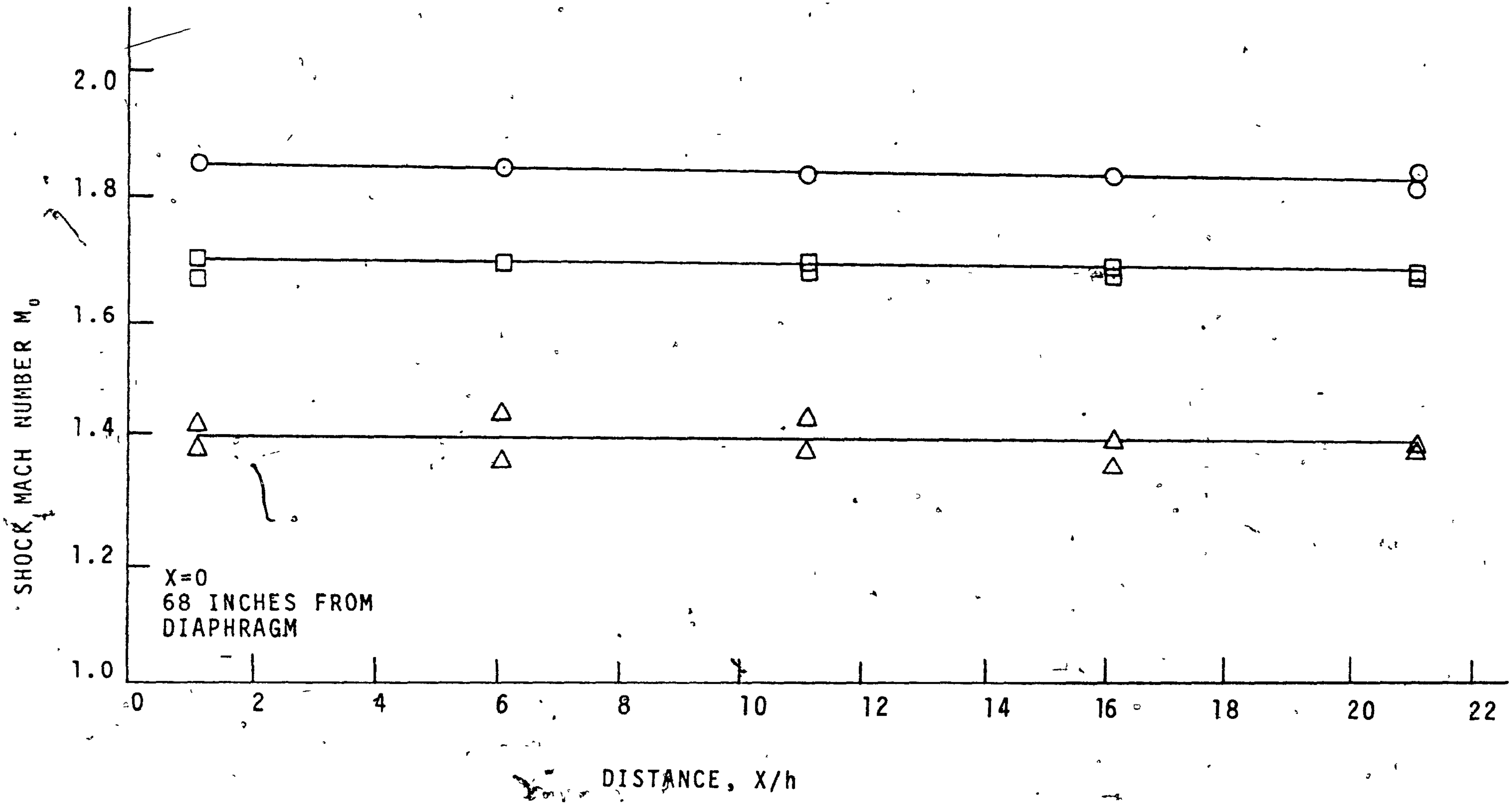

FIGURE 4.5: MEASUREMENTS OF SHOCK ATTENUATION DUE TO VISCOUS FORCES ALONE (NO SLIT).

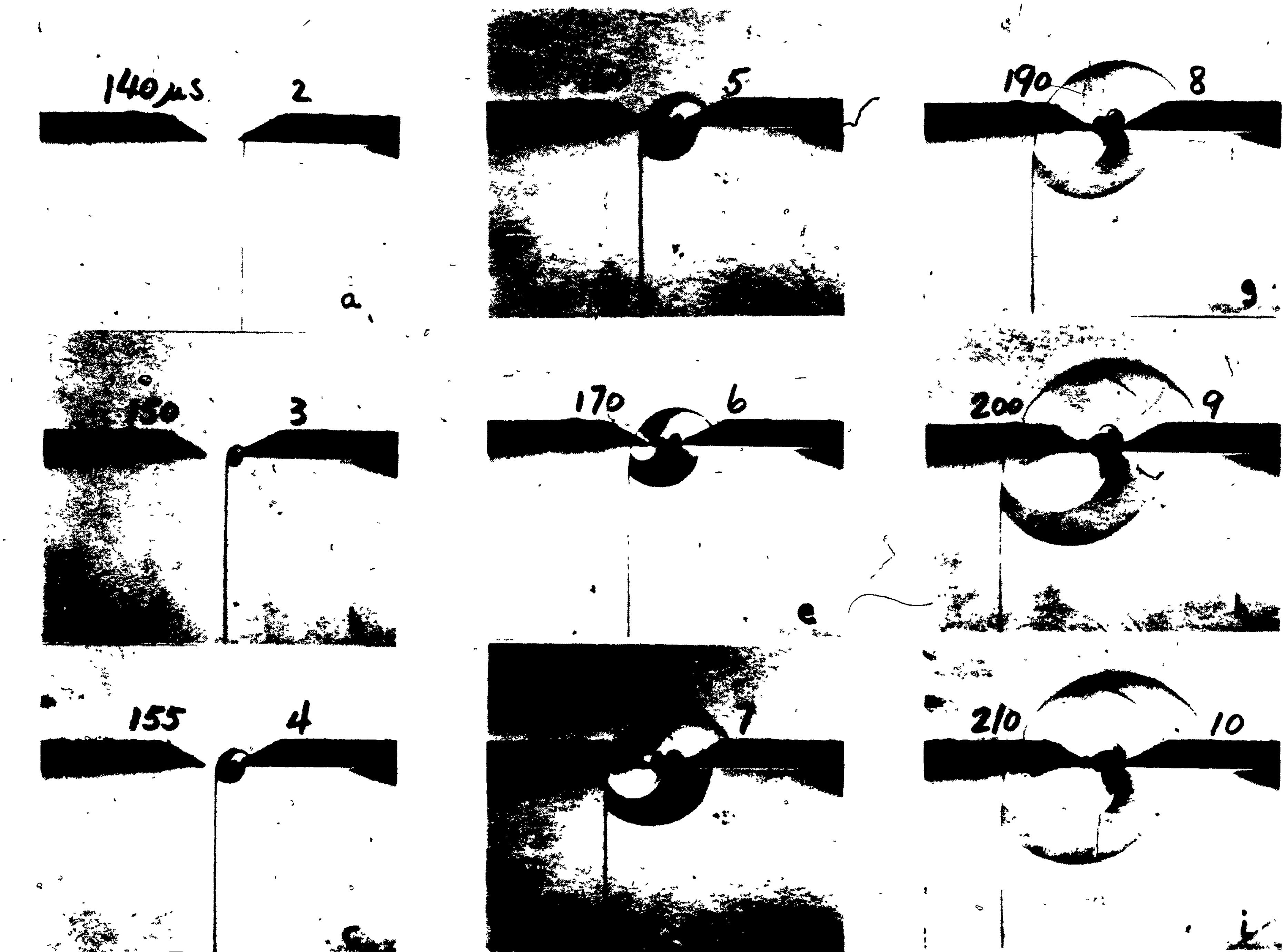

FIGURE 5.1. SHOCK-SLIT INTERACTION FOR M_0 = 1.41, [illegible] = 0.275 INCHES. MAGNIFICATION = 0.80

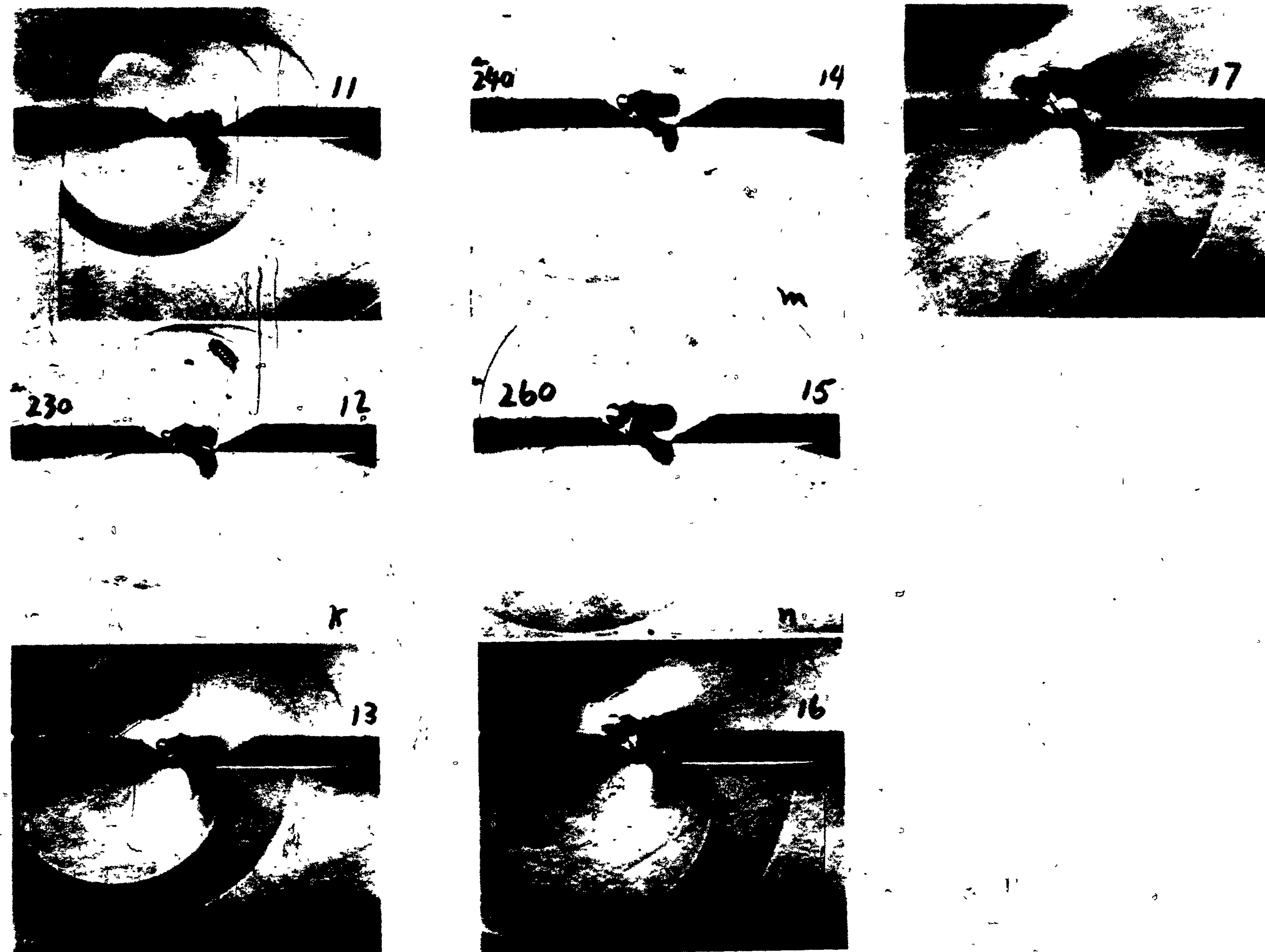

FIGURE 5.1: CONTINUED.

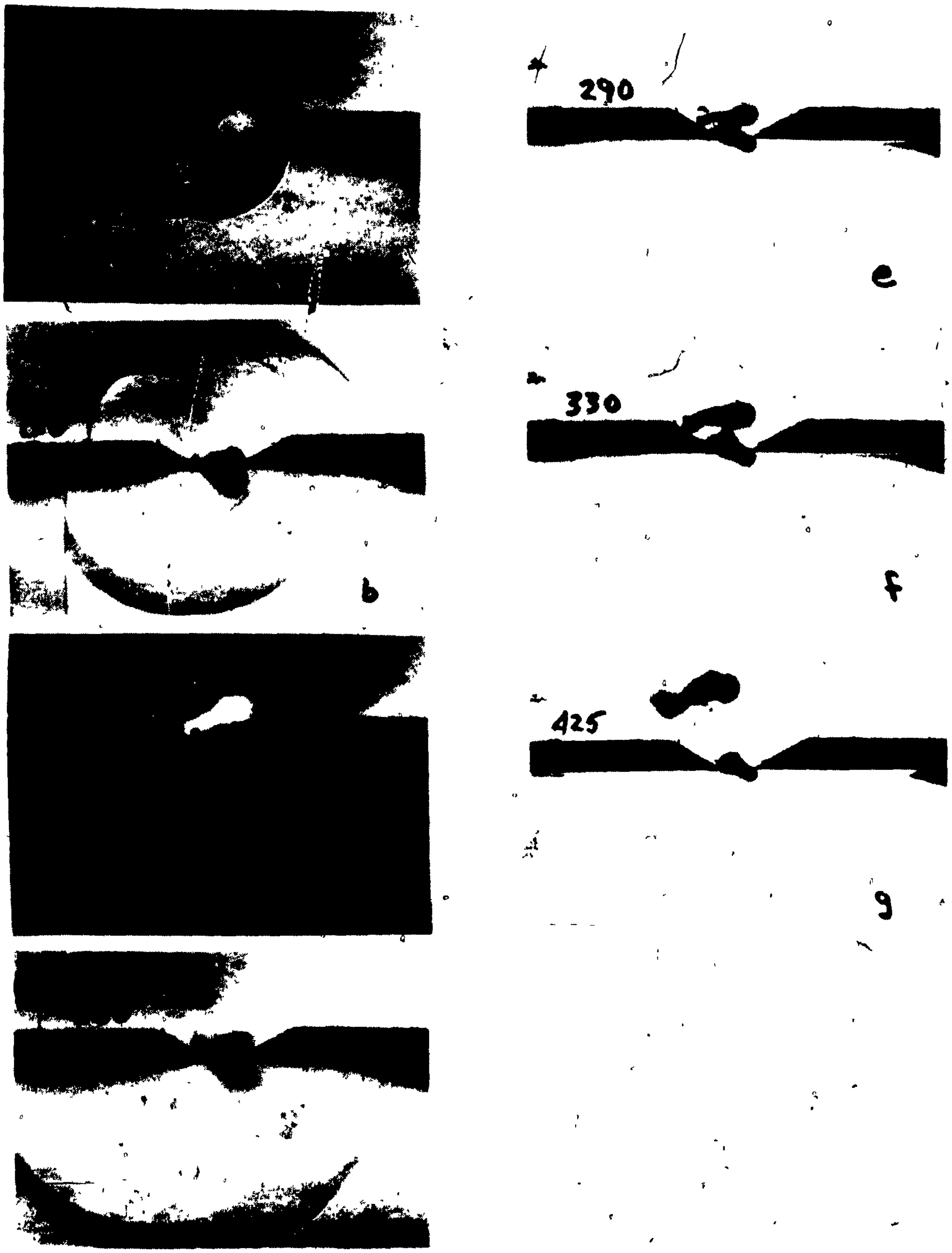

[illegible] INTERACTION FOR M_0 [illegible]
MAGNIFICATION [illegible]

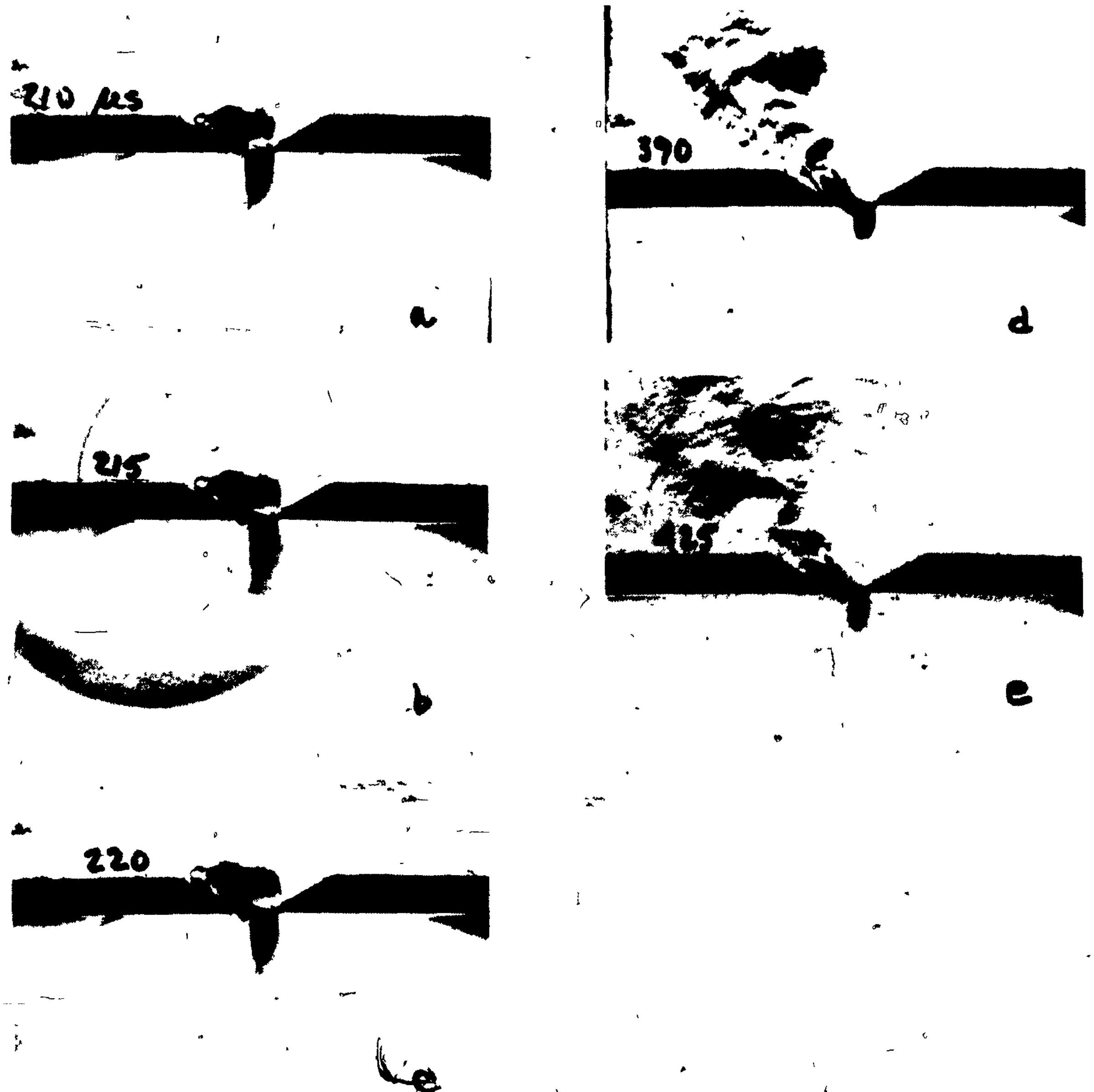

FIGURE 5.8. SHOCK-SLIT INTERACTION FOR $M_0 = 1.45$, [illegible] = .275.
MAGNIFICATION = .84.

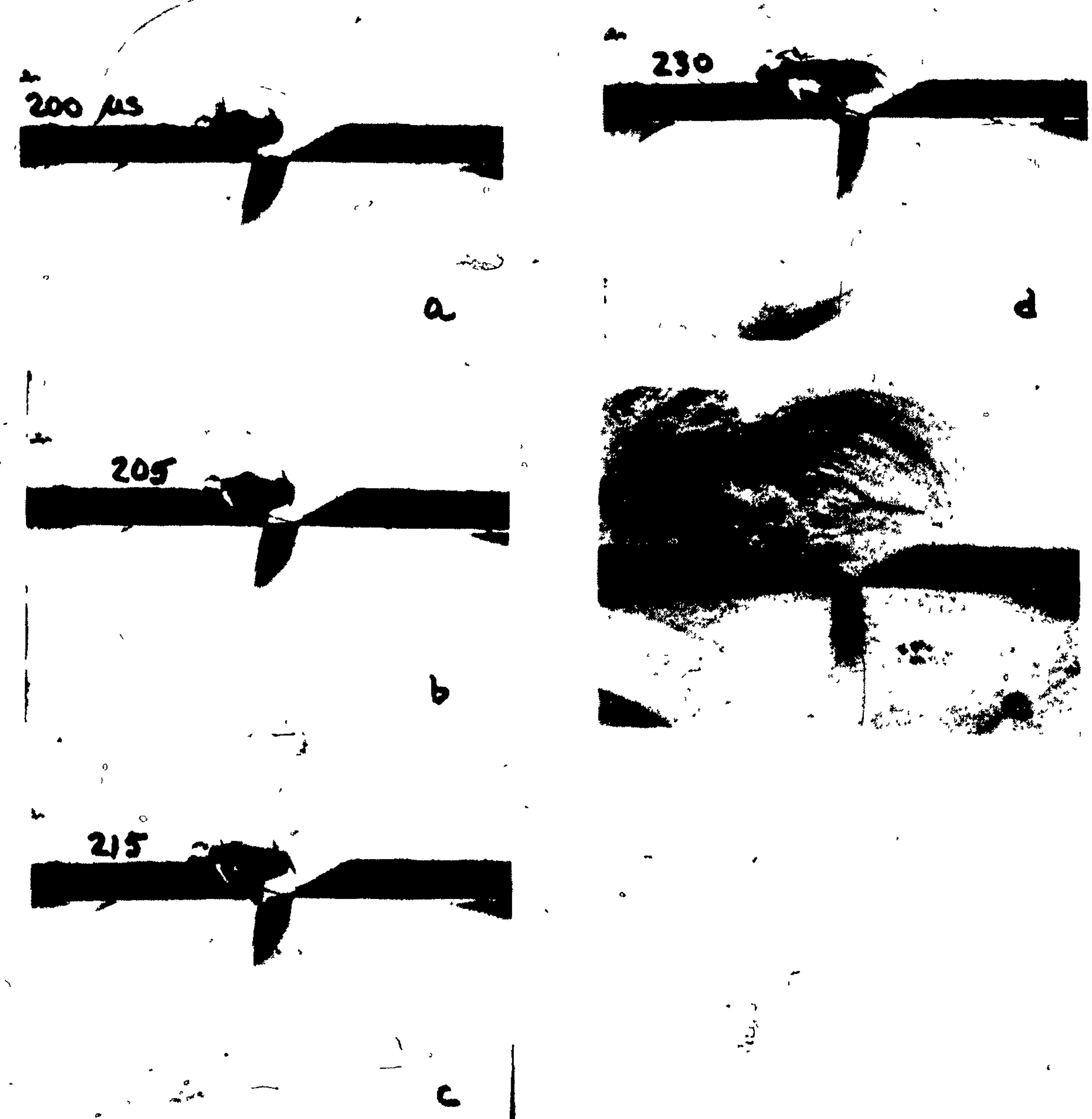

FIGURE 5.4: SHOCK-SLIT INTERACTION FOR M_0 = 1.60, w = .275 INCHES.

MAGNIFICATION = 0.84.

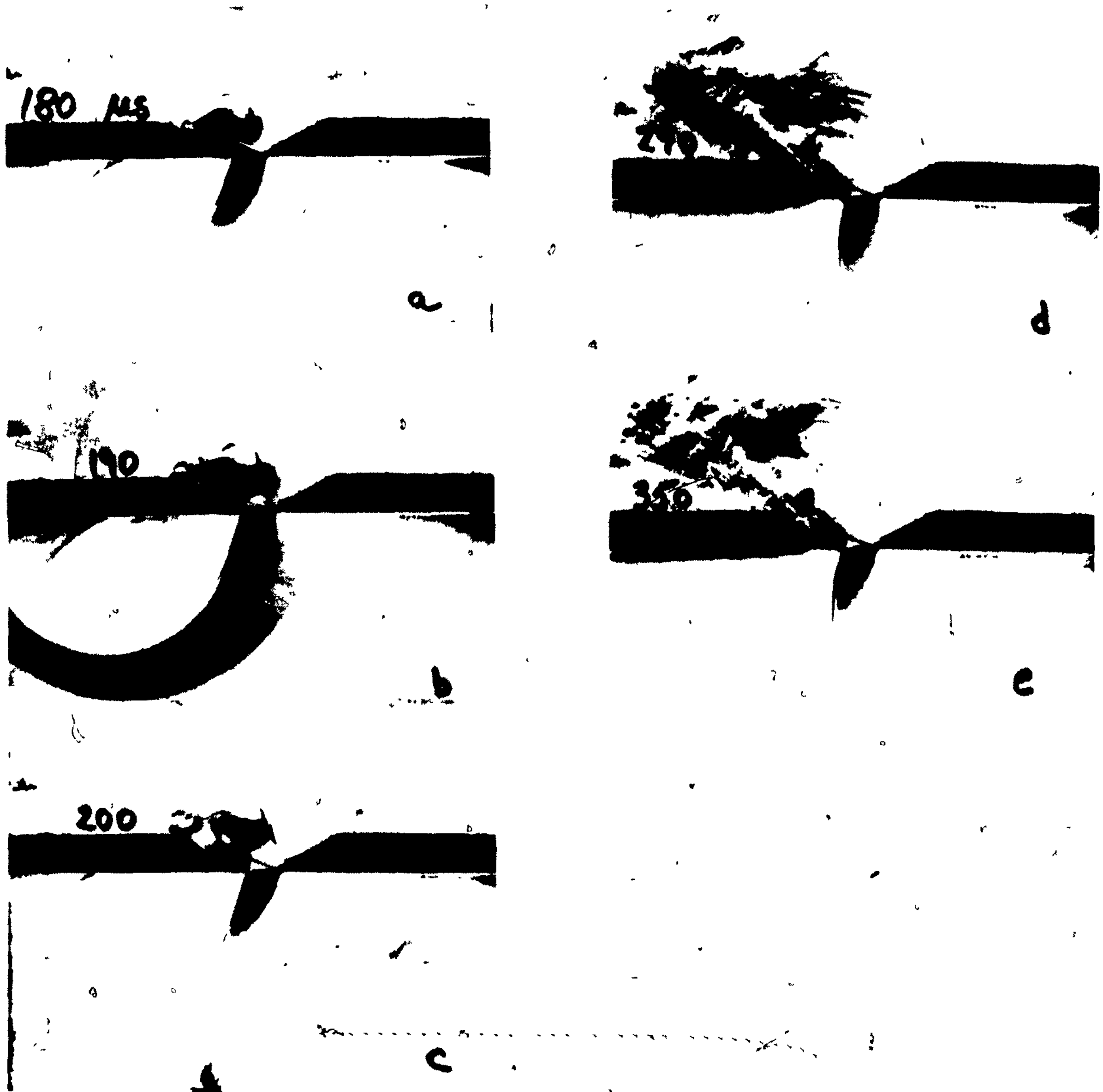

FIGURE 5.5: SHOCK-SLIT INTERACTION FOR M_0 = 1.67, ω = .275 INCHES.
MAGNIFICATION = .84.

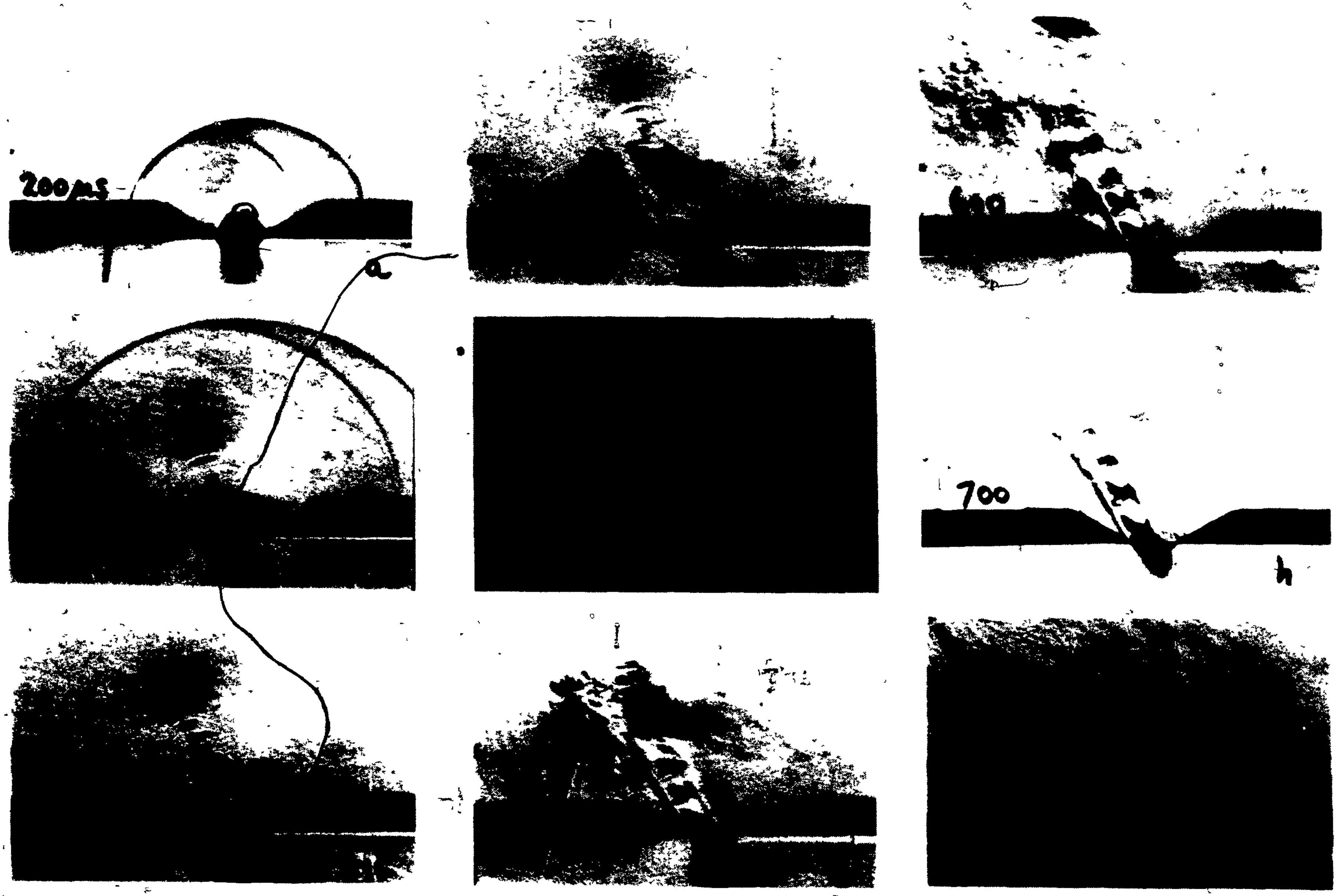
200μs
a
700
h

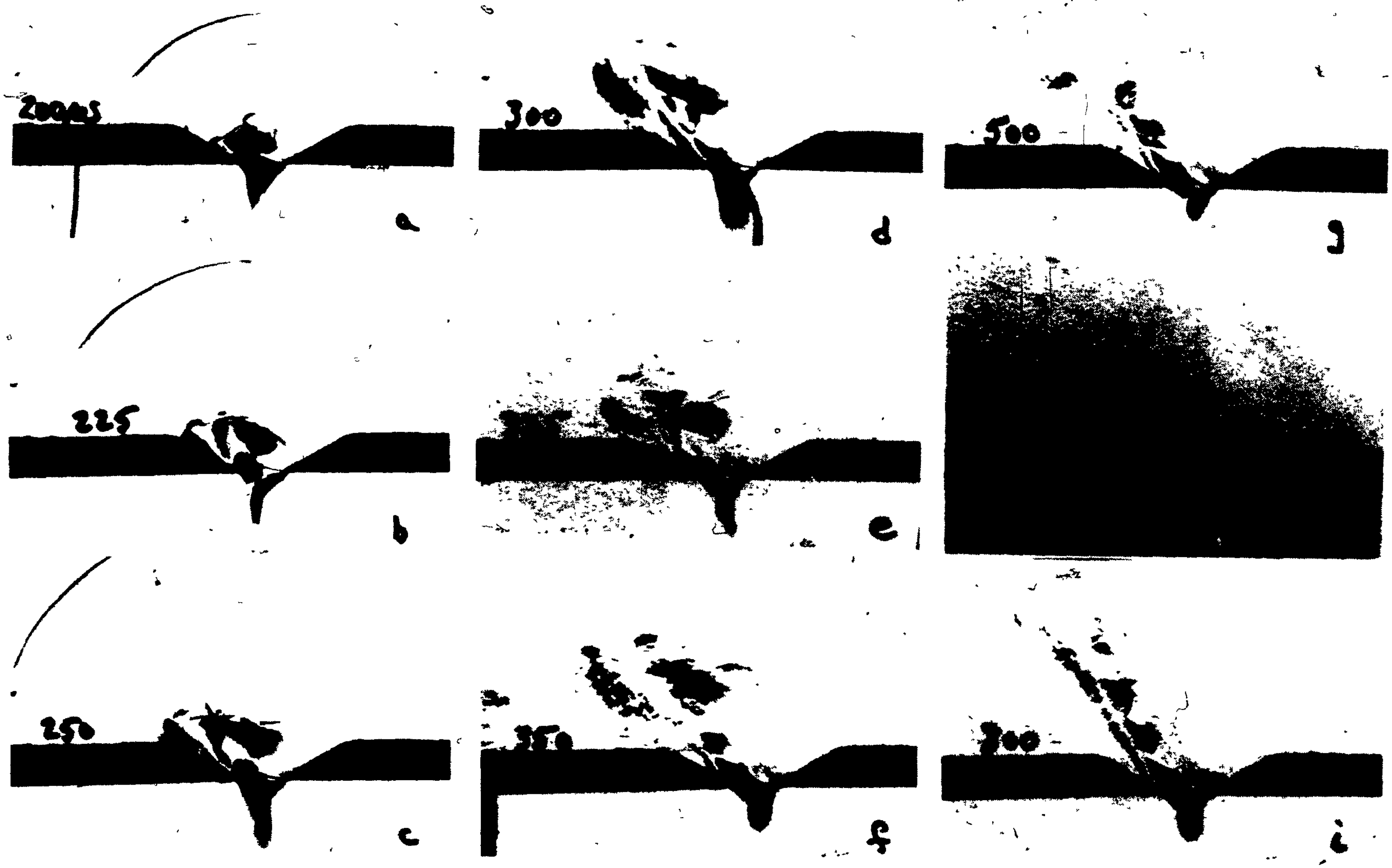

FIGURE 8.7? JET DEVELOPMENT FOR M_0 = 1.55, = 275. MAGNIFICATION = 1.0.

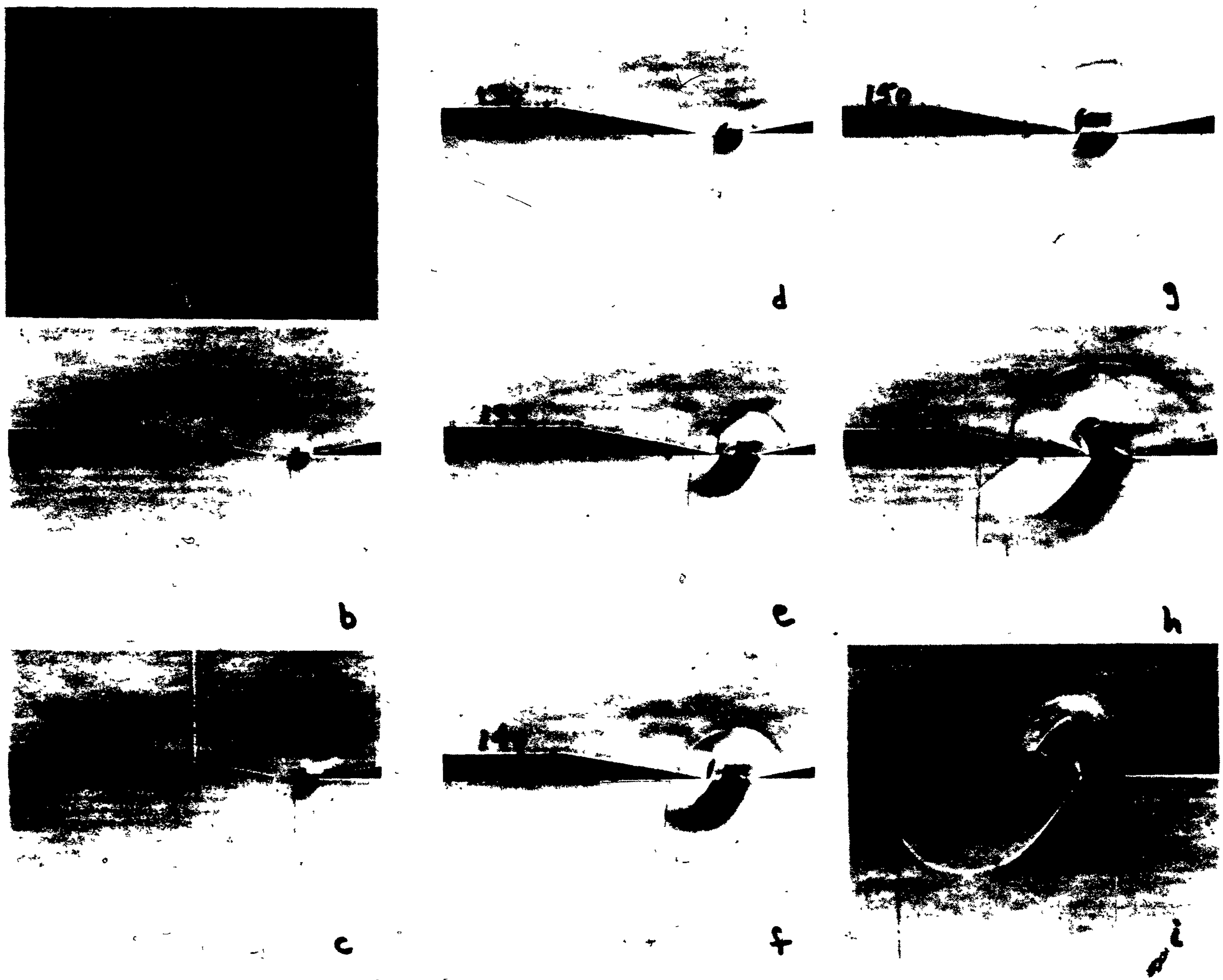
150
d
g
b
e
h
c
f
i

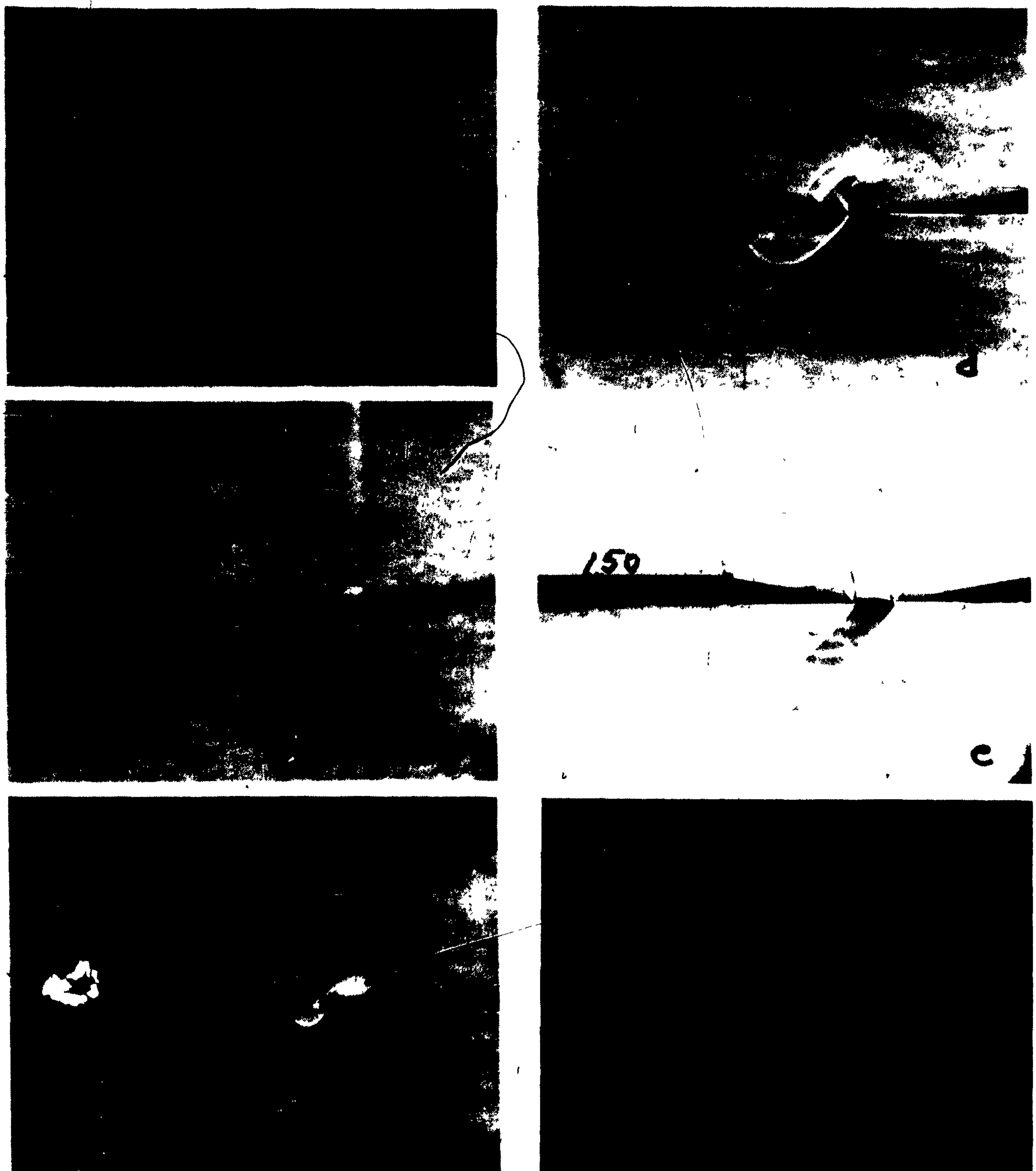

FIGURE 6.9 SHOCK-SLIT INTERACTION FOR M_0 [illegible] 2.44, [illegible] = .375 INCHES.

MAGNIFICATION [illegible] 4

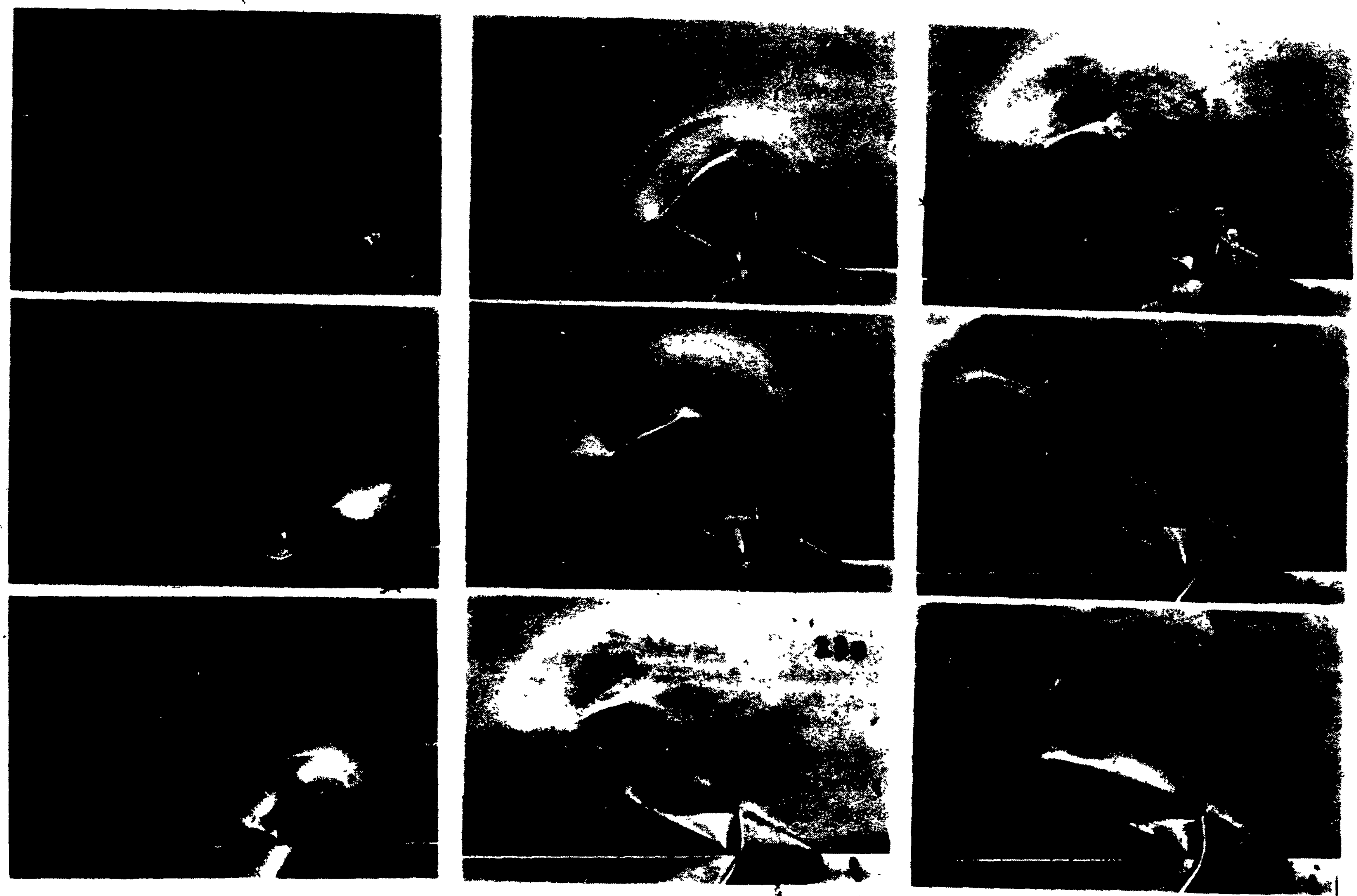

FIGURE 5.10 JET DEVELOPMENT FOR M = 2.14, [illegible]

FIGURE 5.11 [illegible] 375 INCHES. MAGNIFICATION = .84.

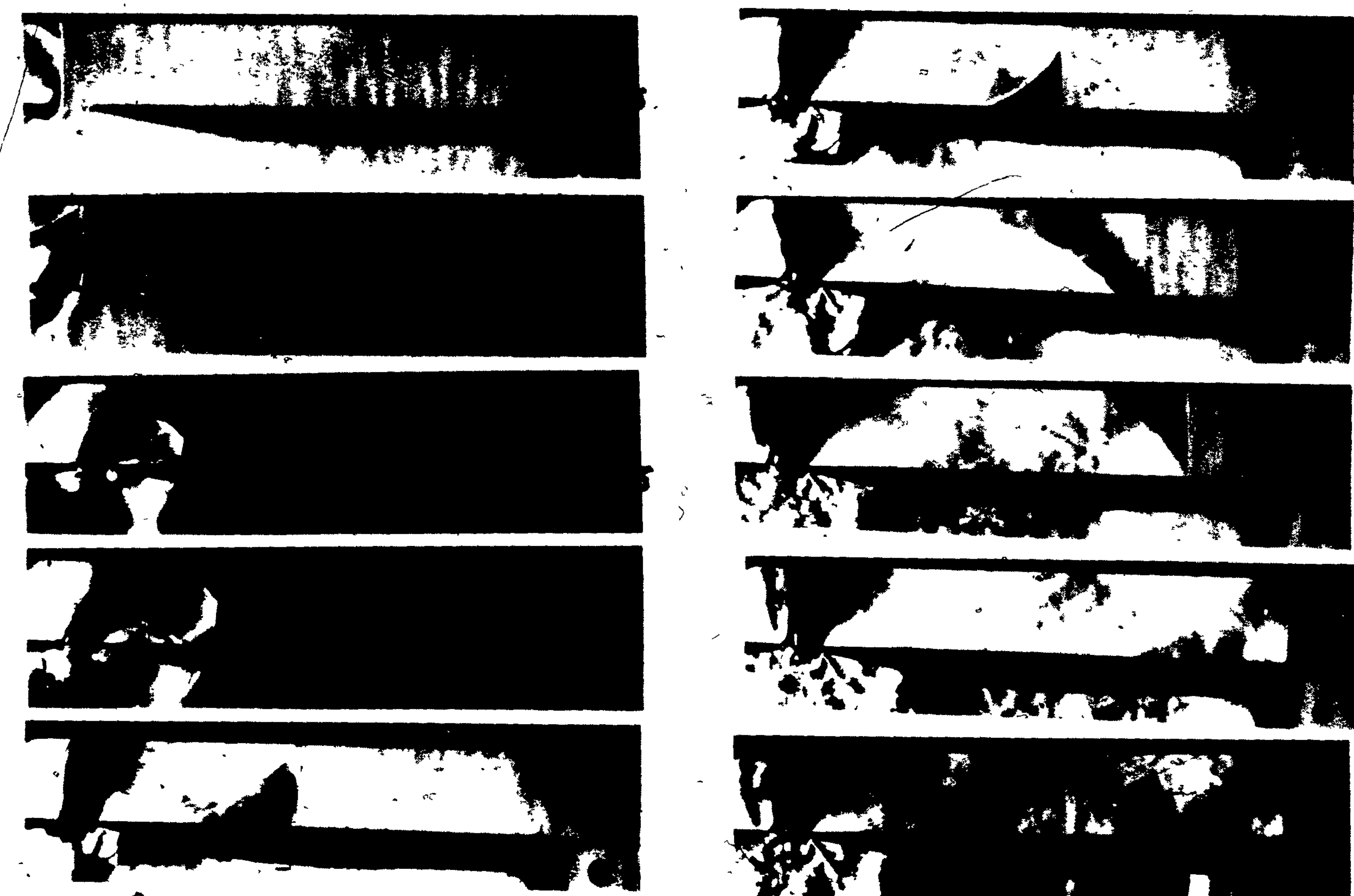

FIGURE [illegible] INTERACTION FOR M_o = 1.4, [illegible] = .35. MAGNIFICATION = .73.

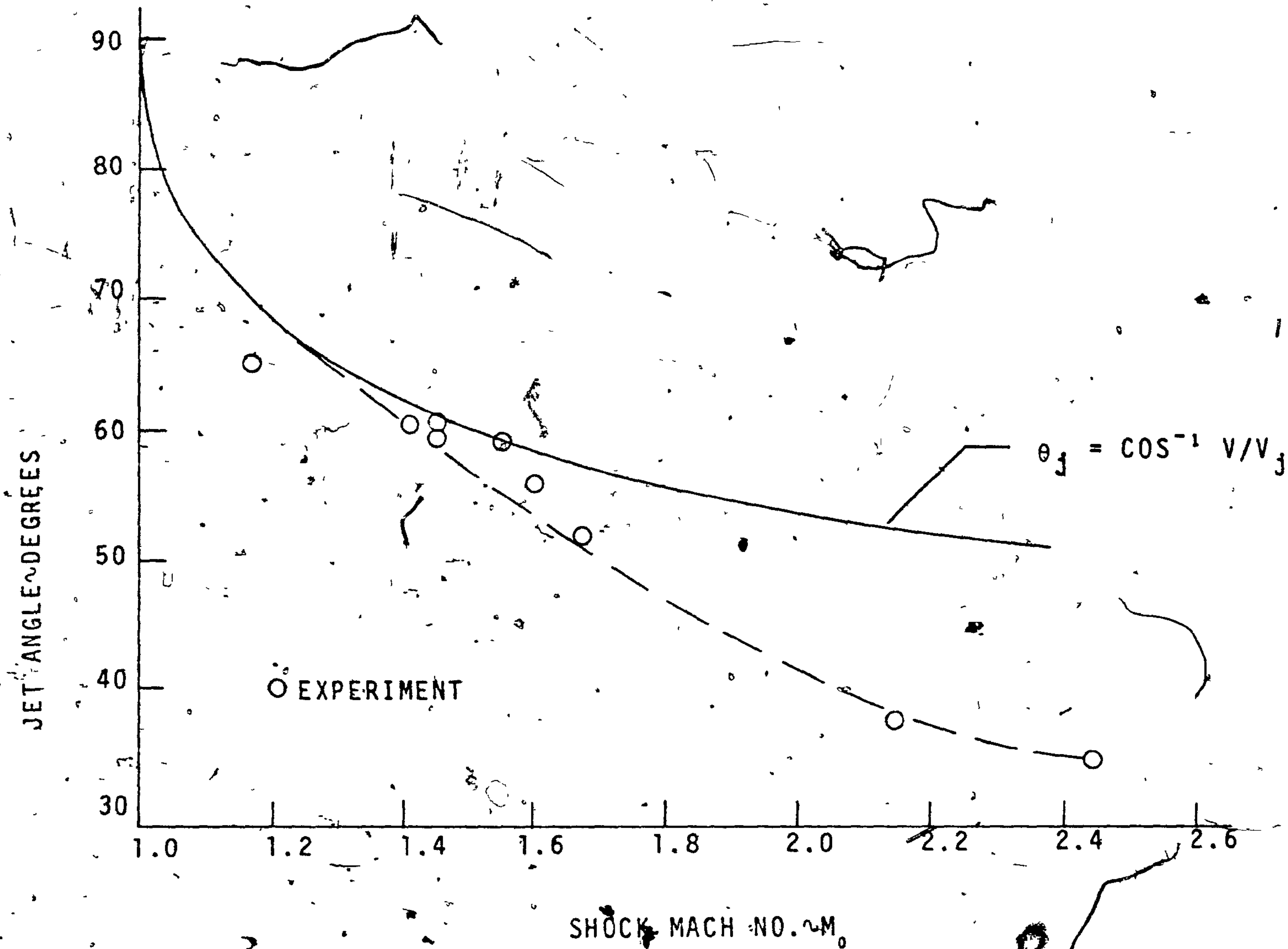

FIGURE 5.13: JET ANGLE

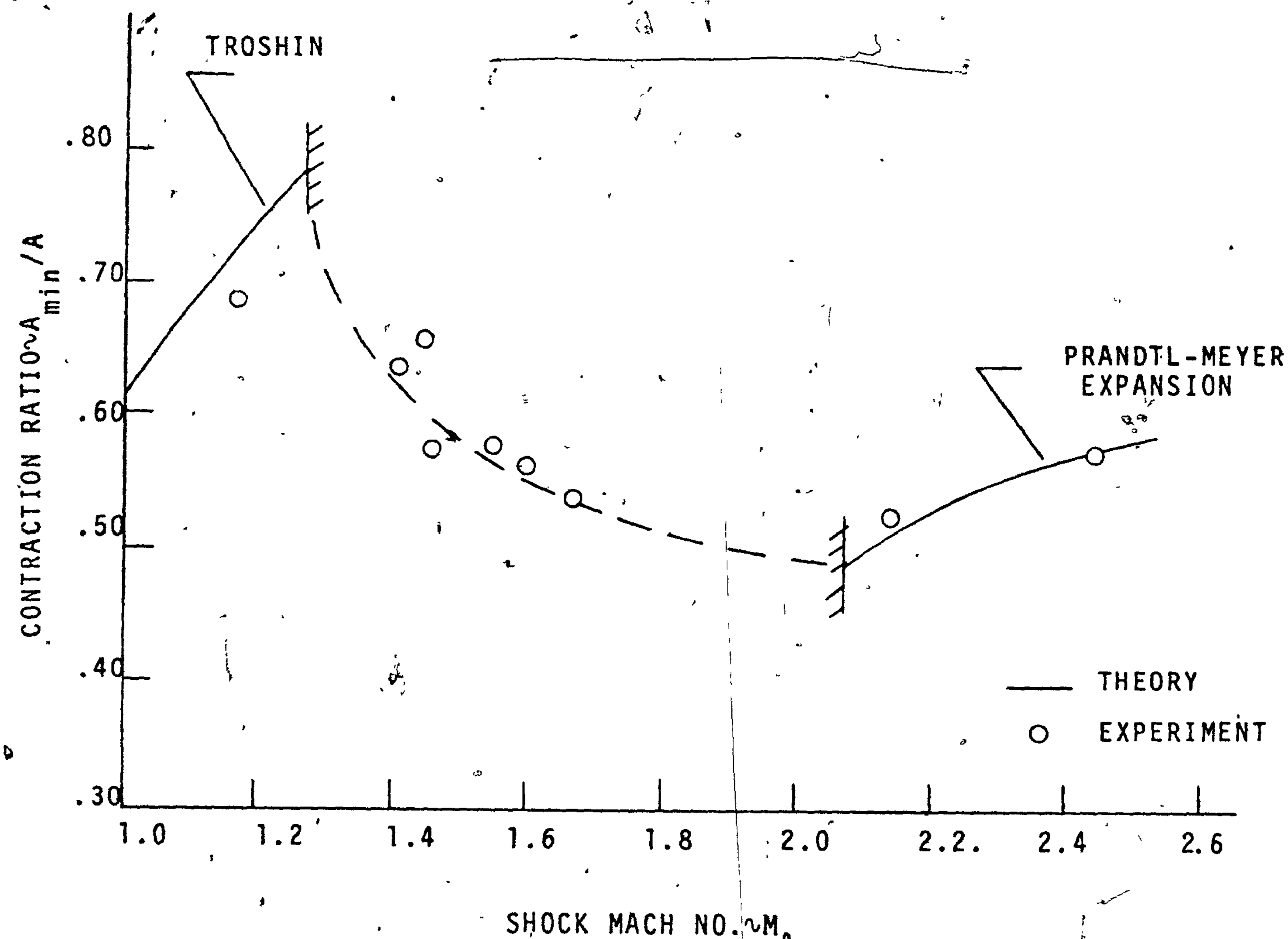

FIGURE 5.14: JET CONTRACTION RATIO.

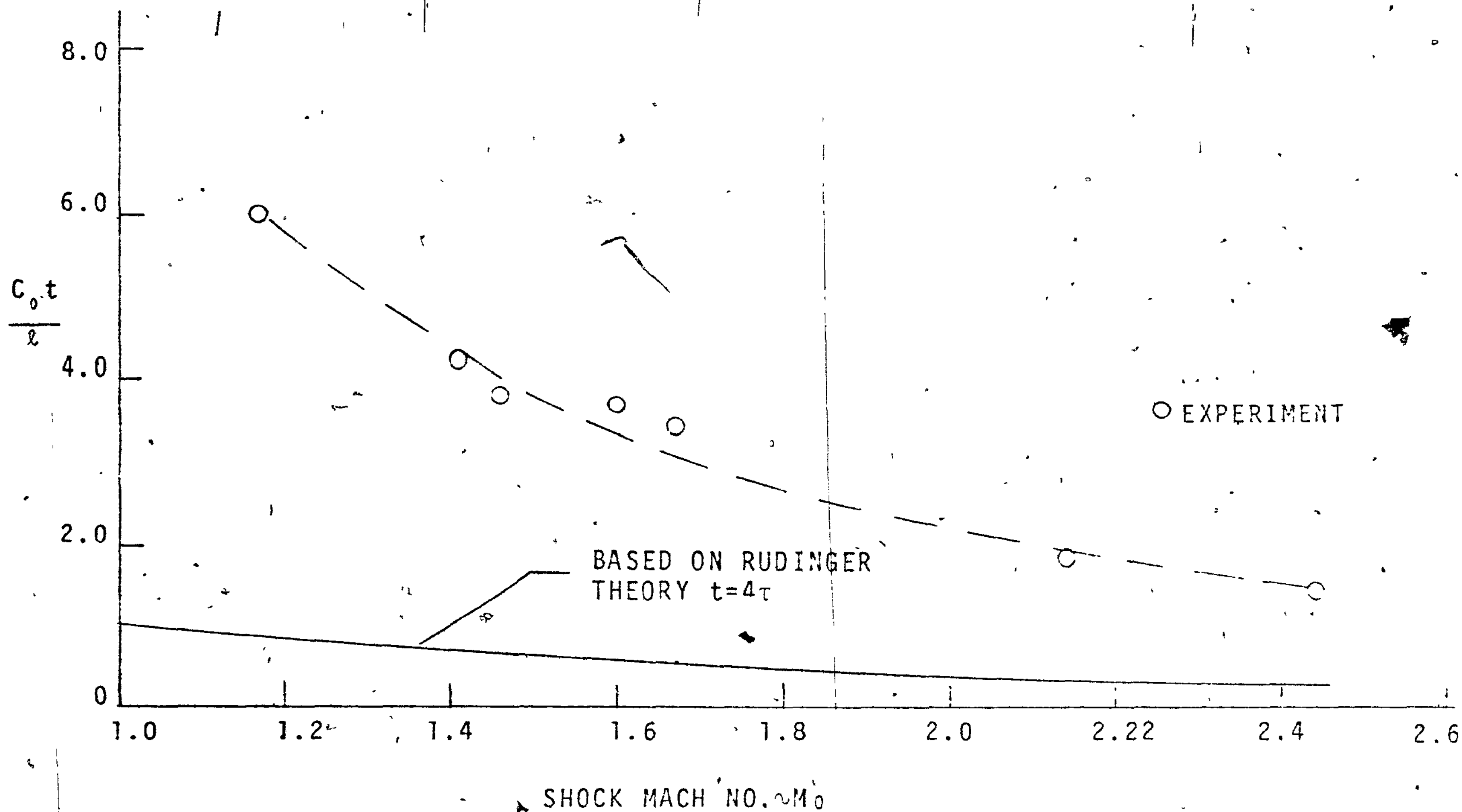

FIGURE 5.15: JET DEVELOPMENT TIME

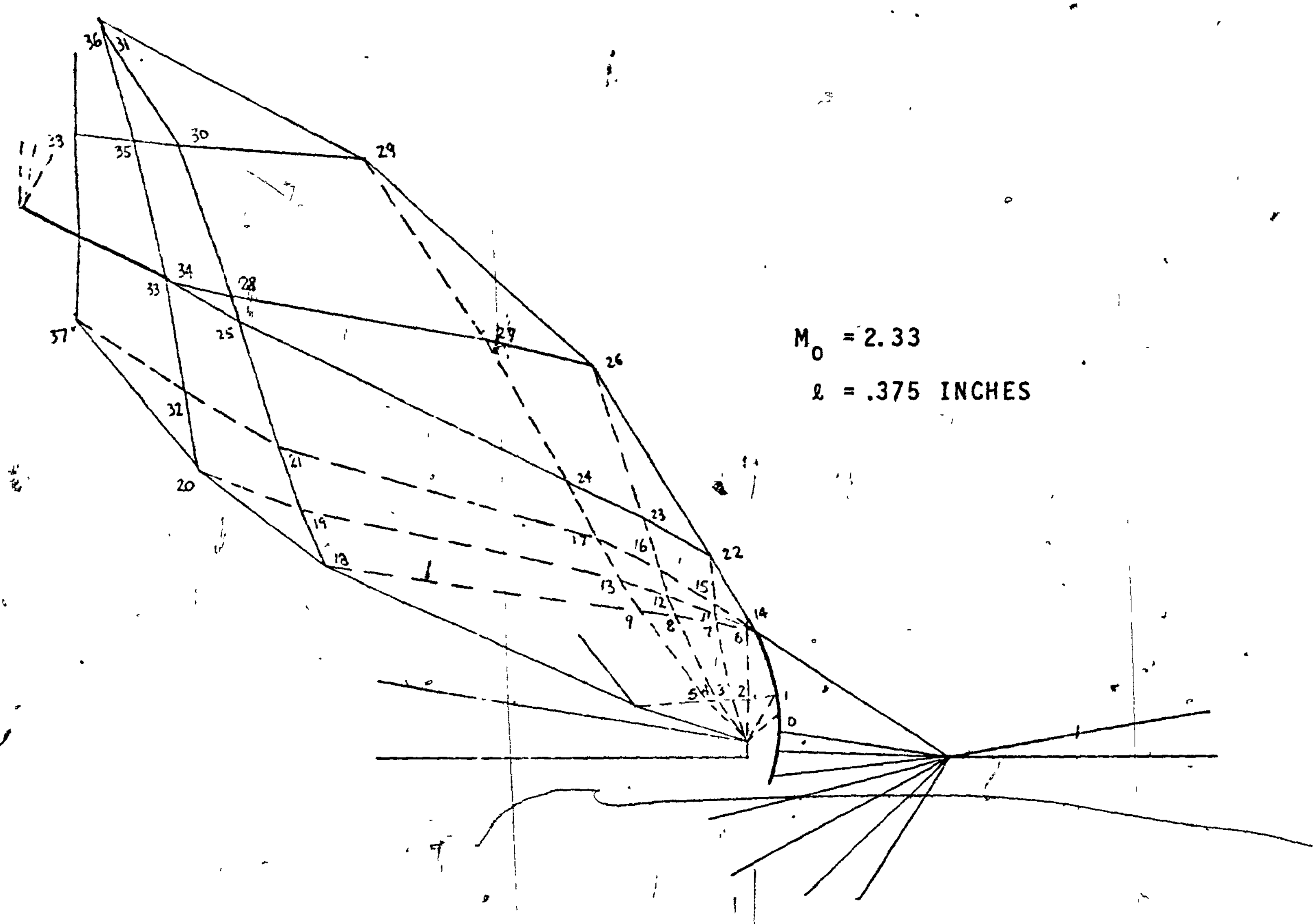

FIGURE 5.16: JET STRUCTURE FOR SUPERSONIC FLOW BEHIND THE INCIDENT SHOCK.

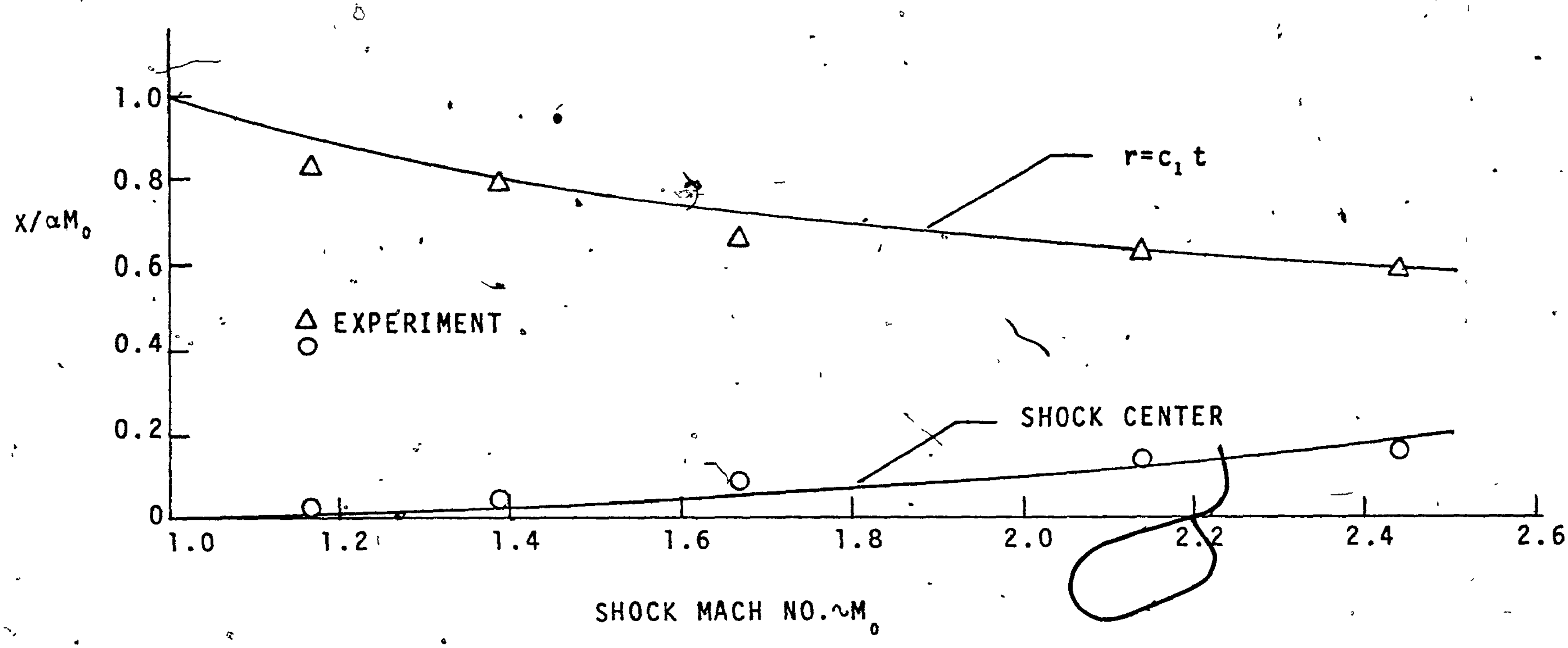

FIGURE 5.17: EXTERNAL DIFFRACTED SHOCK

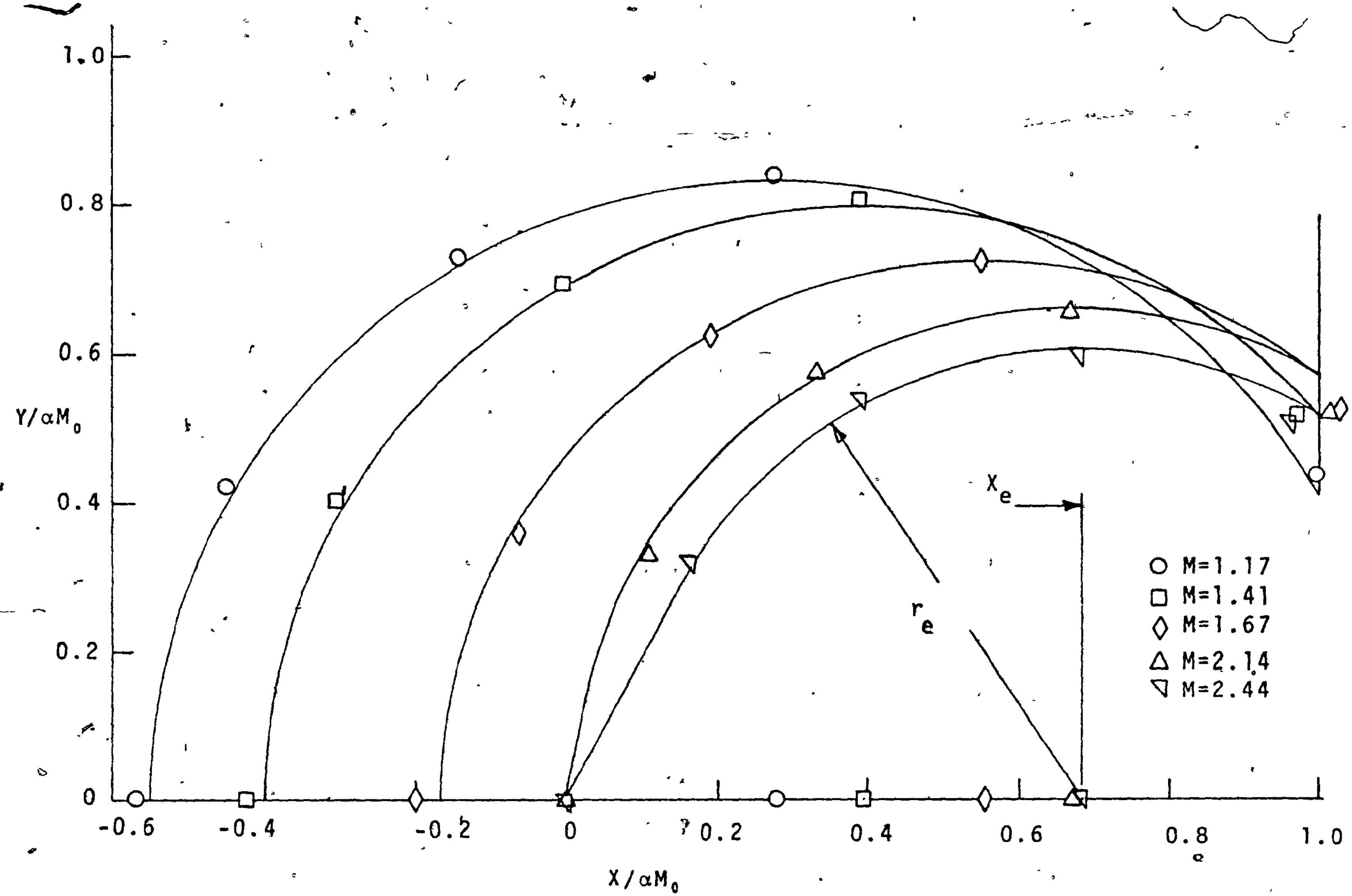

FIGURE 5.18: EXPANSION WAVE MEASUREMENTS

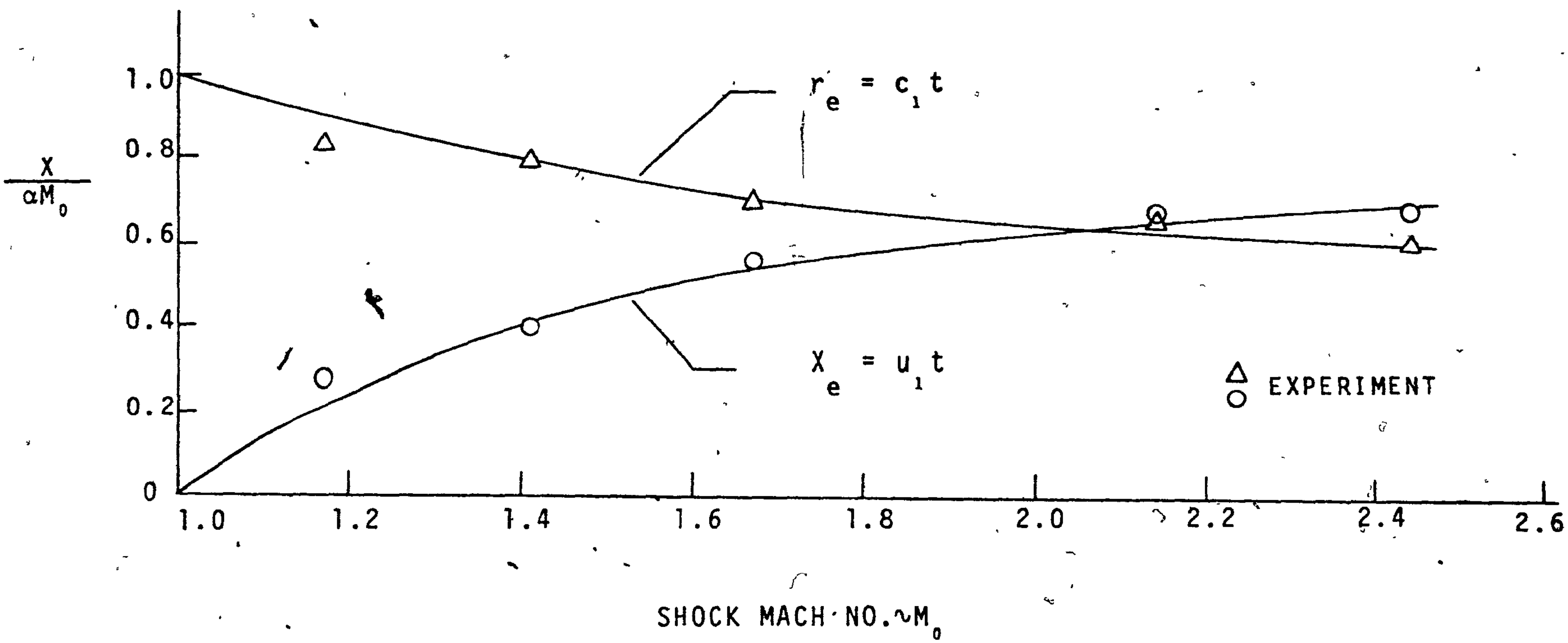

FIGURE 5.19: EXPANSION WAVE CENTER AND RADIUS

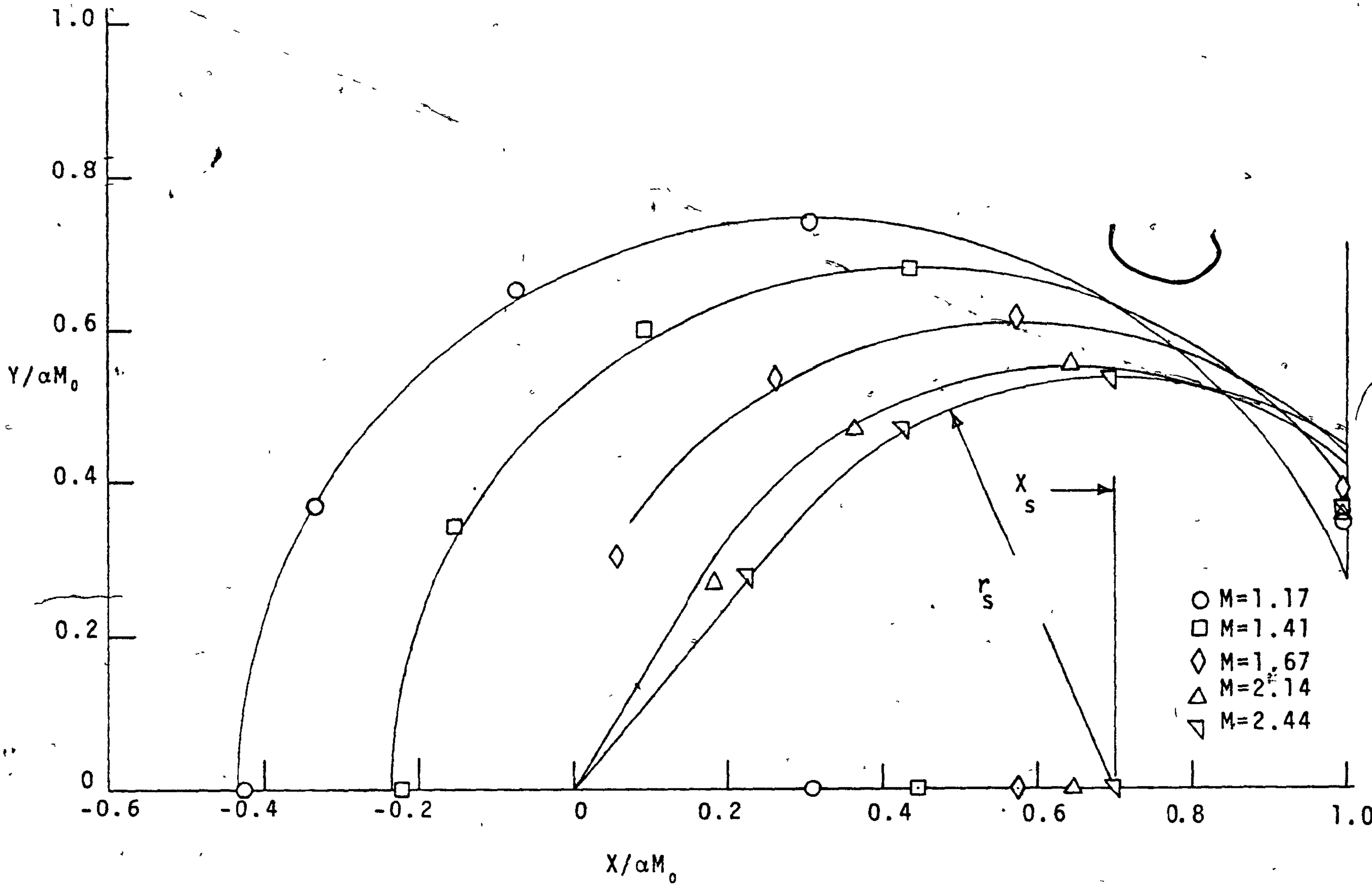

FIGURE 5.20: REFLECTED SHOCK MEASUREMENTS.

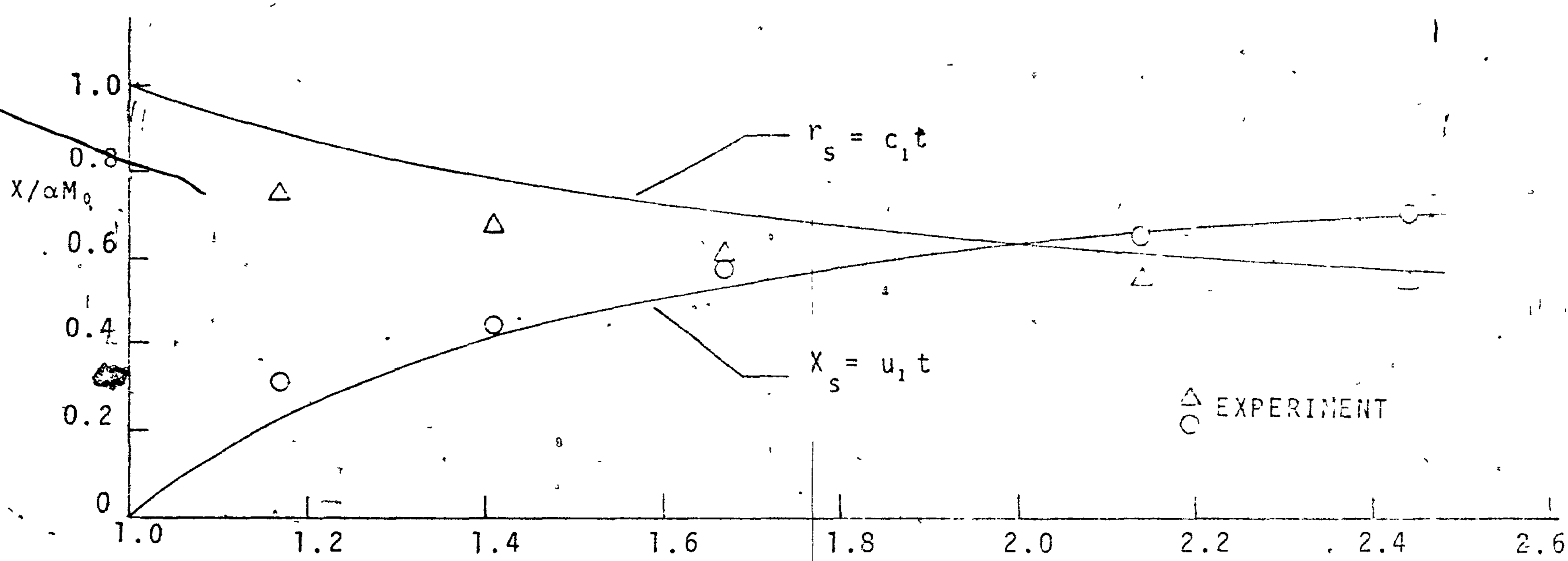

FIGURE 5.21: REFLECTED SHOCK CENTER AND RADIUS

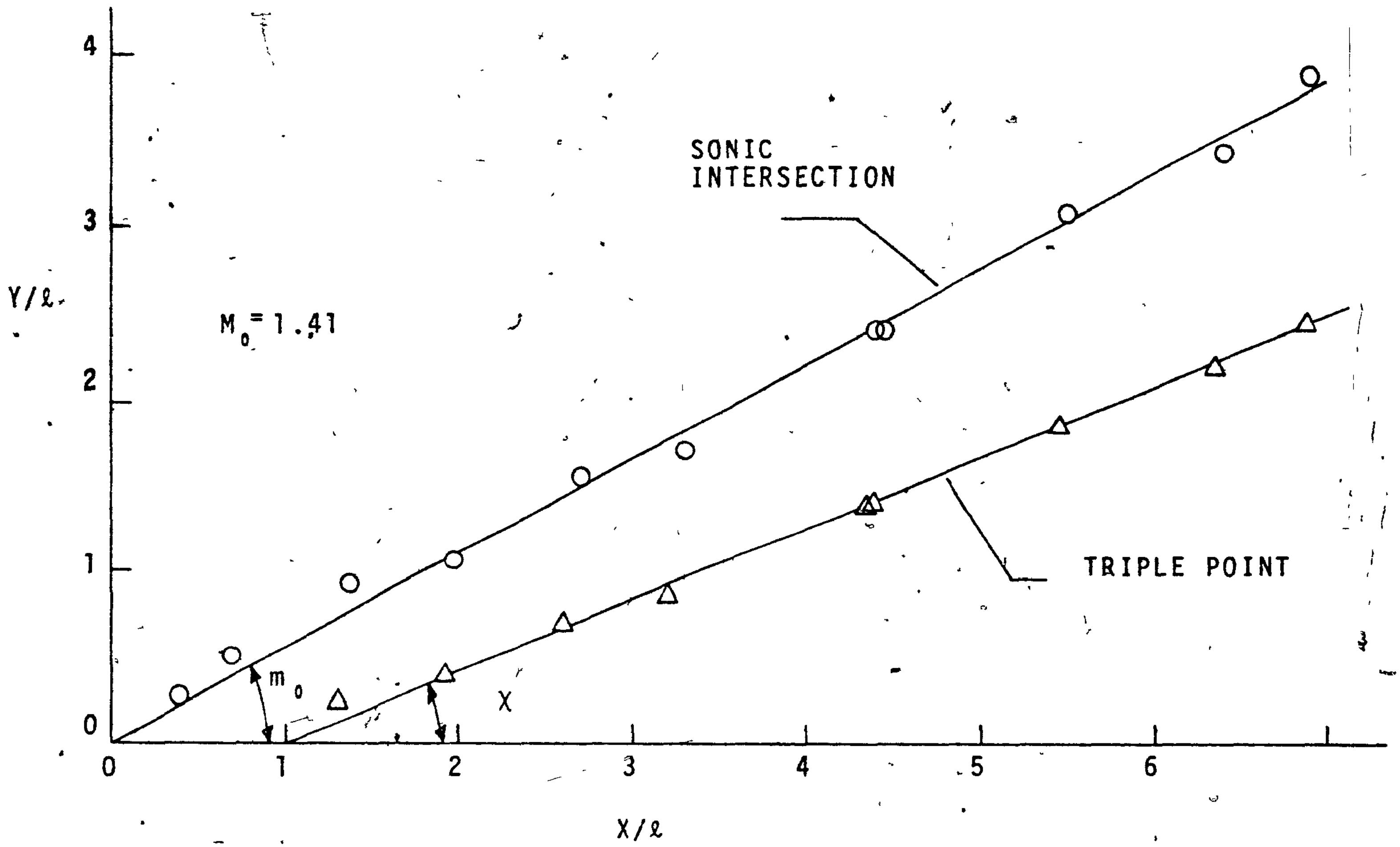

FIGURE 5.22: SONIC INTERSECTION AND TRIPLE POINT LOCUS FOR $M_0 = 1.41$ AND $\ell = 0.275$ INCHES

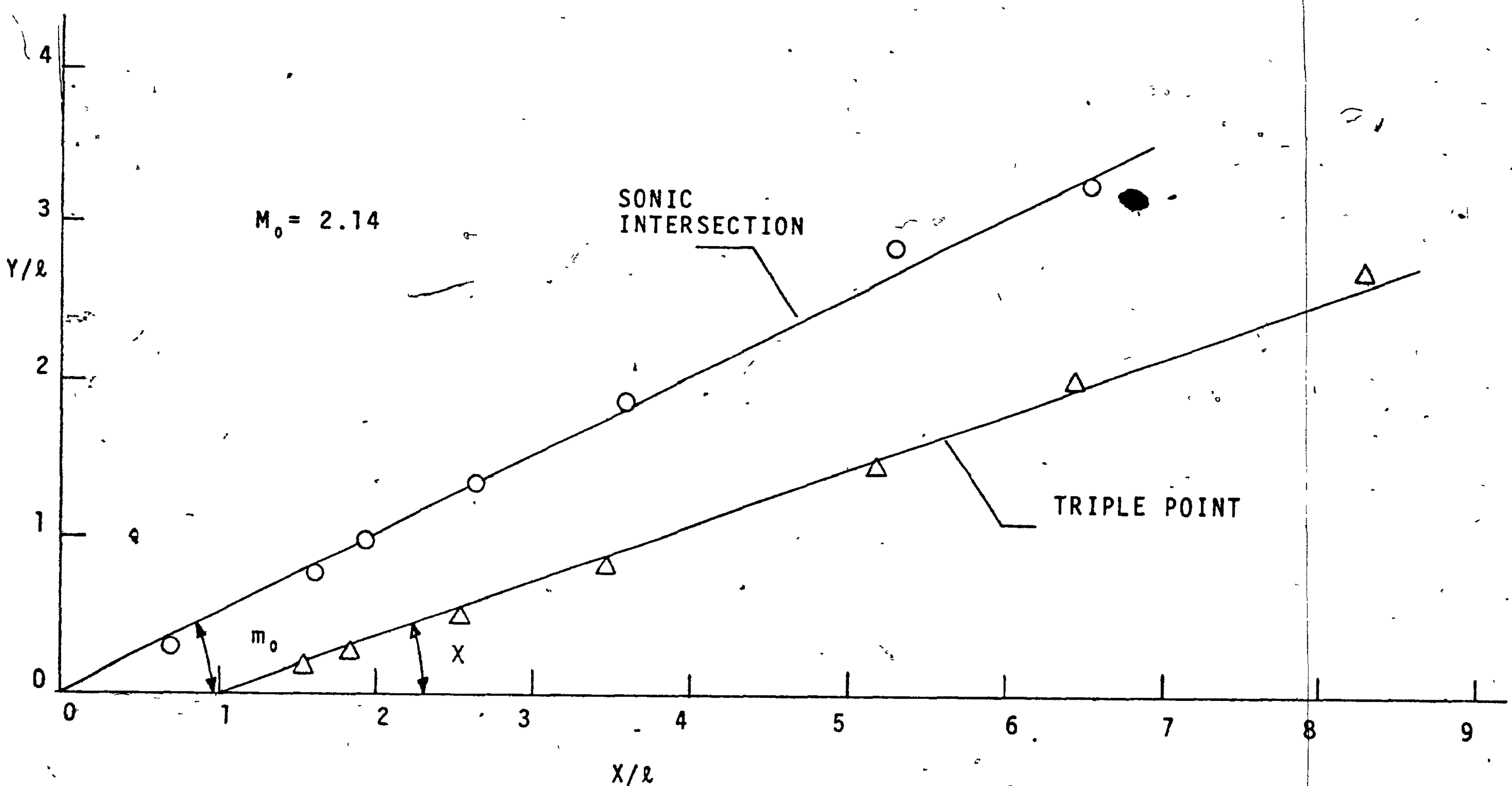

FIGURE 5.23: SONIC INTERSECTION AND TRIPLE POINT LOCUS FOR $M_0 = 2.14$ AND $\ell = 0.375$ INCHES.

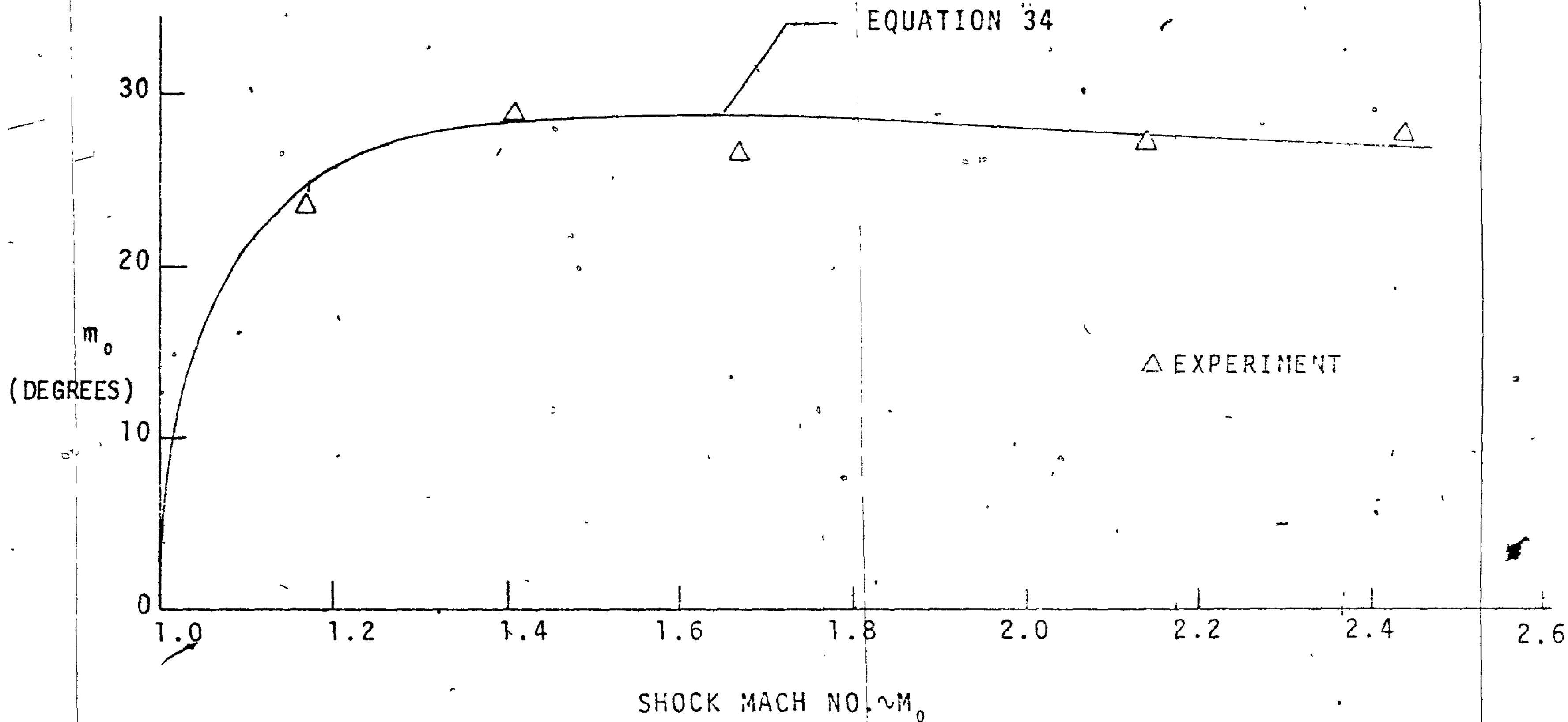

FIGURE 5.24: THE CHARACTERISTIC ANGLE m_0

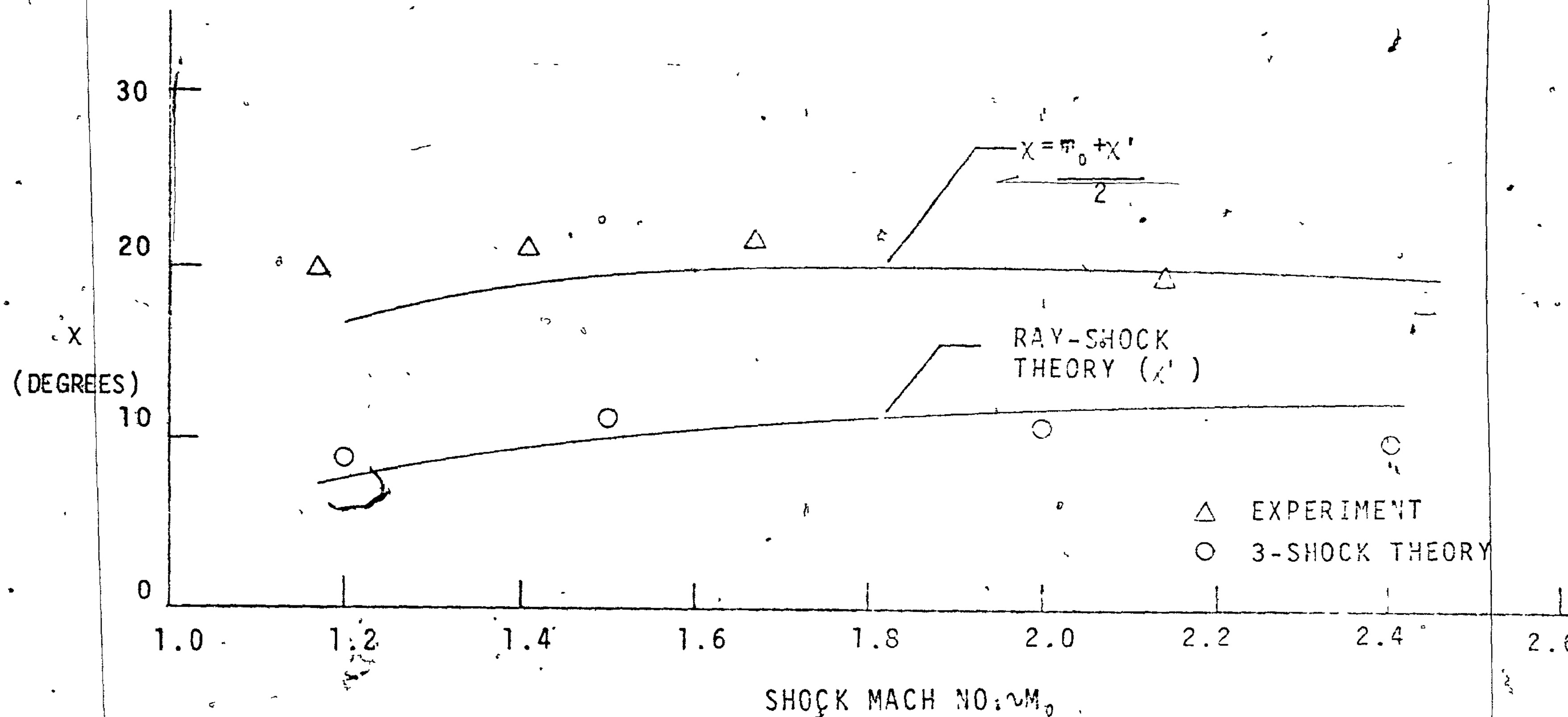

FIGURE 5.25: TRIPLE POINT LOCUS ANGLE χ

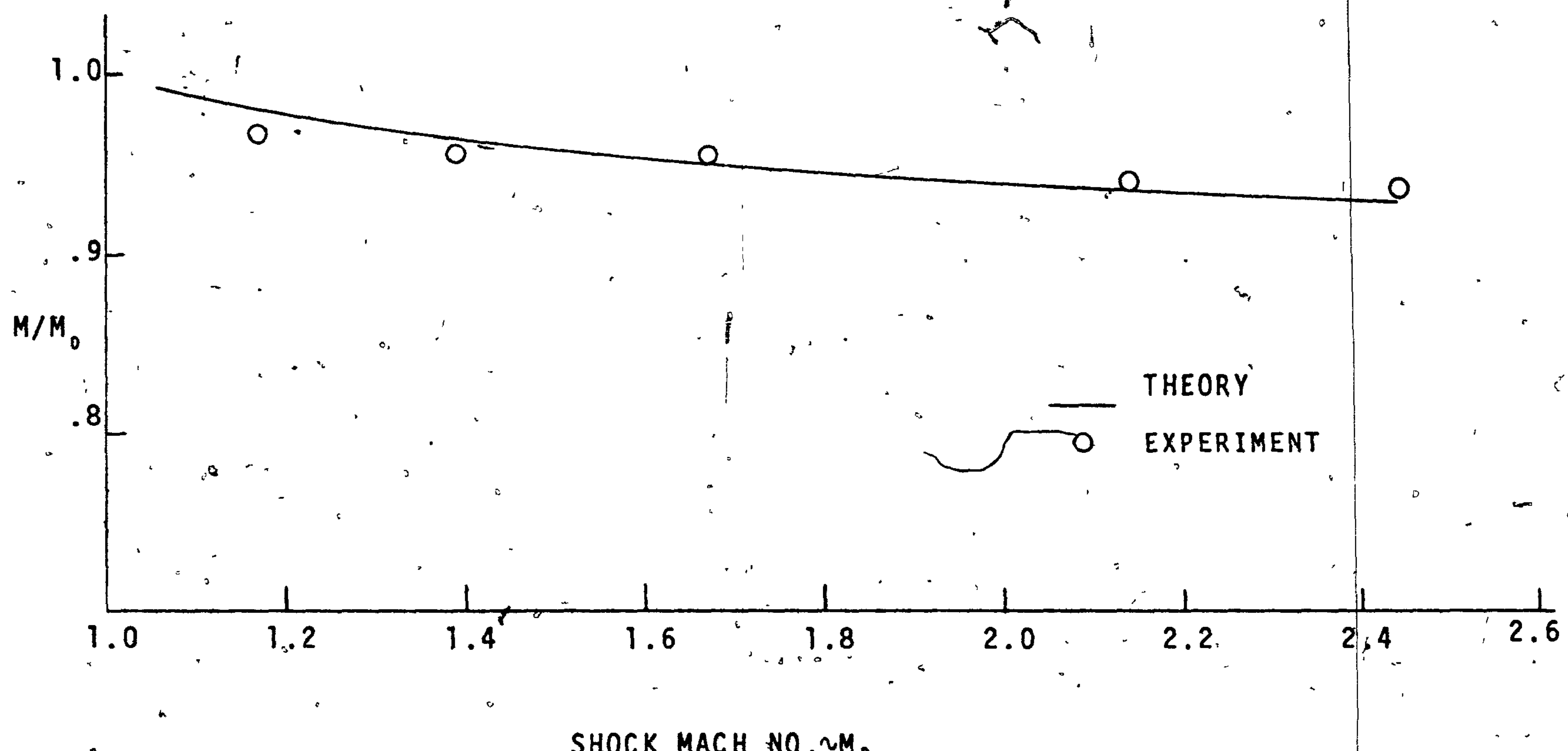

FIGURE 5.26: SHOCK WAVE ATTENUATION NEAR THE SLIT

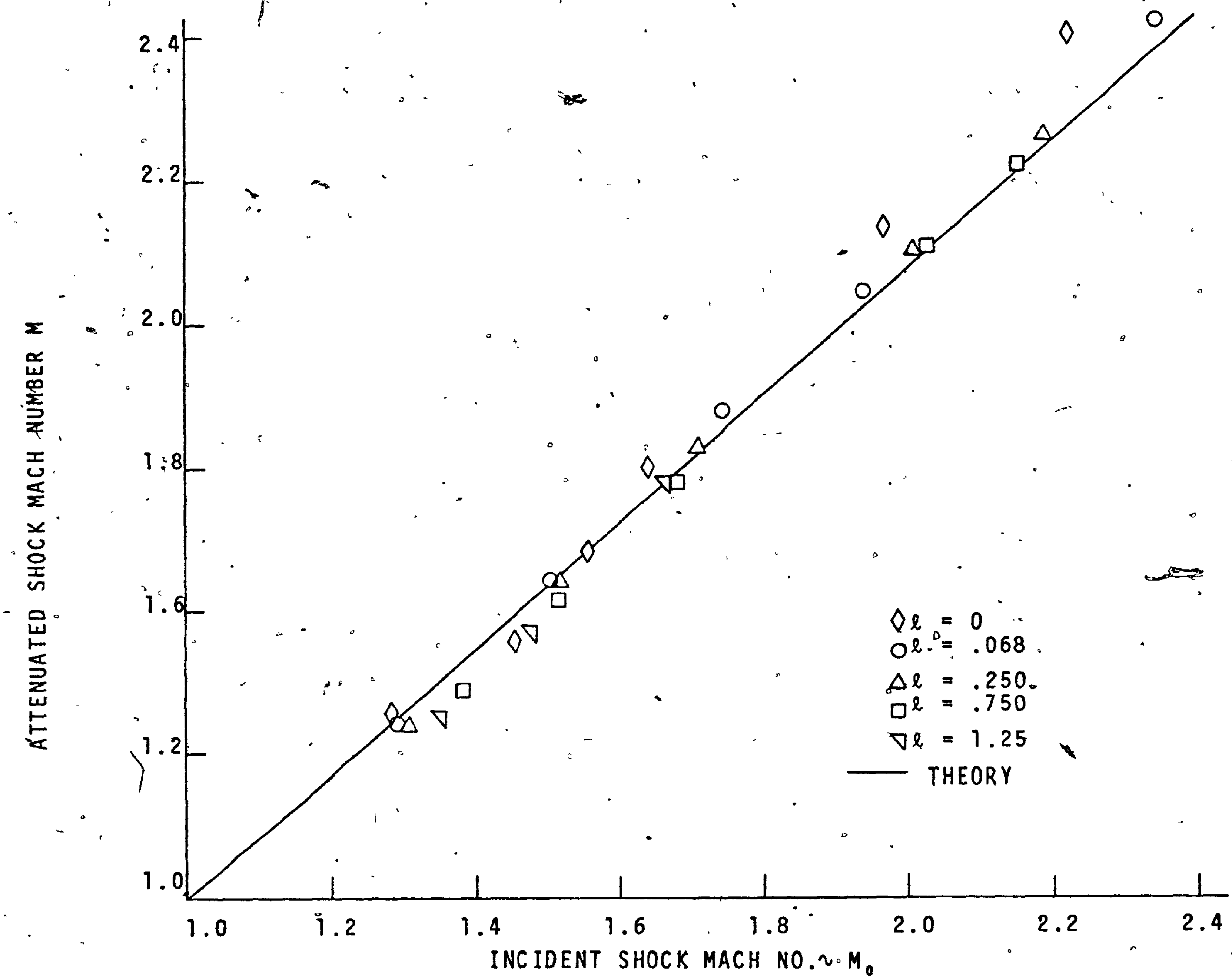

FIGURE 5.27: SHOCK WAVE ATTENUATION FAR DOWNSTREAM OF THE SLIT

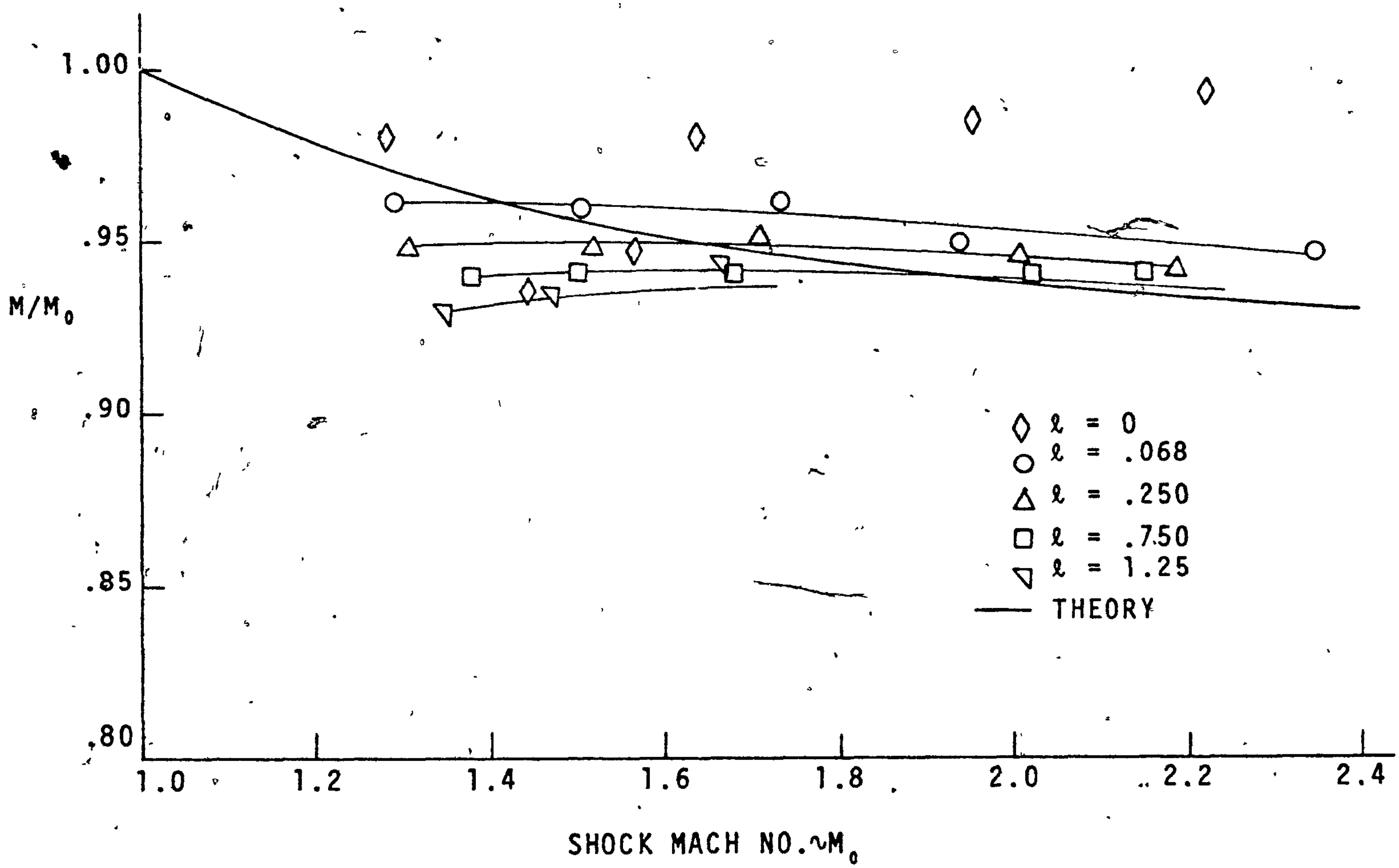

FIGURE 5.28: SHOCK WAVE ATTENUATION FAR DOWNSTREAM OF THE SLIT

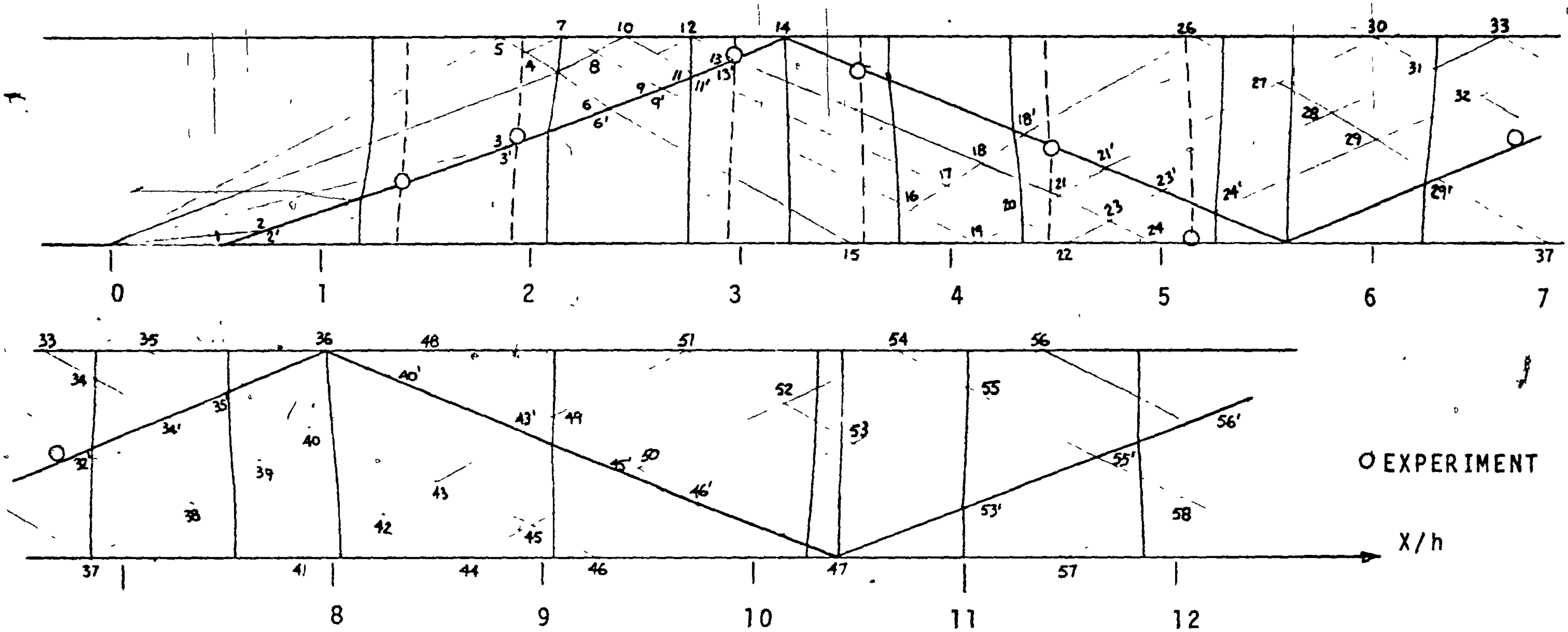

FIGURE 5.29: WAVE DIAGRAM SHOWING TRANSVERSE WAVE MOTION ON THE SHOCK FRONT FOR $M_0 = 1.4$, $\ell = .35$ INCHES, $h = .68$ INCHES.

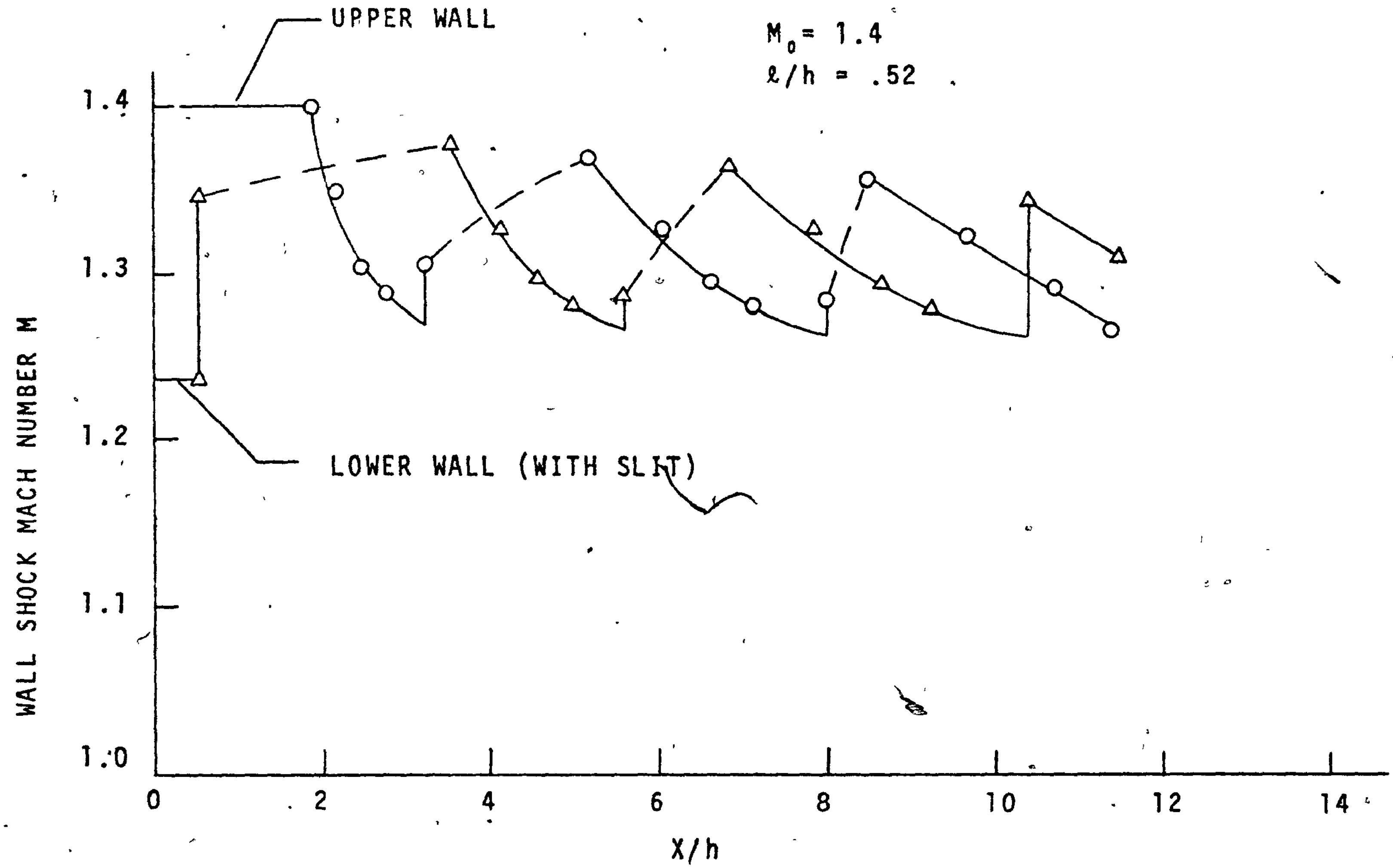

FIGURE 5.30: SHOCK MACH NUMBER VARIATION ALONG THE DUCT WALLS FOR $M_0 = 1.4$ ACCORDING TO THE WAVE DIAGRAM.

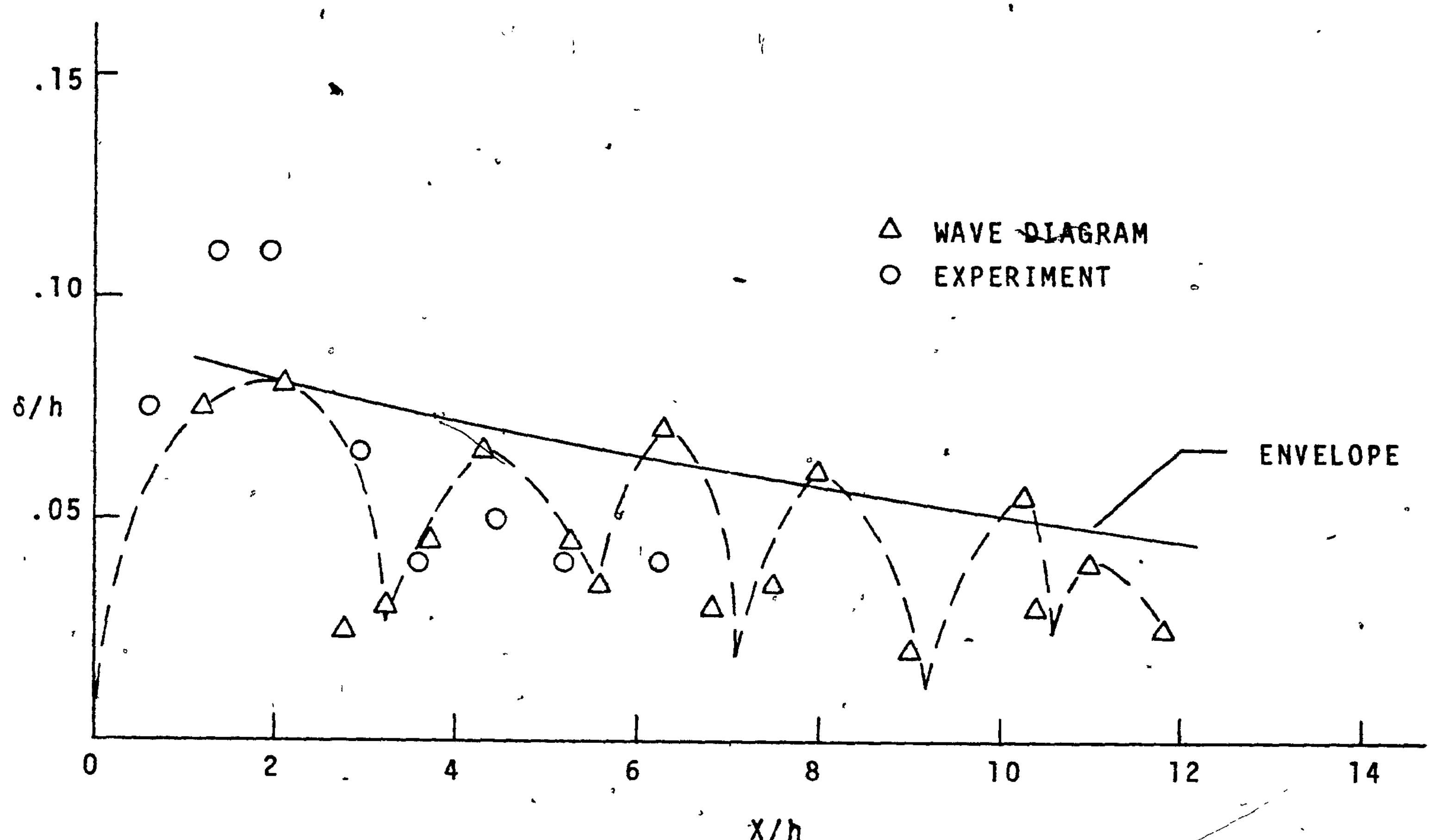

FIGURE 5.31: CYCLIC VARIATION IN SHOCK FRONT PERTURBATION FOR $M_0 = 1.4$

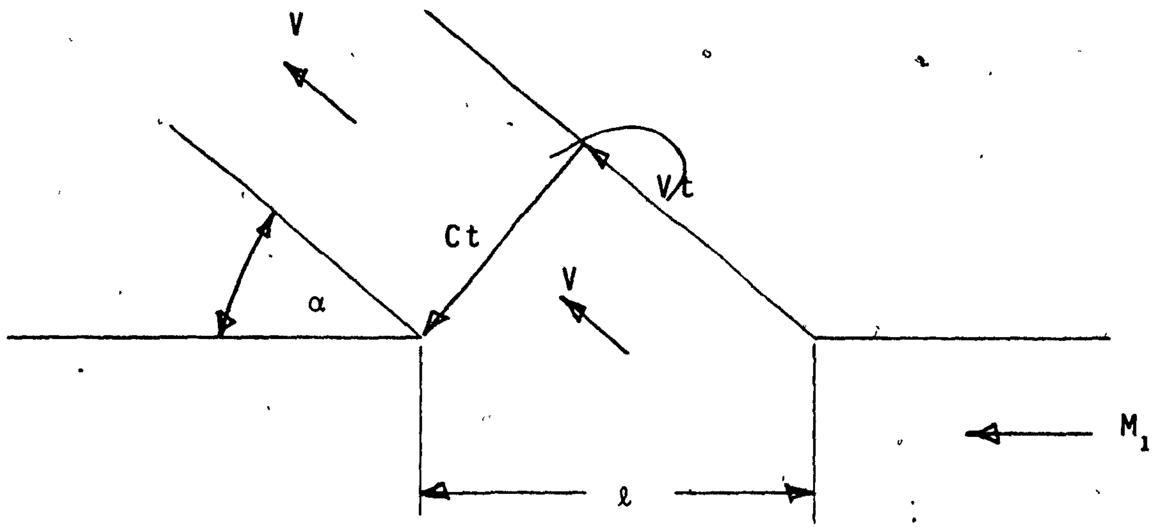

FIGURE A1: IDEALIZED FLOW THROUGH THE SLIT AFTER THE JET HAS BEEN ESTABLISHED.

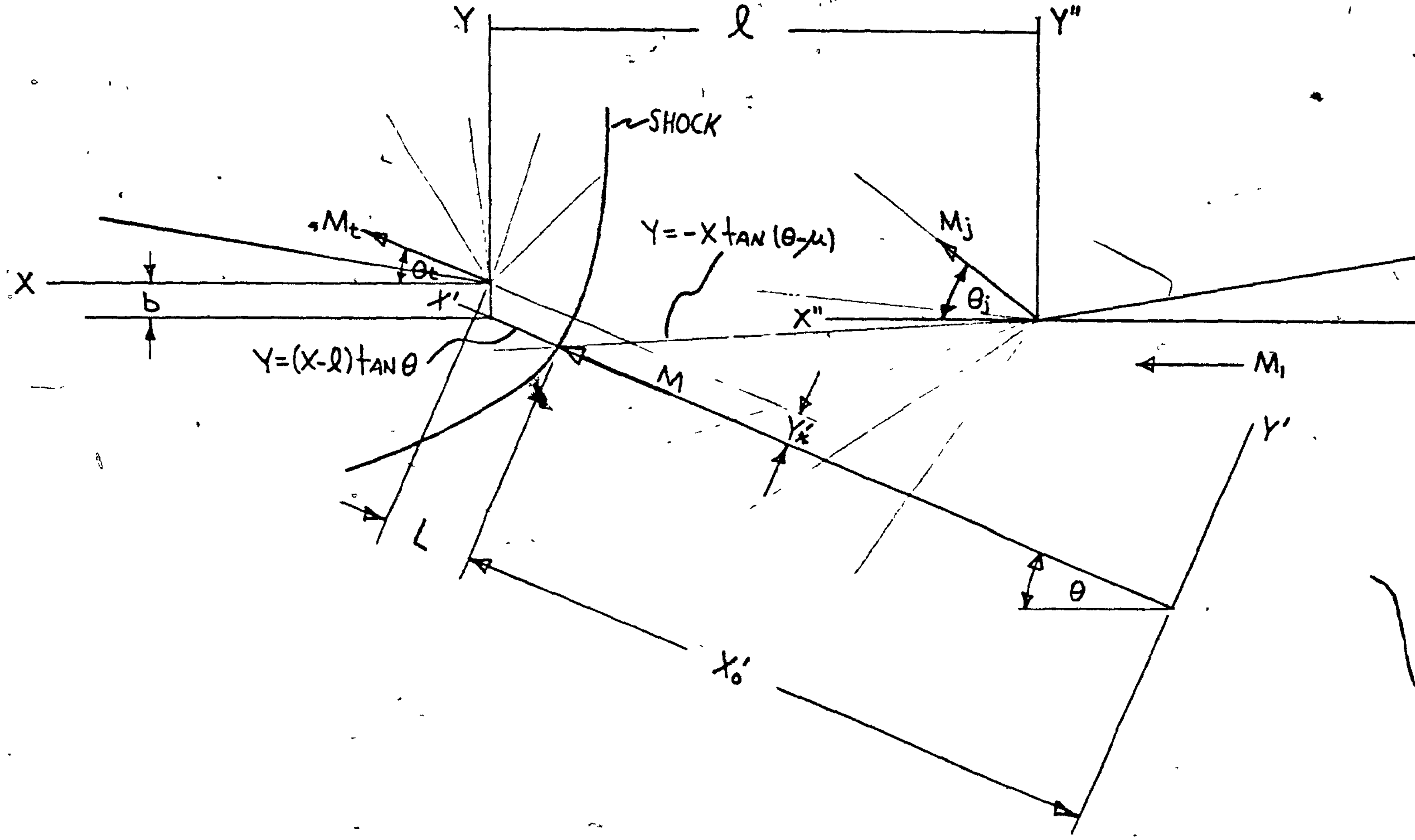

FIGURE B1: THE FLOW FIELD SURROUNDING THE SLIT FOR $M_1 > 1.0$

<u>TABLE 5.1</u>

Point	P	Q	M	θ	ω	m	θ+m	θ-m
1	-45.96	0	1.237	-22.98	-22.98	22.98	0	-45.96
2	-42.00	0	1.250	-21.00	-21.00	26.75	5.75	-47.75
3	-26.85	0	1.300	-13.43	-13.43	27.50	14.07	-40.93
4	-12.88	0	1.350	-6.44	-6.44	28.00	21.56	-34.44
5	0	0	1.400	0	0	28.25	28.25	-28.25
1^{1}	-7.0	7.00	1.347	0	-7.0	27.9	27.90	-27.90
2^{1}	-6.10	3.70	1.363	-1.20	-4.90	28.10	26.90	-29.3
3^{1}	-6.38	3.12	1.364	-1.63	-4.75	28.10	26.47	-29.73
6	-24.06	0	1.310	-12.03	-12.03	27.60	15.57	-39.63
6^{1}	-6.23	2.77	1.366	-1.73	-4.50	28.20	26.47	-29.93
7	-6.44	6.44	1.350	0	-6.44	28.00	28.00	28.00
8	-12.88	6.44	1.328	3.22	-9.66	27.75	30.97	-24.53
9	-16.38	6.44	1.315	-4.97	-11.41	27.70	22.73	-32.67
9^{1}	-10.17	9.63	1.326	-0.27	-9.90	27.75	27.48	-28.02
10	-12.88	12.88	1.304	0	-12.88	27.55	27.55	-27.55
11	-17.53	12.88	1.288	-2.33	-15.21	27.35	25.02	-29.68
11^{1}	-11.63	13.97	1.305	1.17	-12.80	27.60	28.77	-26.43
12	-15.21	15.21	1.288	0	-15.21	27.35	27.35	-27.35
13	-18,47	15.21	1.277	-1.63	-16.84	27.20	25.57	-28.83
13^{1}	-11.75	16.25	1.296	2.25	-14.00	27.45	29.70	-25.20
14^{1}			1.306	0				
15	-2.77	2.77	1.378	0	-2.77	28.15	28.15	-28.15
16	-2.77	9.63	1.353	3.43	-6.20	28.00	31.43	-24.57
17	-2.77	13.97	1.337	5.60	-8.37	27.90	33.50	-22.30
18	-2.77	16.25	1.328	6.74	-9.51	27.80	34.54.	-21.05
19	-9.63	9.63	1.327	0	-9.63	27.77	27.77	-27.77
20	-9.63	13.97	1.311	2.17	-11.80	27.60	29.77	25.43
21	-9.63	16.25	1.303	3.31	-12.94	27.55	30.86	-24.24
22	-13.97	13.97	1.297	0	-13.97	27.50	27.50	-27.50
23	-13.97	16.25	1.289	1.14	-15.11	27.35	28.49	-26.21
24	-16.25	16.25	1.280	0	-16.25	27.25	27.25	-27.25
18^{1}	-3.76	12.24	1.340	4.24	-8.00	27.85	32.09	-23.61
21^{1}	-9.99	13.61	1.311	1.81	-11.80	27.60	29.41	-25.79
23^{1}	-14.16	14.44	1.294	0.14	-14.30	27.40	27.54	-27.26
24^{1}	-16.46	15.14	1.284	-0.66	-15.80	27.30	26.64	-27.96
25^{1}			1.287	0				
26	-3.76	3.76	1.370	0	-3.76	28.1	28.1	-28.1
27	-9.99	3.76	1.348	-3.12	-6.88	26.7	23.58	-29.82
28	-14.16	3.76	1.332	-5.20	-8.96	27.85	22.65	-33.05
29	-16.46	3.76	1.323	-6.35	-10.11	27.75	21.40	-34.10
30	-9.99	9.99	1.326	0	-9.99	27.77	27.77	-27.77
31	-14.16	9.99	1.310	-2.09	-12.08	27.60	25.51	-29.69
32	-16.46	9.99	1.301	-3.24	-13.23	27.50	24.26	-30.74
33	-14.16	14.16	1.295	0	-14.16	27.45	27.45	-27.45
34	-16.46	14.16	1.287	-1.15	-15.31	27.35	26.20	-28.50
35	-16.46	16.46	1.279	0	-16.46	27.20	27.20	-27.20
29^{1}	-13.05	4.75	1.333	-4.15	-8.90	27.85	23.70	-32.00

TABLE 5.1 Continued

Point	P	Q	M	θ	ω	m	θ+m	θ-m
32[1]	-14.18	9.88	1.310	-2.15	-12.03	27.60	25.45	-29.75
34[1]	-15.35	14.45	1.290	-0.45	-14.90	27.35	26.90	-27.80
35[1]	-15.80	16.60	1.281	+0.40	-16.20	27.25	27.65	-26.85
36[1]			1.283	0				
37	-4.75	4.75	1.364	0	-4.75	28.10	28.10	-28.10
38	-4.75	9.88	1.345	2.57	-7.32	27.90	30.47	-25.33
39	-4.75	14.45	1.329	4.85	-9.60	27.80	32.65	-22.95
40	-4.75	16.60	1.320	5.93	-10.68	27.70	33.63	-21.77
41	-9.88	9.88	1.326	0	-9.88	27.75	27.75	-27.75
42	-9.88	14.45	1.310	2.29	-12.17	27.60	29.89	-25.31
43	-9.88	16.60	1.301	3.36	-13.24	27.50	30.86	-24.14
44	-14.45	14.45	1.293	0	-14.45	27.40	27.40	-27.40
45	-14.45	16.60	1.286	1.08	-15.53	27.35	28.43	-26.27
46	-16.60	16.60	1.278	0	-16.60	27.20	27.20	-27.20
40[1]	-5.67	13.53	1.329	3.93	-9.60	27.80	31.73	-23.87
41[1]	-10.49	14.71	1.306	2.11	-12.60	27.55	29.66	-25.44
45[1]	-14.63	15.79	1.288	0.58	-15.21	27.35	27.93	-26.77
46[1]	-18.42	5.67	1.310	-6.25	-12.17	27.60	21.35	-33.85
47[1]			1.343	0				
48	-5.67	5.67	1.356	0	-5.67	28.0	28.0	-28.0
49	-10.44	5.67	1.339	-2.41	-8.08	27.90	25.49	-30.31
50	-14.63	5.67	1.323	-4.48	-10.15	27.75	23.27	-32.23
51	-10.49	10.49	1.322	0	-10.49	27.75	27.75	-27.75
52	-14.63	10.49	1.307	-2.07	-12.56	27.55	25.48	-29.62
53	-18.42	10.49	1.293	-3.97	-14.46	27.40	23.43	-31.37
54	-14.63	14.63	1.290	0	-14.63	27.35	27.35	-27.35
55	-18.42	14.63	1.279	-1.90	-16.53	27.20	25.30	-29.10
56	-18.42	18.42	1.266	0	-18.42	27.05	27.05	-27.05
53[1]	-8.76	12.22	1.322	1.73	-10.49	27.75	29.48	-26.02
54[1]	-9.50	15.70	1.305	3.10	-12.60	27.55	30.65	-24.45
56[1]	-10.71	19.71	1.288	4.5	-15.21	27.35	31.85	22.85
57	-12.22	12.22	1.309	0	-12.22	27.60	27.60	-27.60
58	-12.22	15.70	1.297	1.74	-13.96	27.50	29.24	-25.76

TABLE B 1

Point	P	Q	Θ	ν	M	μ	Θ−μ	θ+μ
0	48.25	-48.25	48.25	0	1.00	90.0	-41.75	138.25
1	54.29	-53.31	53.80	0.49	1.05	72.25	-18.45	126.05
2	54.29	-41.95	48.12	6.17	1.30	50.28	-2.16	98.40
3	54.29	-24.57	39.43	14.86	1.60	38.68	0.75	78.11
4	54.29	-7.11	30.70	23.59	1.90	31.76	-1.06	62.46
5	54.29	6.03	24.13	30.16	2.14	27.86	-3.73	51.99
6	68.19	-25.01	46.60	21.59	1.83	33.12	13.48	79.72
7	68.19	-24.51	46.38	21.81	1.84	32.92	13.46	78.30
8	68.19	-7.11	37.65	30.54	2.16	27.65	10.00	65.30
9	68.19	6.03	31.08	37.11	2.42	24.46	6.62	55.54
10	81.59	-25.01	53.30	28.29	2.07	28.89	24.41	82.19
11	81.59	-24.57	53.08	28.51	2.08	28.74	24.34	81.82
12	81.59	-7.11	44.35	37.24	2.42	24.41	19.94	68.76
13	81.59	6.03	37.78	43.81	2.71	21.65	16.13	59.43
14	94.33	-25.01	59.67	34.66	2.31	25.59	34.08	85.26
15	94.33	-24.57	59.45	34.88	2.33	25.47	33.98	84.92
16.	94.33	-7.11	50.72	43.61	2.70	21.74	28.98	72.46
17	94.33	6.03	44.15	50.18	3.08	18.98	25.17	63.13
18	68.19	-7.97	38.03	30.16	2.14	27.86	10.17	65.89
19	81.59	-7.97	44.78	36.81	2.41	24.57	20.21	69.35
20	81.59	-21.27	51.43	30.16	2.14	27.86	23.57	79.29
21	94.33	-7.97	51.15	43.18	2.68	21.91	29.24	73.06
22	93.89	-24.57	59.23	34.66	2.31	25.59	33.64	84.82
23	93.89	-7.11	50.50	43.39	2.69	21.82	28.68	72.32
24	93.89	6.03	43.80	49.96	3.01	19.40	24.40	63.20
25	93.89	-7.97	50.93	42.96	2.67	22.00	28.93	72.93
26	76.43	-7.11	41.77	34.66	2.31	25.59	16.18	67.36
27	76.43	6.03	35.20	41.23	2.59	22.71	12.49	57.91
28	76.43	-7.97	42.20	34.23	2.30	25.77	7.97	76.43
29	63.29	6.03	28.63	34.66	2.31	25.59	3.04	54.22
30	63.29	-7.97	35.64	27.66	2.05	29.27	6.37	64.91
31	42.63	-7.97	25.30	34.66	2.31	25.59	-0.29	50.89
32	94.33	-21,27	57.80	36.53	2.39	24.73	33.07	82.53
33	93.89	-21.27	57.58	36.31.	2.39	24.79	32.79	82.37
34	76.43	-21.27	48.85	27.58	2.05	29.27	19.58	78.12
35	63.29	-21.27	42.28	21.01	1.81	33.54	8.74	75.82
36	42.63	-21.27	31.95	10.68	1.49	42.16	-10.21	74.11
37	94.33	-34.01	64.17	30.16	2.14	27.86	36.31	92.03
38	63.29	-34.01	48.65	14.64	1.60	38.83	4.91	87.48